

THERMAL MODELING AND TESTING OF THE BLUE THERMAL VACUUM CHAMBER

A Thesis
Presented to
the Faculty of California Polytechnic State University,
San Luis Obispo

In Partial Fulfillment
of the Requirements for the Degree
Master of Science in Aerospace Engineering

by
Madeline Renee Jensma
June 2020

© 2020
Madeline Renee Jensma
ALL RIGHTS RESERVED

COMMITTEE MEMBERSHIP

TITLE: Thermal Modeling and Testing of the Blue Thermal
Vacuum Chamber

AUTHOR: Madeline Renee Jensma

DATE SUBMITTED: June 2020

COMMITTEE CHAIR: Pauline Faure, Ph.D.

Assistant Professor of Aerospace Engineering

COMMITTEE MEMBER: Kira Abercromby, Ph.D.

Professor of Aerospace Engineering

COMMITTEE MEMBER: Kim Shollenberger, Ph.D.

Professor of Mechanical Engineering

COMMITTEE MEMBER: Daniel Wait, M.S.

Lecturer of Aerospace Engineering

ABSTRACT

Thermal Modeling and Testing of the Blue Thermal Vacuum Chamber

Madeline Jensma

The Blue Thermal Vacuum Chamber (TVAC) located in the Space Environments Laboratory at California Polytechnic State University, San Luis Obispo (Cal Poly), may be used for thermal vacuum testing of test articles that fit within the semi cylindrical test section that has a radius of approximately 18 cm and a length of 61 cm. The potential test articles include CubeSat systems and subsystem. The Blue TVAC can also be used for educational and research purposes. The goal of this thesis project is to develop a thermal model of the Blue TVAC to predict and analyze the thermal response of the chamber. Thermal vacuum testing is conducted to verify the repeatability of a test and validate the thermal model.

Thermal vacuum tests were conducted according to the ISO Standard 19683 to measure the temperature at various points in the chamber. This data was used to determine the thermal response of the chamber and the distribution of heat within the chamber. After conducting a total of fifteen thermal vacuum tests, eleven without a test article and four with a test article, a repeatable testing procedure was written to ensure that results from such tests are consistent. A thermal model was developed using Thermal Desktop to predict the temperature distribution within the chamber during the cooling phase, cold soak phase, heating phase, and hot soak phase of a thermal vacuum test.

The simulations of the empty thermal vacuum test predict the platen temperature in the Blue TVAC with a thermal uncertainty margin of less than 10°C. The simulations of the thermal vacuum test with a 3U CubeSat mass model predict the platen temperature in the Blue TVAC with a thermal uncertainty margin of less than 30°C. These simulations can predict the mass model temperature with a thermal uncertainty margin of less than 15°C. The thermal model can

be used to analyze how future changes to the Blue TVAC may affect the thermal distribution in the chamber. Finally, recommendations are made to further improve the performance and repeatability of the Blue TVAC as well as the thermal model with specific instruction for implementing changes and verifying potential improvements.

ACKNOWLEDGMENTS

This thesis project could not be completed without the significant contributions from many people. Thank you first to my parents, Marlo and Jim Jensma, who have been my continuous support through every phase of my education. Their sacrifices have allowed me to pursue my own dreams and passions.

Thank you, Dr. Faure, for your constant guidance and advice despite less than ideal circumstances and schedules. You never fail to offer your time and help when it is needed. Thank you, Dr. Abercromby, for your advice and expertise as I have tried to learn as much as I can about vacuum chamber hardware. Thank you, Dan Wait, for always being willing to help me make progress and for pointing me in the right directions for research and problem-solving strategies. Thank you, Dr. Shollenberger, for offering your valuable instruction for modeling heat transfer and understanding the mechanics of the system.

Special thanks to Cody Thompson for the endless wisdom and creative ideas for solving most, if not every, hardware problem encountered. Thank you also for the special coordinating of liquid Nitrogen weekly refills. Thank you to Eric Beaton for being generous in allowing me to use your time and resources for liquid Nitrogen refills as well.

Thank you, Kendra Bubert, for handling all of the behind the scenes logistics and finances that were required for us all to complete our thesis projects. Also, thank you, Brandon Goddard, for equipping me with the technological resources I needed to complete my project in the most unexpected circumstances.

Finally, thank you to my fellow graduate students, many of whom offered their time to sit in the lab with me during testing to provide safety assistance in case of emergency. Thank you also to all the peers I reached out to for help with software and hardware struggles along the way.

TABLE OF CONTENTS

	Page
LIST OF TABLES	xi
LIST OF FIGURES	xiii
LIST OF ACRONYMS	xx
CHAPTER	
1. INTRODUCTION	1
1.1 Thesis Overview	1
1.2 Thesis Statement	1
1.3 Space Environment	2
1.4 Thermal Modeling	4
1.5 Thermal Testing	5
1.5.1 Thermal Balance Test	5
1.5.2 Thermal Cycle Test	6
1.5.3 Thermal Vacuum Test	7
1.6 ISO Standard 19683	8
2. TECHNICAL BACKGROUND	10
2.1 Heat Transfer	10
2.2 Thermal Desktop	14
3. EXPERIMENTAL APPARATUS	18
3.1 Overview of the System	18
3.2 Thermal Vacuum Chamber	18
3.2.1 Vacuum System	19
3.2.2 Convectron Gauges	22
3.2.3 Ion Gauge	23
3.2.4 Platen	24
3.2.5 Shroud	26
3.2.6 Heating System	27
3.2.7 Cooling System	28
3.2.8 PID Temperature Controller	32
3.3 Data Acquisition (DAQ) System	33
3.4 Test Article	34
4. PRIOR WORK	36
4.1 Initial Testing and Modeling	36

4.2 Additional Heating System Testing	37
4.3 Cooling System Testing	38
4.4 Thesis Motivation	39
5. PROJECT METHODOLOGY	41
5.1 General Methodology	41
5.2 Modeling Methodology	43
5.3 Testing Methodology	50
6. RESULTS	56
6.1 Analytical Model Results	56
6.2 Preliminary Test Results	57
6.3 Empty Thermal Vacuum Test Results	62
6.4 Empty Thermal Vacuum Simulation Results	69
6.5 Test Article Thermal Vacuum Test Results	82
6.5.1 Test 14 Results	84
6.5.2 Test 15 Results	86
6.6 Test Article Thermal Vacuum Simulation Results	89
7. CONCLUSION	101
7.1 General Results	101
7.2 Empty Thermal Vacuum Tests	101
7.3 Thermal Vacuum Tests with Test Article	102
7.4 Thermal Vacuum Test Repeatability	104
7.5 Lessons Learned	105
7.5.1 Thermal Analysis Lessons	105
7.5.2 Operational Lessons	106
7.5.3 Personal Lessons	107
8. FUTURE WORK	109
8.1 LN ₂ Supply	109
8.1.1 Purchase of Worthington 50 Liter Dewar	109
8.1.2 Purchase of 250 lbs LN ₂ Dewar	109
8.2 PID Temperature Controller Analysis	110
8.3 Testing	111
8.4 Thermal Modeling	112
8.5 Chamber Vacuum Leak Investigation	113
REFERENCES	115

APPENDICES

A. Vacuum System Analysis 117

 A.1 Initial Observations 117

 A.2 Initial Hypothesis 118

 A.3 Current Vacuum Status 119

B. Thermocouple Application Procedure..... 120

C. Prior Test Results 122

 C.1 Test Results by Caudill 122

 C.2 Test Results by Caudill and Diamond..... 126

D. Thermal Vacuum Test Setups 128

 D.1 Tests 1-5 Setup..... 128

 D.2 Test 6 Setup..... 130

 D.3 Test 7 Setup..... 132

 D.4 Test 8-9 Setup 133

 D.5 Test 10-11 Setup 135

 D.6 Test 12 Setup..... 136

 D.7 Test 13 Setup..... 138

 D.8 Tests 14-15 Setup..... 138

E. Analytical Model Calculations 141

F. Test Results..... 143

 F.1 Test 1 Data..... 143

 F.2 Test 2 Data..... 144

 F.3 Test 3 Data 145

 F.4 Test 4 Data 146

 F.5 Test 5 Data..... 147

 F.6 Test 6 Data..... 148

 F.7 Test 7 Data..... 149

 F.8 Test 8 Data..... 150

 F.9 Test 9 Data..... 151

 F.10 Test 10 Data..... 152

 F.11 Test 11 Data..... 153

 F.12 Test 12 Data..... 154

 F.13 Test 13 Data..... 155

 F.14 Test 14 Data..... 156

F.15 Test 15 Data.....	157
G. Thermocouple Build/Repair Procedure.....	158
H. Thermal Model Results.....	161
H.1 Additional Cooling Phase Simulation Results	161
H.2 Additional Cold Soak Phase Simulation Results	163
H.3 Additional Heating Phase Simulation Results	165
H.4 Additional Hot Soak Phase Simulation Results	167

LIST OF TABLES

Table	Page
1. ISO Standard 19683 Thermal Vacuum Test Parameters [8].....	8
2. Overview of Recommendations Made by Past Students [4, 18, 19].....	39
3. Blue TVAC Thermophysical Properties [21, 22, 23]	44
4. Blue TVAC Optical Properties [21].....	44
5. Discretization of the Blue TVAC Thermal Model.....	45
6. Thermal Vacuum Test Parameters.....	51
7. Purpose of Each Thermal Vacuum Test	52
8. Thermocouple Description and Locations During Testing.....	54
9. Empty Cooling Phase Temperature Comparison.....	72
10. Empty Cold Soak Temperature Comparison	75
11. Empty Heating Phase Temperature Comparison.....	78
12. Empty Hot Soak Temperature Comparison	81
13. Cooling Phase with Mass Model Temperature Comparison.....	92
14. Cold Soak with Mass Model Temperature Comparison	94
15. Heating Phase with Mass Model Temperature Comparison.....	97
16. Hot Soak with Mass Model Temperature Comparison.....	99
17. Thermal Uncertainty Margin for Empty Thermal Vacuum Simulations	102
18. Thermal Uncertainty Margin for Thermal Vacuum Simulations with Mass Model.....	103
19. Comparison of Chamber Pump Down Time.....	117

20. Thermocouple Application Equipment..... 120

LIST OF FIGURES

Figure	Page
1. Spacecraft Thermal Environment [7].....	4
2. Thermal Balance Test Profile [2].....	6
3. Thermal Cycle Test Profile [2]	6
4. Thermal Vacuum Test Profile [2]	7
5. Uniform Radiation Between Two Flat Parallel Plates	12
6. Two Flat Plates with a View Factor.....	13
7. Thermal Desktop Software Module Relationships [10].....	15
8. Schematic of the Blue TVAC	18
9. Wiring Diagram of Single Phase Induction Motor	20
10. Turbomolecular Pump Diagram	21
11. Turbo Pump Control Panel on Blue TVAC	21
12. Chamber Gauge (Left) and Line Gauge (Right) Locations	22
13. Vacuum Gauge Controller	23
14. Ion Gauge Illuminated	24
15. Platen Dimensions	25
16. Strip Heater Dimensions in Platen.....	25
17. LN ₂ Plumbing into Platen	26
18. Test Section within the Blue TVAC	27
19. Heat Strips Attached to Bottom of Platen.....	28

20. 35 Liter Dewar of LN ₂	29
21. LN ₂ Plumbing Diagram [4].....	30
22. LN ₂ Plumbing Through Chamber Door Shroud [4].....	31
23. PID Temperature Controller	32
24. General 12-Channel Temperature Recorder	34
25. 3U CubeSat Mass Model Dimensions	35
26. Project Methodology.....	41
27. Platen and Shroud Meshes	46
28. LN ₂ Plumbing Meshes Through Platen (Left) and On Shroud (Right).....	47
29. Chamber Door and Inner Cylinder Meshes	47
30. 3U CubeSat Mass Model Mesh	48
31. Model Interfaces Without the Test Article	48
32. Model Interfaces with the Test Article	49
33. Nondimensionalized Thermal Vacuum Test Profile.....	51
34. Thermocouple Application Method.....	53
35. Analytical Platen Temperature Calculations.....	57
36. Thermocouple Configuration on Platen for Test 3	58
37. Thermal Response of Platen During Test 3	59
38. External T Type Thermocouple Panel Jack with K Type Thermocouples	61
39. Omega Thermocouple Types [22]	62
40. Thermocouple Configuration on Platen for Test 12	63

41. Thermocouple Configuration on Copper Shroud for Test 12	64
42. Thermocouple Configuration on Door Shroud for Test 12.....	64
43. Thermal Response of Platen During Test 12	65
44. Thermal Response of Copper Shroud and Door Shroud During Test 12.....	66
45. Thermocouple Configuration for Test 13	67
46. Thermal Response of Platen During Test 13	68
47. Predicted Temperature of Platen After Empty Cooling Phase.....	70
48. Predicted Temperature of Shroud After Empty Cooling Phase	71
49. Predicted Temperature of Inner Cylinder and Door After Empty Cooling Phase	71
50. Predicted Temperature of Platen After Empty Cold Soak	73
51. Predicted Temperature of Shroud After Empty Cold Soak	74
52. Predicted Temperature of Inner Cylinder and Door After Empty Cold Soak.....	74
53. Predicted Temperature of Platen After Empty Heating Phase.....	76
54. Predicted Temperature of Shroud After Empty Heating Phase	77
55. Predicted Temperature of Inner Cylinder and Door After Empty Heating Phase	77
56. Predicted Temperature of Platen After Empty Hot Soak.....	79
57. Predicted Temperature of Shroud After Empty Hot Soak	80
58. Predicted Temperature of Inner Cylinder and Door After Empty Hot Soak	80
59. Thermocouple Configuration on Mass Model for Tests 14 and 15 (Right, Top and Bottom Sides).....	82
60. Thermocouple Configuration on Mass Model for Tests 14 and 15 (Left Side).....	83

61. Thermocouple Configuration on Platen for Tests 14 and 15	83
62. Thermal Response of Platen and Mass Model During Test 14.....	84
63. DAQ Thermocouple with Aluminum Tape Attached.....	87
64. Thermal Response of Platen and Mass Model During Test 15.....	88
65. Predicted Temperature of Platen After Cooling Phase with Mass Model	90
66. Predicted Temperature of Mass Model After Cooling Phase	91
67. Predicted Temperature of Platen After Cold Soak with Mass Model.....	93
68. Predicted Temperature of Mass Model After Cold Soak.....	93
69. Predicted Temperature of Platen After Heating Phase with Mass Model.....	95
70. Predicted Temperature of Mass Model After Heating Phase.....	96
71. Predicted Temperature of Platen After Hot Soak with Mass Model	98
72. Predicted Temperature of Mass Model After Hot Soak.....	98
73. Caudill Presentation Slide 15	122
74. Caudill Presentation Slide 16.....	123
75. Caudill Presentation Slide 17	123
76. Caudill Presentation Slide 18.....	124
77. Caudill Presentation Slide 19.....	124
78. Caudill Presentation Slide 20.....	125
79. Caudill Presentation Slide 21	125
80. Caudill Presentation Slide 22.....	126
81. Caudill and Diamond Slide 10.....	126

82. Caudill and Diamond Slide 11	127
83. Caudill and Diamond Slide 12.....	127
84. Tests 1-5 Thermocouple Configuration on Platen	128
85. Tests 1-5 Thermocouple Configuration in Chamber	129
86. Tests 1-5 Thermocouple Configuration on Door Shroud	129
87. Test 6 Thermocouple Configuration on Platen	130
88. Test 6 Thermocouple Configuration in Chamber	131
89. Test 6 Thermocouple Configuration on Door Shroud	131
90. Test 7 Thermocouple Configuration on Platen	132
91. Test 7 Thermocouple Configuration in Chamber	132
92. Test 7 Thermocouple Configuration on Door Shroud	133
93. Tests 8-9 Thermocouple Configuration on Platen	133
94. Tests 8-9 Thermocouple Configuration in Chamber	134
95. Tests 8-9 Thermocouple Configuration on Door Shroud	134
96. Tests 10-11 Thermocouple Configuration Mass Model (Right and Top).....	135
97. Tests 10-11 Thermocouple Configuration Mass Model (Bottom and Left)	135
98. Tests 10-11 Thermocouple Configuration on Platen	136
99. Test 12 Thermocouple Configuration on Platen	136
100. Test 12 Thermocouple Configuration in Chamber	137
101. Test 12 Thermocouple Configuration on Door Shroud	137
102. Test 13 Thermocouple Configuration on Platen	138

103. Tests 14-15 Thermocouple Configuration on Mass Model (Right and Top).....	138
104. Tests 14-15 Thermocouple Configuration on Mass Model (Bottom).....	139
105. Tests 14-15 Thermocouple Configuration on Mass Model (Left).....	139
106. Tests 14-15 Thermocouple Configuration on Platen	140
107. Thermocouple Data from Test 1	143
108. Thermocouple Data from Test 2	144
109. Thermocouple Data from Test 3	145
110. Thermocouple Data from Test 4	146
111. Thermocouple Data from Test 5	147
112. Thermocouple Data from Test 6	148
113. Thermocouple Data from Test 7	149
114. Thermocouple Data from Test 8	150
115. Thermocouple Data from Test 9	151
116. Thermocouple Data from Test 10	152
117. Thermocouple Data from Test 11	153
118. Thermocouple Data from Test 12	154
119. Thermocouple Data from Test 13	155
120. Thermocouple Data from Test 14	156
121. Thermocouple Data from Test 15	157
122. Screws on Back of Thermocouple Connector.....	158
123. Screws Inside Thermocouple Connector	158

124. Stripped Thermocouple Wires	159
125. Thermocouples positioned in Insulative Disk.....	159
126. Exposed Thermocouple Wires Positioned Between Probes and Plates	160
127. Assembled Thermocouple	160
128. Predicted Temperature of Shroud During Cooling Phase with Mass Model.....	161
129. Predicted Temperature of Door and Inner Cylinder During Cooling Phase with Mass Model.....	162
130. Predicted Temperature of Shroud During Cold Soak Phase with Mass Model.....	163
131. Predicted Temperature of Door and Inner Cylinder During Cold Soak Phase with Mass Model.....	164
132. Predicted Temperature of Shroud During Heating Phase with Mass Model	165
133. Predicted Temperature of Door and Inner Cylinder During Heating Phase with Mass Model.....	166
134. Predicted Temperature of Shroud During Hot Soak Phase with Mass Model.....	167
135. Predicted Temperature of Door and Inner Cylinder During Hot Soak Phase with Mass Model.....	168

LIST OF ACRONYMS

CAD	Computer Aided Design
DAQ	Data Acquisition
ECSS	European Cooperation for Space Standardization
FDM	Finite Difference Model
FEM	Finite Element Model
FLUINT	Fluid Integrator
GEVS	General Environmental Verification Standard
IR	Infrared
ISO	International Standards Organization
LEO	Low Earth Orbit
LN ₂	Liquid Nitrogen
PID	Proportional-Integral-Derivative
RMF	Rotating Magnetic Fields
RPM	Revolution per Minute
SD	Secure Digital
SINDA	Systems Improved Numerical Differencing Analyzer
TC	Thermocouple
TD	Thermal Desktop
TVAC	Thermal Vacuum Chamber

Chapter 1

INTRODUCTION

1.1 Thesis Overview

This chapter serves as an introduction to this thesis project as well as the various thermal testing methods used for spacecraft systems and subsystems. Chapter 2 provides a technical background to the concepts and tools used for the analytical aspects of the project. In Chapter 3, relevant information about the experimental apparatus used is presented. The previous work conducted on the Blue TVAC as well as the gaps in this past work that motivated this thesis project are described in Chapter 4. The methodology of the modeling and testing involved for this project is discussed in Chapter 5. The thermal vacuum test results and associated simulation results are presented in Chapter 6. The conclusions made from testing and modeling are discussed in Chapter 7 and recommendations for future work with the Blue TVAC are made in Chapter 8.

1.2 Thesis Statement

Spacecraft design involves an iterative process of analysis, design, and testing [1]. During its lifetime, a spacecraft will experience temperature fluctuations as a result of heat transfer from both environmental and internal sources [2]. Each component on a spacecraft operates most efficiently within a specific temperature range defined by the component manufacturer specifications. A spacecraft shall be designed to maintain these temperatures despite the varying thermal environment [2]. A TVAC is a machine that simulates both the thermal environment and vacuum environment of space. By mechanically pumping the ambient air out of the chamber, the vacuum environment of space is simulated. While in orbit around Earth, or elsewhere, a spacecraft will experience periods of time in sunlight and in eclipse. The varying amounts of incident sunlight and other heat loads on the spacecraft result in cyclical temperature changes that can also be simulated in a TVAC with heating and cooling systems. With a TVAC, various types of thermal tests are conducted to verify and validate that the spacecraft operates as expected in the

space environment and that all components maintain operational temperatures [3]. For TVAC tests to be validated, it is important that the heating and cooling processes of the chamber are understood and analyzed. The required inputs such as duration of testing, component heat dissipation, and radiative environments must be determined before conducting thermal vacuum testing. Furthermore, the TVAC must also operate in a way that produces repeatable results.

The Blue TVAC at Cal Poly has the potential to be used for educational and research purposes [4]. For this thesis project, the thermal response of the chamber is measured and modeled to determine the repeatability and performance of thermal vacuum tests conducted with this chamber. This is done to validate the chamber's performances and ensure repeatable testing. Moreover, this thesis provides recommendations for improving the performance of the chamber and increasing the validity of thermal vacuum tests and simulations with the thermal model.

1.3 Space Environment

A spacecraft must be designed to operate in the space environment, which is significantly different than the familiar environment on Earth. The general space environment includes, but is not limited to, the vacuum environment, thermal environment, particulate environment, and plasma environment [2]. Each of these environments pose unique design challenges for a spacecraft to perform as required throughout its lifetime. Extensive design, analysis, and testing must be conducted on Earth to verify and validate the spacecraft performance before it is launched [1].

In a low Earth orbit (LEO) of altitudes less than 2,000 km above the surface of Earth, the pressure of the ambient air is approximately 10^{-8} Pa which is twelve orders of magnitude less than the pressure of ambient air at sea level on Earth [5]. This is because air pressure decreases as altitude increases. Since pressures are so low in space relative to on Earth, the physical properties of the surrounding air are different, such as the thermal conductivity, electrical conductivity, sound propagation, and optical transmission and absorption. The vacuum environment is also

responsible for the phenomena of outgassing from a spacecraft which is the process that occurs when molecules of a solid material are spontaneously released due to the lack of surrounding pressure holding the particles to the material [6].

In a vacuum environment, heat transfer is different than on the surface of Earth as there are few to no particle collisions to transfer heat via convection. The primary mode of heat transfer from the space environment to the spacecraft is radiation, which is the process by which electromagnetic waves are emitted from one source and absorbed by another [2]. These electromagnetic waves carry energy that causes the emitting surface to cool and the absorbing surface to heat. The secondary mode of heat transfer in the space environment is conduction. The heat absorbed from environmental factors as well as the heat generated from internal components of the spacecraft is conducted throughout the spacecraft and eventually reemitted as infrared (IR) radiation.

The thermal environment of a spacecraft in orbit around Earth includes the environmental heating from various sources including, but not limited to, direct solar radiation, infrared (IR) radiation from the Earth, and albedo radiation from Earth [2]. The internal heat generated by components on a spacecraft also contributes to the thermal response of the spacecraft while in orbit as this heat is conducted to other components and emitted to space [2]. Figure 1 shows a visual representation of the thermal environment that a spacecraft is exposed to while in orbit.

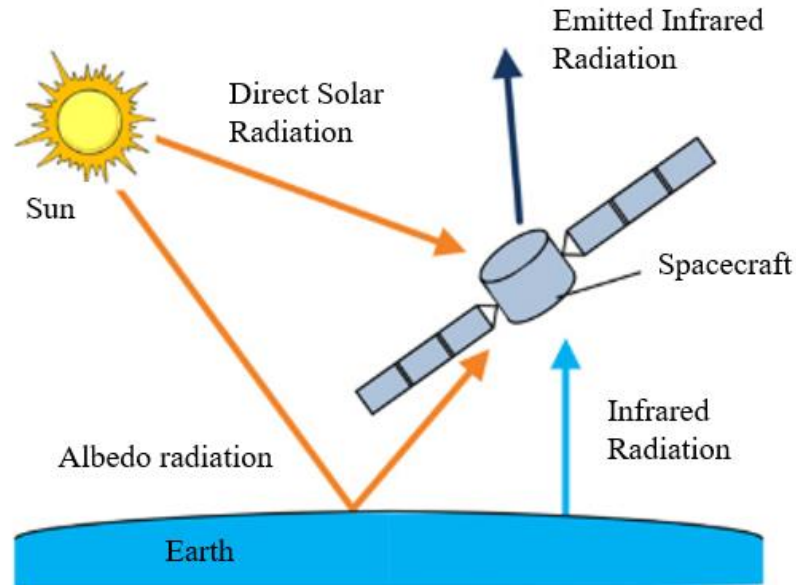


Figure 1: Spacecraft Thermal Environment [7]

Direct solar radiation is the incident electromagnetic radiation on a spacecraft surface from the sun. Solar radiation that is absorbed by a planetary body is reemitted as IR radiation [2]. This IR radiation can then be absorbed by a spacecraft. Solar radiation is also reflected by planetary bodies. This reflected sunlight is known as albedo, which can then be absorbed by a spacecraft. The magnitudes of these heat inputs to a spacecraft depend on its orbital parameters and physical properties. This thermal environment can be predicted and used for thermal analysis and testing of a spacecraft.

1.4 Thermal Modeling

Prior to manufacturing and testing flight hardware, a thermal model of a spacecraft system or subsystem is developed to conduct low-cost and repeatable thermal simulations [2]. A thermal model is a tool that makes numerical approximations to problems that have complex, coupled, and non-linear partial differential equations of integral equations with no direct solution. Once the power dissipation, structural design, mission phases, and orbital parameters of the spacecraft are known, a thermal model will make an estimation of the temperature response using

numerical approximation methods such as finite element method or finite difference method. A thermal model is developed early in the spacecraft project and it is continuously updated as design decisions are made. Once the design and model are complete, thermal testing is conducted to verify the results of the model predictions. If needed, the model is then refined to more accurately predict the results of the test. Once the spacecraft is launched, the thermal model can be used to analyze the causes and corrective actions needed for any anomalies that may occur during the mission [2]. In general, thermal models provide engineers an adaptable tool to analyze and predict the temperature response of a spacecraft system or subsystem.

1.5 Thermal Testing

To ensure mission success, space programs commonly conduct thermal balance tests, thermal cycle tests, and thermal vacuum tests [2]. A TVAC is used to simulate the vacuum environment of space as well as the expected heat loads on the spacecraft during its various mission phases. Heating sources and cryogenic cooling systems are implemented to simulate these heat fluxes. The Blue TVAC can be used to perform the thermal tests as described in the subsequent sections.

1.5.1 Thermal Balance Test

A thermal balance test simulates the hot and cold temperature conditions to verify the thermal subsystem and the correlation of the analytic thermal model of the system. Figure 2 shows a general nondimensionalized profile of a thermal balance test.

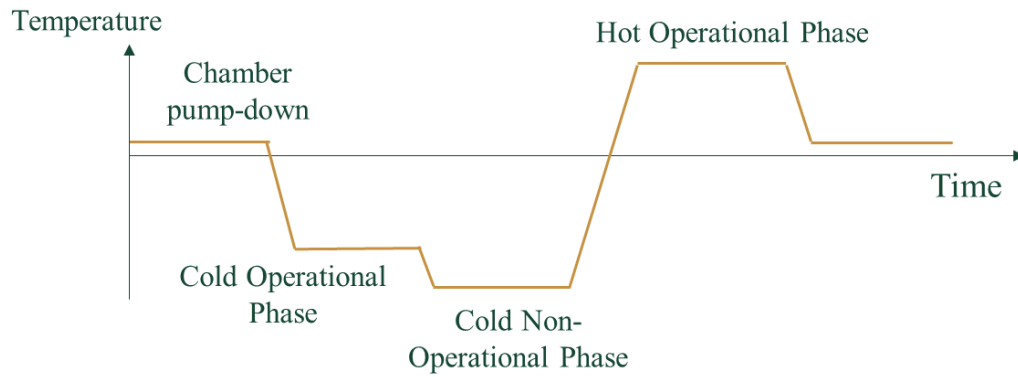


Figure 2: Thermal Balance Test Profile [2]

Dedicated test phases simulate flight conditions to gather steady-state temperature data that is compared to the model predictions [2]. It is critical that the spacecraft maintains an equilibrium or quasi-equilibrium temperature state during the thermal balance test because even a slight rate of change of temperature can accumulate over time and result in temperatures that exceed the tolerated ranges.

1.5.2 Thermal Cycle Test

A thermal cycle test subjects a test article to a number of cycles of hot and cold temperature plateaus in an ambient or gaseous Nitrogen environment. Figure 3 shows a general nondimensionalized profile of a thermal cycle test.

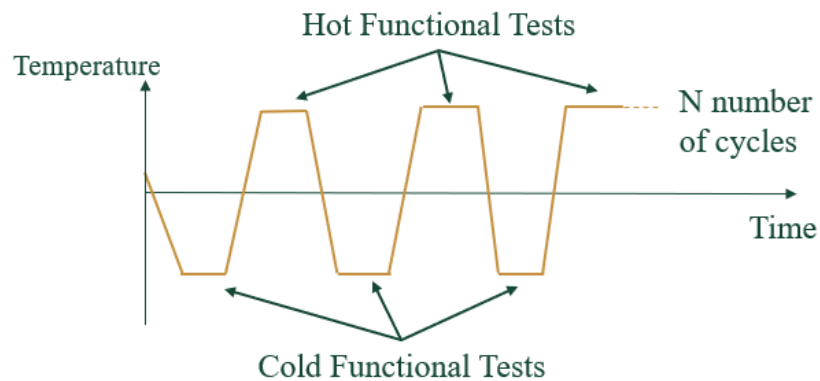


Figure 3: Thermal Cycle Test Profile [2]

The plateaus of hot and cold temperatures are hereafter referred to as soaks. The primary objective of a thermal cycle test is to serve as an environmental stress screen by revealing material defects and workmanship flaws [2]. Functional tests can be performed at the hot and cold plateaus to verify performance as a secondary objective of a thermal cycle test [2].

1.5.3 Thermal Vacuum Test

A thermal vacuum test subjects a test article to cycles of hot and cold temperature plateaus in a vacuum environment. Figure 4 shows a general profile of a thermal vacuum test.

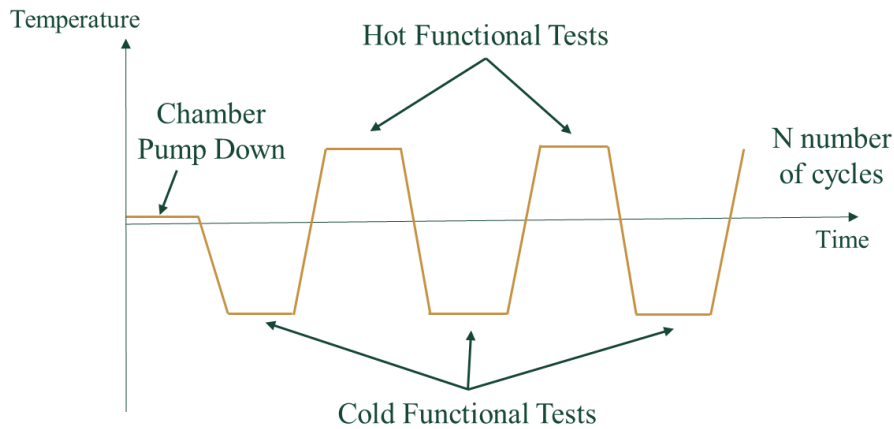


Figure 4: Thermal Vacuum Test Profile [2]

This test is most similar to the actual flight environment as radiative and conductive heat transfer dominates due to the lack of convection. A thermal vacuum test is intended to verify test article performance with functional testing [2]. The testing parameters such as the number of cycles and temperature ranges of a thermal vacuum test depend on what type of test is being conducted. A qualification test is conducted on hardware that is not flown while an acceptance test is conducted on flight hardware and requires smaller temperature margins than a qualification test [2]. A qualification test will subject hardware to temperatures approximately 5-10 degrees higher and lower than the maximum and minimum acceptance test temperatures [2]. The thermal vacuum

test is often the last test conducted in the verification process of the thermal subsystem of a spacecraft.

1.6 ISO Standard 19683

To ensure repeatable and valid tests are conducted by space programs, standards are developed to provide baseline testing parameters. The International Standards Organization (ISO) Standard 19683 is a reference used for various environmental testing of small spacecraft [8]. Other testing standards such as the NASA General Environmental Verification Standard (GEVS) and U.S. Military Standards are also used in industry. The ISO Standard 19683 is referenced for this thesis project because the Blue TVAC will potentially be used for testing of CubeSats and other small spacecraft test articles. Within the ISO Standard 19683, there is a section that provides test parameters for thermal vacuum tests. Table 1 shows the values that were referenced as a guideline for the tests conducted with the Blue TVAC for this thesis project.

Table 1: ISO Standard 19683 Thermal Vacuum Test Parameters [8]

Temperature Range	-15°C to 50°C
Number of Cycles	2 or more
Thermal Dwell	1 hour or longer
Tolerance Limit	3°C
Temperature Ramp Rate	+5°C/min or slower -5°C/min or slower
Chamber Pressure	1.0×10^{-3} Pa or lower ($\sim 7.5 \times 10^{-6}$ Torr)

According to the ISO Standard 19683, a thermal vacuum test is conducted with at least two cycles of hot and cold soaks within the temperature range of -15°C and 50°C. The minimum and maximum temperatures are to be maintained for at least one hour with a tolerance of 3°C. Between the hot and cold soaks, the temperature shall change at a rate of 5 °C/min or slower. The

chamber pressure must be lower than 1.0×10^{-3} Pa or approximately 7.5×10^{-6} Torr. The testing parameters as defined in ISO Standard 19683 were used for the tests conducted for this thesis project. The only testing parameter not followed was the chamber pressure as the lowest achievable pressure in the Blue TVAC was approximately 10^{-5} Torr. The root cause analysis for this discrepancy is provided in Appendix A.

Chapter 2

TECHNICAL BACKGROUND

2.1 Heat Transfer

Heat transfer is the transfer of energy in a closed system that cannot be categorized as work. There are three modes of heat transfer that occur in nature: convection, conduction, radiation. Convection involves the combined effect of conduction and advection. It is the transfer of heat through a fluid that is caused by molecular motion. In the vacuum environment, particles of ambient air are so sparse that convective heat transfer is negligible [2]. With the Blue TVAC, convective heat transfer occurs between the cryogenic fluid and the pipes that it flows through, but for modeling purposes, the cryogenic fluid in the chamber is modeled as surfaces of the pipes with constant temperatures due to the high heat transfer coefficient of the Liquid Nitrogen (LN₂) that is used. This eliminates the need for convective computational tasks while maintaining the thermal uncertainty and efficiency of the model. For these reasons, radiative and conductive heat transfer are the primary focus for the scope of this thesis.

Radiation is defined as the transfer of energy by means of photons in electromagnetic waves. Photons carry the energy from a relatively hot surface to a relatively colder surface. The amount of energy that a photon carries depends on its wavelength as shown in Eq. 1.

$$E = \frac{hc}{\lambda} \quad (\text{Eq. 1})$$

where E is the photon energy [J], h is the Planck constant [J-s], c is the speed of light in vacuum [m/s] and λ is the wavelength of the photon [m]. Photons with wavelengths in the infrared and visible wavelength ranges are the most prevalent in space and therefore transfer the majority of heat to a spacecraft. Incident radiation onto a surface is either reflected from the surface, absorbed by the surface material, or transmitted through the material completely [9]. The proportion of incident radiation reflected from a surface depends on the reflectance of the surface material. The

proportion of incident radiation that is absorbed by the surface depends on the absorptance of the surface material. The absorbed radiation can then be reemitted from a surface primarily as infrared radiation. The proportion of radiation a surface will emit depends on the emittance of the material. Finally, the proportion of incident radiation that is completely transmitted through a material depends on the transmittance of the material.

The amount of heat that is radiated from a surface is quantified by the Stefan-Boltzmann Law, which is shown in Eq. 2

$$q = \varepsilon\sigma AT^4 \quad (\text{Eq. 2})$$

where q is the rate of energy is emitted [W], ε is the emissivity of the radiating surface [-], σ is the Stefan-Boltzmann constant [W/m²-K⁴], A is the area of the radiating surface [m²], and T is the absolute temperature of the radiating surface [K]. For uniform radiative heat transfer between two surfaces, i and j , the equation is shown in Eq. 3.

$$q_{net} = \varepsilon\sigma A_i(T_i^4 - T_j^4) \quad (\text{Eq. 3})$$

where q_{net} is the total rate of energy transferred from surface i to surface j [W], ε is the emissivity of surface i [-], A_i is the area of surface i [m²], T_i is the temperature of surface i [K] and T_j is the temperature of surface j [K]. This equation assumes that all the energy radiated from one surface is incident on the other surface [9]. Uniform radiation between two parallel flat plates is shown in Figure 5 to show a scenario when this equation would be used.

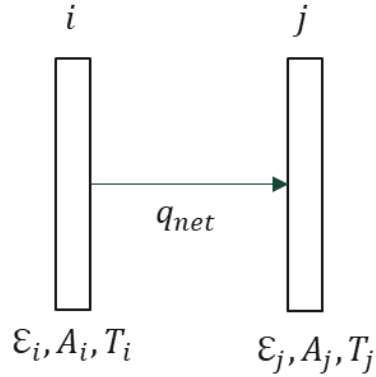


Figure 5: Uniform Radiation Between Two Flat Parallel Plates

In reality, the amount of energy incident on one surface depends on its orientation to the other surface. The orientation of two surfaces with respect to each other is accounted for by a view factor, which is the proportion of radiation which leaves one surface and strikes another. The view factor is dependent on the angle between the normal of each surface and the distance between each surface as shown in Eq. 4

$$F_{i \rightarrow j} = \frac{1}{A_i} \int_{A_i} \left(\int_{A_j} \frac{\cos \theta_i \cos \theta_j}{\pi s^2} dA_j \right) dA_i \quad (\text{Eq. 4})$$

where $F_{i \rightarrow j}$ is the view factor from a general surface i to a general surface j [-], A_i and A_j are the respective areas of surface i and surface j [m^2], θ_i and θ_j are the respective angles between the surface normals and a ray between the two differential surface [radians], and s is the distance between each differential surface [m]. These parameters are shown below in Figure 6 for two flat plates. For this situation, the view factor must be included in the radiation calculation.

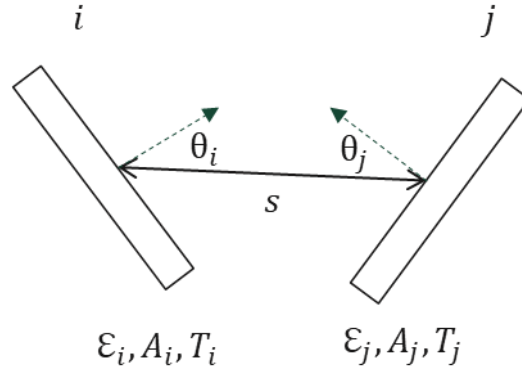


Figure 6: Two Flat Plates with a View Factor

The total rate of energy transferred from surface i to surface j for uniform radiation when the view factor, $F_{i \rightarrow j}$ is accounted for is shown in Eq. 5.

$$q_{net} = \epsilon \sigma A_i F_{i \rightarrow j} (T_i^4 - T_j^4) \quad (\text{Eq. 5})$$

In application, the view factor between surfaces may be continuously changing and complex for hand calculations. For these reasons, numerical approximations are used to calculate radiative heat exchange between surfaces.

Conductive heat transfer is defined as the transfer of energy through direct particle collisions. In conduction, heat flows within and through a body itself as opposed to thermal radiation where heat is transferred between bodies that may be separated spatially. How easily heat flows through a material is defined by the thermal conductivity of the material. The inverse of the thermal conductivity is the thermal resistivity, which is a measure of how well a material prevents heat flow. Fourier's law states that for conduction, the rate of heat transfer through a material is proportional to the negative gradient in the temperature and to the area, at right angles to that gradient, through which the heat flows. In differential form, for a homogeneous material of 1-D geometry between two endpoints at constant temperature, the heat flow can be calculate as shown in Eq. 6

$$\frac{Q_x}{dt} = -kA \frac{dT}{dx} \quad (\text{Eq. 6})$$

where $\frac{Q_x}{dt}$ is the rate of heat transfer in the x-direction [W], k is the thermal conductivity of the material [W/m-K], A is the cross-sectional area [m²], and $\frac{dT}{dx}$ is the temperature change in the x direction [K/m]. In practice, this equation is not useful for complex thermal analysis because it does not account for heat transfer in multiple dimensions or for transient analysis. Computational iterative methods are used to solve for conductive heat transfer in multiple dimensions and for transient analysis [9].

2.2 Thermal Desktop

When analytic solutions to real life problems do not exist, numerical approximations are used to obtain a solution. Systems of complex geometries and/or physical properties can be simplified and discretized to create a system that can be solved with the numerical methods. The thermal modeling process involves the following steps:

- Discretizing the system into nodes
- Determining the system material properties and geometries
- Defining subsystem interfaces
- Applying heat loads to surfaces
- Defining boundary conditions and initial conditions of the system
- Specifying a steady state analysis or the time for a transient analysis
- Iterating to converge on an approximate solution

As the number of defined parameters increases, the thermal uncertainty of the model approximation increases, but the computation time also increases. This poses a trade-off that must be made between model thermal uncertainty and computational time. A thermal model is a tool for predicting the temperature response of a system when various parameters are changed.

Resources are conserved because the system does not need to be manufactured and tested for these predictions to be made. Various software exist to perform these computational tasks.

Thermal Desktop is a software product from C&R Technologies that is used for this thesis project due to its prevalence in the Aerospace Industry and its efficiency in calculating radiation models. Thermal Desktop is an overlay of AutoCAD, which is a software used to create 2-D and 3-D drawings [10]. Thermal Desktop is used to calculate dimensions, material properties, and distances between surfaces. Thermal Desktop uses two subset modules for additional calculations. RadCAD is used to calculate the radiation heat exchange between surfaces while FloCAD is used to create flow networks and calculate convective heat transfer [10]. The data from Thermal Desktop, RadCAD, and FloCAD is then passed to the SINDA/FLUINT solver to calculate the temperature changes of the defined discretized nodes [10]. Figure 7 shows what the Thermal Desktop modules are used for and how they interact with each other.

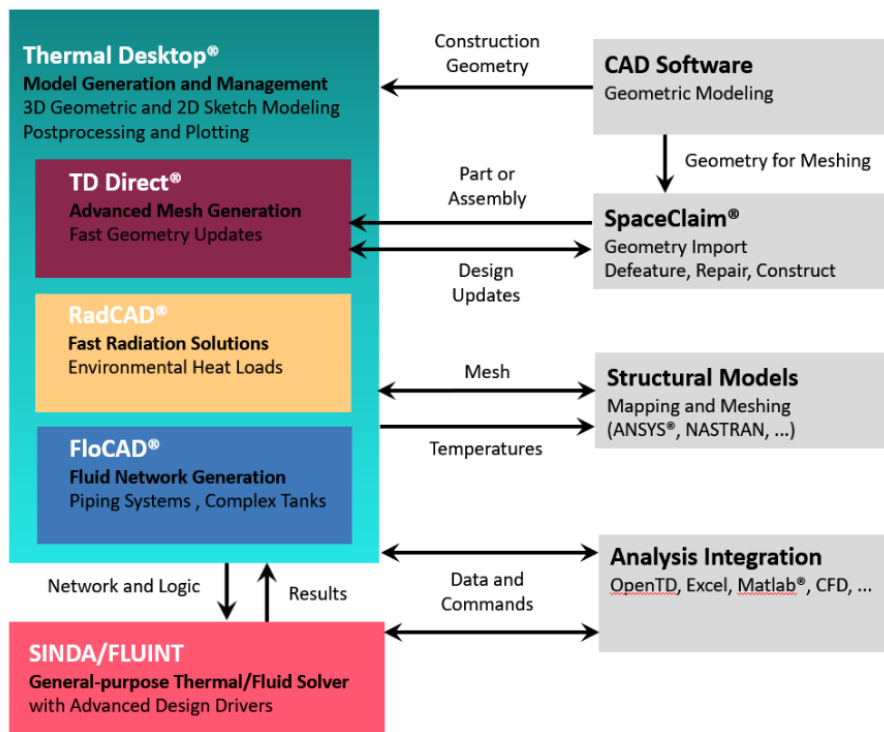


Figure 7: Thermal Desktop Software Module Relationships [10]

The SINDA produces network solutions, where a network represents finite element models (FEMs), finite difference models (FDMs), or a combination of both. The network is composed of finite volume discretizations called nodes. This is to allow the heat equation to be discretized and solved numerically.

Thermal Desktop allows users to define a node in three different ways:

- Diffusion node
- Arithmetic node
- Boundary node

A diffusion node represents a normal material with a finite thermal mass that changes temperature as a result of heat flow into or out of the node. An arithmetic node has zero thermal mass and responds instantly to its surroundings. This is not physically possible but may be useful for modelling certain system features like vapor, which is not relevant to this thesis. A boundary node represents a boundary or sink with a fixed temperature. For each node, the thermophysical and optical properties must be defined, if applicable.

After discretizing the system into nodes, the user must define the interfaces between the nodes. Contactors represent the physical connections between nodes that allow for conductive heat transfer.

The radiative heat transfer is defined by the user with Radiation Analysis Groups, which allow the user to define which nodes are exchanging heat via radiation. Once the interfaces between nodes are defined, the heat loads on the nodes are defined. A node can also be defined as a heat source or “heater” which outputs a defined amount of heat power to the nodes it interfaces with. If a negative amount of power is defined, the “heater” can alternatively be modeled as a “cooler” in the system [10].

Once the system is fully defined, a simulation can be run as a steady-state or transient analysis. A steady-state analysis solves the system for the state that is established when thermal equilibrium is achieved. The transient analysis solves the system for increments of time between the start and end of a certain amount of time. The user defines both the duration of the transient analysis and the increments of time that are analyzed for the transient analysis. The transient analysis method was used for this thesis project to approximate the temperature in the Blue TVAC during heating and cooling phases as well as during the hot and cold soak phases of a thermal vacuum test.

Chapter 3

EXPERIMENTAL APPARATUS

3.1 Overview of the System

The Blue TVAC was used for every experiment for this thesis project. This chamber was originally used by MDA Corporation in the development of the Mars exploration rover's robotic arm. Since its donation to the Cal Poly Space Environments lab in 2017, it has been refurbished and modified to improve its performance [4]. This section will describe the current components of the chamber to provide a deeper understanding as to how the experiments were conducted for this thesis project. A detailed description for how to operate the Blue TVAC and each subsystem is provided in [11].

3.2 Thermal Vacuum Chamber

The Blue TVAC consists of various components that allow for the vacuum and thermal environments of space to be simulated and measured. Figure 8 shows the general schematic of the chamber with the most critical components included.

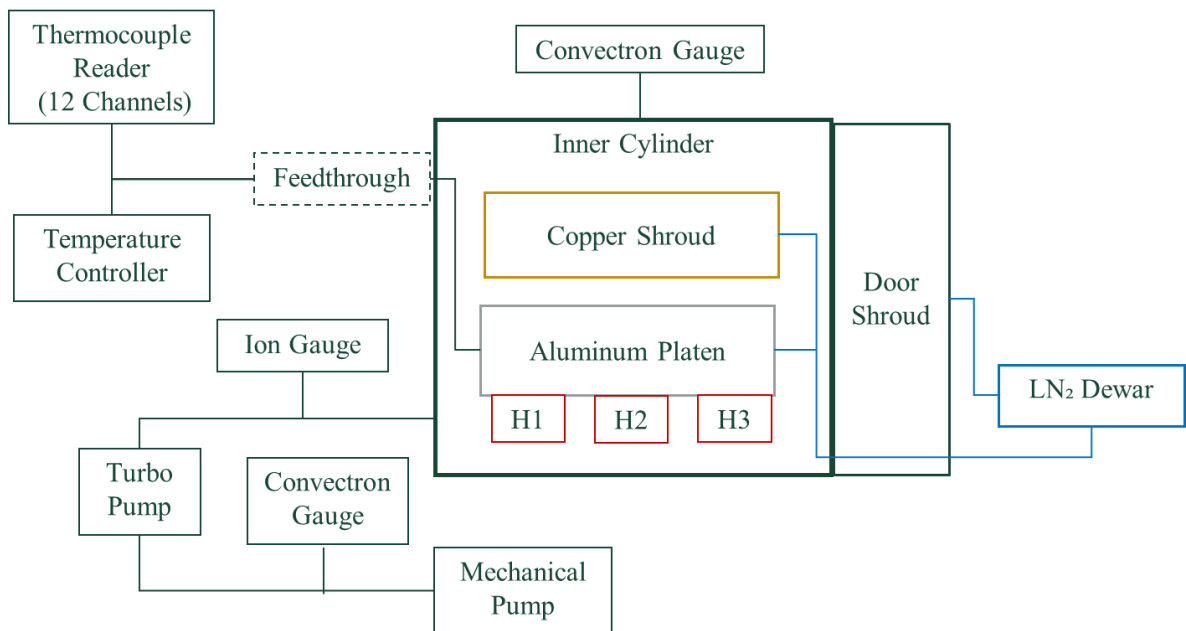


Figure 8: Schematic of the Blue TVAC

Note that in Figure 8, each of the three heaters are referred to as H1, H2, and H3. The following descriptions of the components involved are the most up to date as of June 2020 and all chamber descriptions provided in documentation prior to June 2020 are no longer relevant.

3.2.1 Vacuum System

The vacuum environment within the Blue TVAC is established by the operation of two different pumps, one mechanical pump and one turbo pump. Together, these pumps allow pressures as low as 16×10^{-5} Torr in the chamber. The mechanical pump is a Galiso Inc. single phase induction motor. The main components of an induction motor are a rotor, a main winding, an auxiliary winding that is placed perpendicular to the main winding, and a capacitor that is connected to the auxiliary winding. When AC current flows through the main winding, a fluctuating magnetic field is created in equal and opposite directions, so the auxiliary winding and capacitor are needed to start the rotation of the rotor. The auxiliary winding and capacitor are used to produce two additional equal and opposite magnetic fields. One of these cancels with one of the main winding rotating magnetic fields (RMF) while the other adds to one of the main RMFs. This provides the starting torque to the rotor and allows the motor to continue to rotate. Figure 9 shows the circuit diagram of this type of pump.

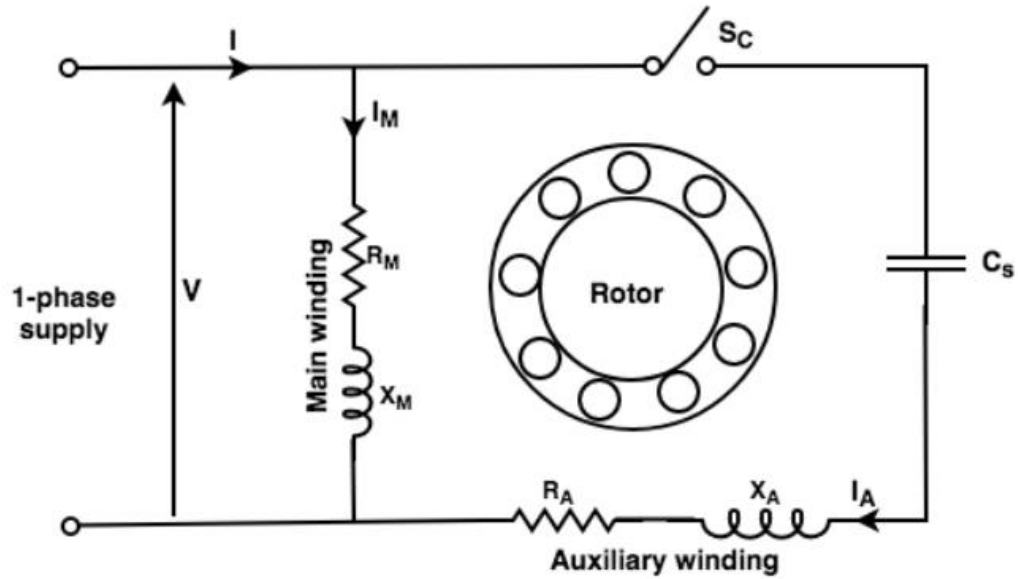


Figure 9: Wiring Diagram of Single Phase Induction Motor

The rotation of the rotor creates a pressure differential and air with higher pressure in the chamber moves to the space of lower pressure air in the motor. When the mechanical pump brings the chamber pressure below 50×10^{-3} Torr, the turbo pump can be activated to achieve much lower chamber pressures.

The turbo pump used is a Leybold Turbovac 151 turbomolecular pump that is designed for low vacuum use. The turbo pump consists of stacks of rotor blades and stationary blades that captures gas and compresses it as it moves through the pump and into the mechanical pump line [12]. Figure 10 shows a diagram of how this pump works.

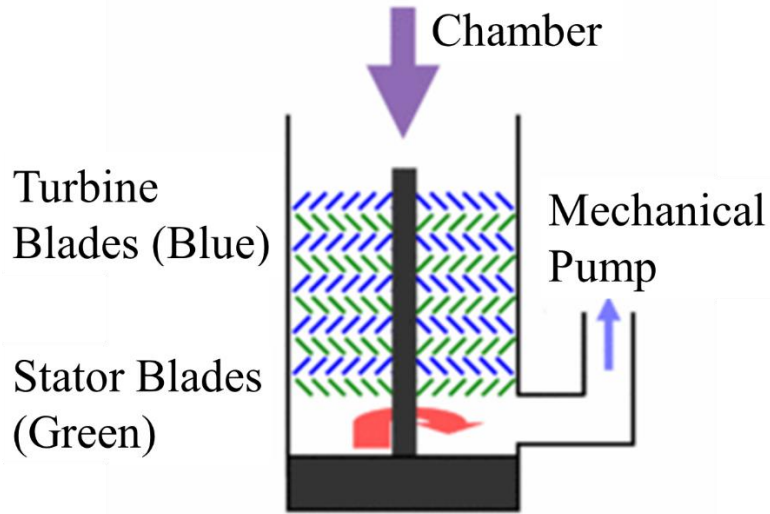


Figure 10: Turbomolecular Pump Diagram

With the turbo pump in use, the chamber currently reaches pressures of approximately 16×10^{-5} Torr after at least four hours of operation. The chamber pressure does not reach pressures below this value even after over eight hours of operation. Note that this pressure is higher than that required by the ISO Standard 19683 for thermal vacuum tests. The potential root causes for this discrepancy are discussed in Appendix A. On the right side of the chamber there is a control panel for the turbo pump, which is shown in Figure 11.



Figure 11: Turbo Pump Control Panel on Blue TVAC

The diagonal bars that are stacked above the Start button represent the increasing pressure load on the pump during operation [12].

3.2.2 Convectron Gauges

There are two Granville-Phillips convectron gauges used to measure pressures in the Blue TVAC. Figure 12 shows a diagram of where they are located.

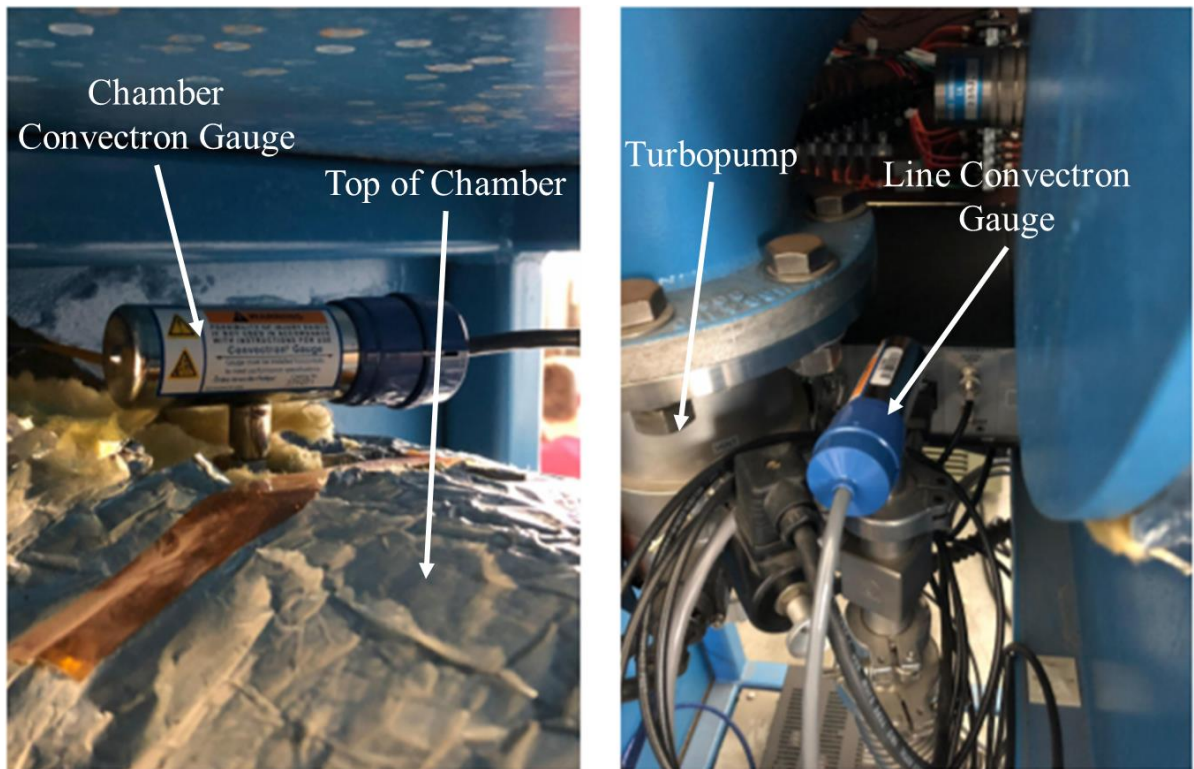


Figure 12: Chamber Gauge (Left) and Line Gauge (Right) Locations

The image on the left shows the gauge used to measure the pressure in the chamber while the image on the right shows the gauge used to measure the pressure in the pumping line after the turbo pump and before the mechanical pump. The convectron gauges display the pressure measurements to the Granville-Phillips 307 Vacuum Gauge controller that is located on the right side panel of the Blue TVAC and shown in Figure 13.



Figure 13: Vacuum Gauge Controller

Line A displays the pumping line pressure reading while line B displays the chamber pressure reading. The pressures displayed are in the unit of Torr with three significant figures included. For example, the atmospheric pressure is displayed as 7.60 +02, which is 760 Torr. The convector gauge only measures the chamber pressure when it is above 1×10^{-4} Torr, below which the display will show only zeros and the ion gauge must be activated to measure the low chamber pressures [13].

3.2.3 Ion Gauge

The Granville-Phillips ion gauge is used to measure pressures below 1×10^{-3} Torr in the chamber. It does so by detecting the individual ions in the chamber. When activated, the chamber pressure measured by the ion gauge will be displayed on the top line of the vacuum gauge controller display labeled IG in Figure 13 [13]. The ion gauge itself will be illuminated when in use as shown in Figure 14.



Figure 14: Ion Gauge Illuminated

3.2.4 Platen

The rectangular platen in the Blue TVAC is made of aluminum and serves as the test section for experiments. The platen is stationary and has no mechanisms for changing its orientation within the chamber. The platen extends about 61 cm into the chamber, it is about 36 cm wide and about 4 cm thick. The dimensions of the platen are shown in Figure 15.

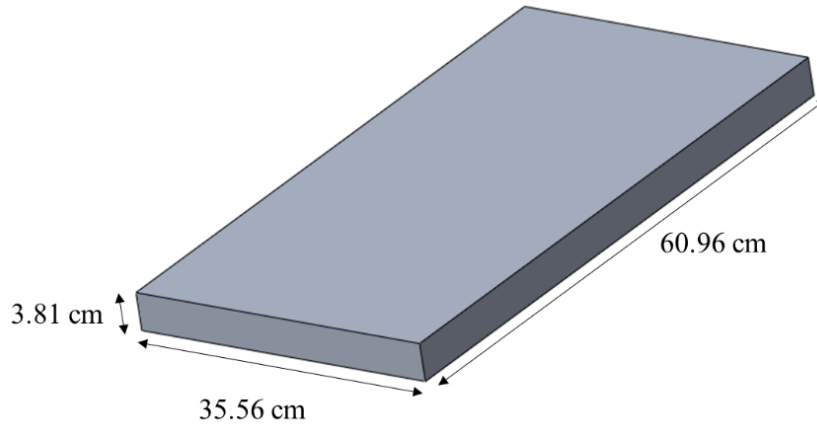


Figure 15: Platen Dimensions

On the bottom side of the platen, three strip heaters are secured in cutouts evenly spaced by about 16 cm. The strip heaters are approximately 25 cm wide and 4 cm long. The dimensions of the heat strips on the bottom side of the platen are shown in Figure 16. The heating system will be described in further detail in Section 3.2.6 Heating System.

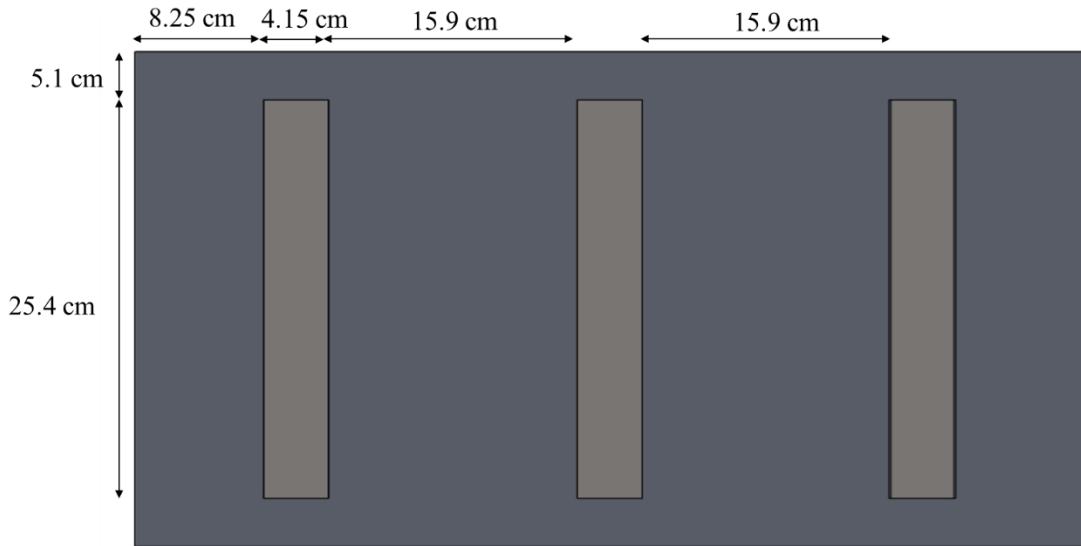


Figure 16: Strip Heater Dimensions in Platen

Plumbing for the cooling system also runs through the platen, although the exact geometry of the plumbing within the platen is currently unknown. The LN₂ flows through these

pipes and cools the platen during tests. Only the inlet and outlet locations of the plumbing are currently known and are shown in Figure 17. The cooling system will be described further in Section 3.2.7 Cooling System.

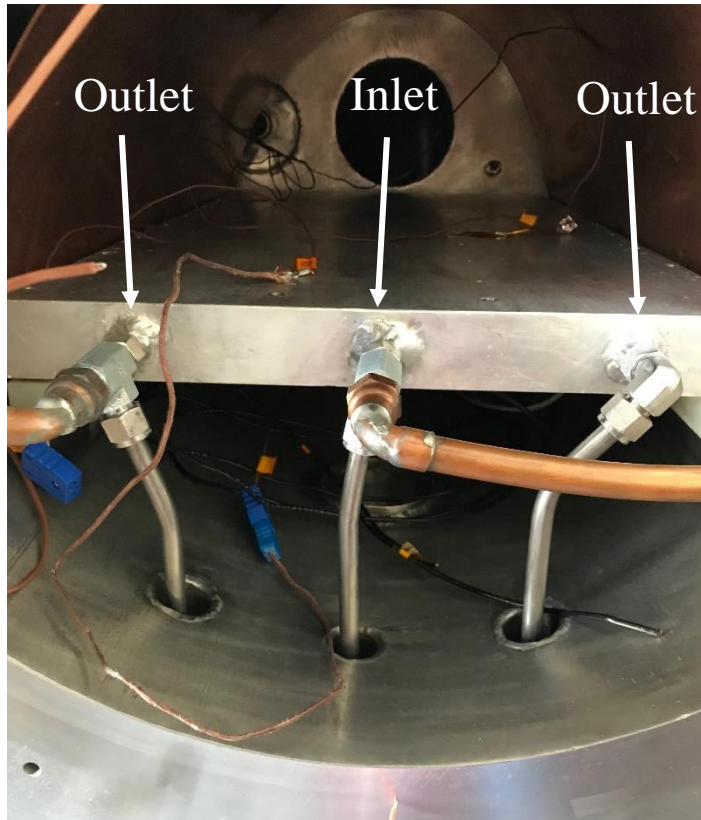


Figure 17: LN₂ Plumbing into Platen

3.2.5 Shroud

A semi cylindrical shroud made of copper extends about 61 cm into the chamber and about 18 cm above the platen surface. The copper shroud is stationary and there is no mechanism for moving it from its current position. The shroud and platen form an area of space in which the test article is subjected to the simulated environment of space. This test volume is approximately 0.121 m³ in volume. An image of the test section in the chamber is shown in Figure 18.

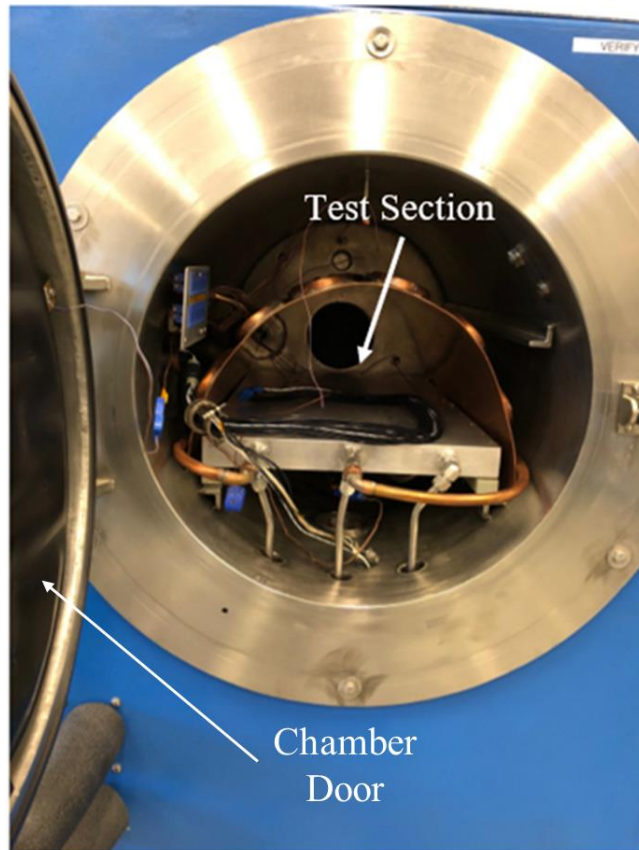


Figure 18: Test Section within the Blue TVAC

There is also LN₂ plumbing that is welded to the top surface of the copper shroud to cool the shroud during experiments. This is to increase the efficiency of cooling the chamber test section. This will be discussed in more detail in Section 3.2.7 Cooling System.

3.2.6 Heating System

There are three Ogden 475 Watt resistive heat strips located below the aluminum platen that conduct heat to the platen, which then radiates heat to the surrounding test section. The locations of each heat strip under the platen are shown in Figure 16. Each heater is attached to the platen with screws of unknown material as shown in Figure 19 below. A small rectangular plate separates the screw heads from the strip heaters.

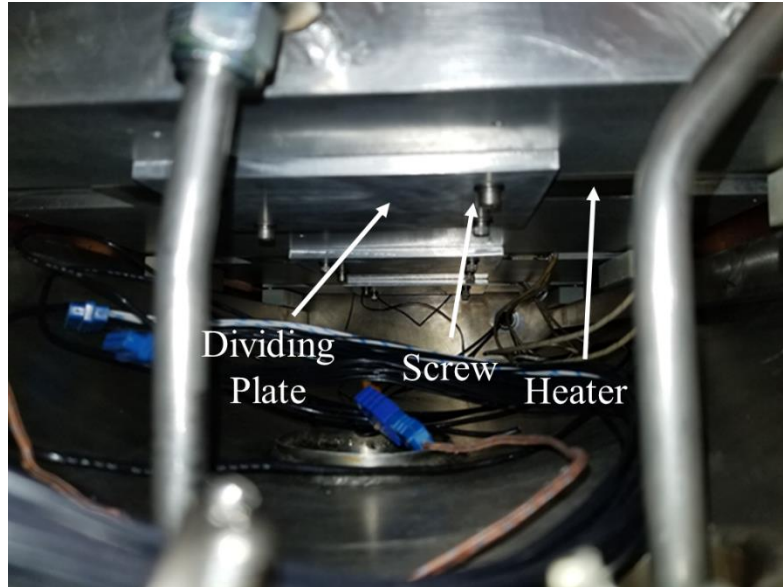


Figure 19: Heat Strips Attached to Bottom of Platen

The Proportional-Integral-Derivative (PID) temperature controller determines the amount of power that is output to each heat strip based on the current temperature of the top surface of the platen. It is important to note that the temperature of the platen is the controlled parameter during heating and cooling of the chamber. A percentage of the total possible power output to the heat strips is displayed on the PID temperature controller screen.

3.2.7 Cooling System

There is a LN₂ cooling system that allows the cryogenic LN₂ to flow across the copper shroud and through the aluminum platen and chamber door shroud. Heat from the chamber is conducted to the LN₂ and removed from the chamber via the exhaust gaseous Nitrogen. The LN₂ is stored in a 35 liter dewar that is stationed next to the chamber and shown in Figure 20.



Figure 20: 35 Liter Dewar of LN₂

This dewar has a liquid withdrawal device that consists of a hose that extends from the top of the dewar to the bottom of it. When the liquid valve at the top of the dewar is manually opened, the back pressure from the Nitrogen in the tank pushes LN₂ from the bottom of the dewar through the hose, through the dewar valve and eventually into the chamber plumbing system. The flow rate from the dewar is dependent on the back pressure in the tank, which is measured by a pressure gauge on the dewar. As the amount of LN₂ in the dewar decreases, the back pressure in the dewar decreases and the flow of LN₂ slows. This dewar of LN₂ can support up to approximately five hours of continuous use and approximately 9 hours of cycled use at a minimum temperature of -15°C. Figure 21 shows the plumbing configuration of the LN₂ through the chamber.

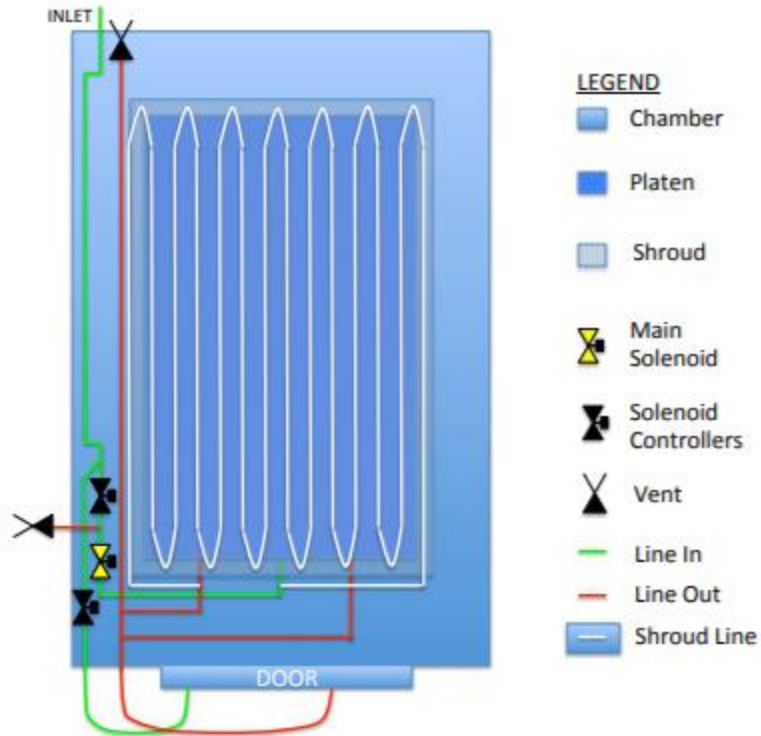


Figure 21: LN₂ Plumbing Diagram [4]

When the dewar fluid valve is manually opened, the LN₂ flows from the dewar until it reaches a junction. After the junction, there are two solenoid valves, one on each flow path, that control the amount of LN₂ that flows into the chamber. The PID temperature controller controls the opening and closing of these solenoid valves. The left most green line after the first junction shows the flow to the chamber door shroud. The right line after the junction in Figure 21 shows the flow to the platen and copper shroud. For this flow, there is another junction inside the chamber that splits the flow between the platen and copper shroud. Within the platen, there is another junction in an unknown location, but is known to exist because there are two exit lines from the platen. After flowing through the platen, across the copper shroud, and through the door shroud, all four exit lines rejoin and the LN₂ is vented from the chamber. The LN₂ plumbing through the door shroud is shown in Figure 22.

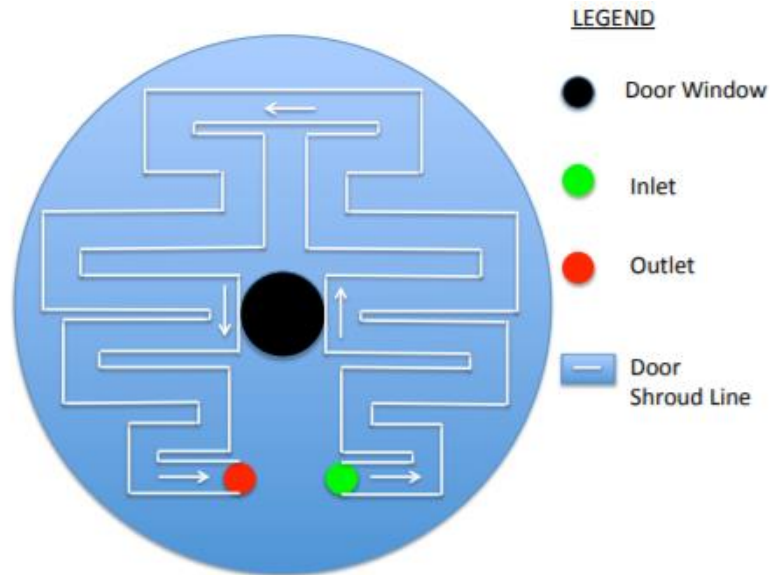


Figure 22: LN₂ Plumbing Through Chamber Door Shroud [4]

The LN₂ that flows to the chamber door enters at the bottom right of the door, circulates around the door as shown, and exits at the bottom left of the door. After which, this flow joins with the exhaust lines from the platen and copper shroud. This exhaust line is extended to vent into a bucket of water outside of the Cal Poly Space Environments Lab. The height of water in the bucket is approximately 0.60 meters. This is done to maintain a sufficient back pressure in the LN₂ dewar when all valves are open during testing. The bucket of water is also used to dampen the noise of the venting LN₂.

Similar to the heating system, the PID temperature controller is used to control the cooling system. When a temperature that is colder than the current temperature is set, the PID temperature controller controls the opening and closing of the solenoid valves based on the input temperature of the platen top surface. The frequency of the opening and closing of these valves depends on the user defined rate of cooling and set temperature. Currently, the solenoid valve controlling the LN₂ flow to the door shroud does not function properly. The manual switch is the only control mechanism for the LN₂ flow to door shroud. The opening and closing of the solenoid

valves for the flow to the platen and copper shroud are controlled by the PID temperature controller.

3.2.8 PID Temperature Controller

The Blue TVAC has a Watlow Winona series F4S/D Ramping Controller for the temperature control of the chamber. The user interface of the PID temperature controller is shown in Figure 23.



Figure 23: PID Temperature Controller

The temperature of the platen measured by the PID temperature controller thermocouples is displayed on the user interface but can only be manually recorded for analysis. This PID temperature controller has one input temperature reading from the platen surface that is used for the temperature control of the platen in the chamber. This PID temperature controller allows the user to design a thermal profile to be run automatically. The user can select a set point temperature, a ramp time or ramp rate, and a soak duration [14]. The PID temperature controller

uses these input parameters to determine the amount of power output to the heating and cooling systems. The set point temperature defined by the user is the desired platen temperature. The ramp time is the amount of time in which the platen changes from the current temperature to the set point temperature. The ramp rate is the degrees per minute that the platen temperature changes as it reaches the set point temperature. The soak duration is the amount of time the set point temperature is sustained for. In theory, with these user inputs, a complete thermal profile can be set and executed automatically.

The PID temperature controller also has two Watlow Series 97 limit controllers integrated into the control system to limit over or under temperature conditions in the Blue TVAC. These controllers provide safety assurances against runaway high or low temperatures that could occur from a shorted input sensor or an output device that could fail in a closed position [15]. These controllers use inputs from thermocouple readings of the platen surface temperature. The thermal profile will not run if the high or low limit temperatures are exceeded or if the thermocouple connection to these controllers are shorted.

3.3 Data Acquisition (DAQ) System

A General 12-channel temperature recorder with an Excel-formatted data logging SD card is used to record the temperatures from twelve Omega T type thermocouples in the chamber. This temperature recorder allows the user to specify which type of thermocouples are being used, the sample rate time, and the duration of data sampling [16]. During sampling, the temperatures from each thermocouple are displayed on the reader, which is shown in Figure 24.



Figure 24: General 12-Channel Temperature Recorder

During sampling, the recorded temperatures are automatically saved to a SD card in an Excel spreadsheet format that is then transferred to a computer for analysis.

The Omega T type thermocouples in use record temperatures at twelve locations in the chamber. These thermocouples can measure temperatures in the range of -250°C to 350°C with an error of 1.0°C [17]. Aluminum tape and polyimide tape are used to secure the welded end to any surface inside the chamber. The procedure for the thermocouple application process is included in Appendix B. Note that T type thermocouples must be used with the Blue TVAC for data collection. Any other type of thermocouple, such as K type, will result in temperature discrepancies between the twelve DAQ thermocouple readings and the PID temperature controller thermocouple reading. This discrepancy is further discussed in Section 6.2.

3.4 Test Article

A 3U CubeSat mass model was used as the test article for four of the fifteen tests conducted for this thesis. This mass model is made of anodized Aluminum 6061-T6. It is 34 cm long, 10 cm wide, and 10 cm tall. The 3U CubeSat mass model with dimensions is shown in

Figure 25. Note that the mass model has internal supporting beams and screws that are not shown in the figure.

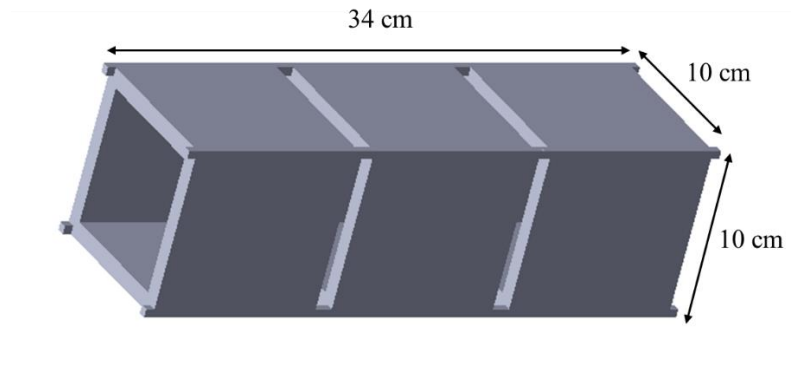


Figure 25: 3U CubeSat Mass Model Dimensions

Chapter 4

PRIOR WORK

4.1 Initial Testing and Modeling

In 2018, Cal Poly graduate student, Adrian Williams, refurbished the chamber, conducted hot soak tests, and modeled these tests with Thermal Desktop. The initial refurbishment efforts by Williams included replacing the preexisting mechanical pump, convectron gauges, and door O-ring. Upon verifying that the vacuum system and heating system operated as expected, Williams conducted a total of six hot soak tests with test articles [4]. The details of each experiment conducted by Williams are found in [4], which can be found on the Cal Poly Digital Commons. The goals of these tests were to prove that the chamber can achieve a vacuum according to the NASA GEVS standards and prove that the heating system of the chamber works properly. During Williams' tests, the chamber did not reach pressures required by the NASA GEVS standards. The lowest chamber pressure reached was approximately 1.0×10^{-5} Torr [2]. Williams also developed a thermal model with Thermal Desktop to simulate each test conducted. This was done to validate the tests conducted in the chamber and help predict future tests [4].

In general, the tests conducted by Williams proved that the Blue TVAC could be used for repeatable hot soak tests with a test article. Upon completion of his thesis project, Williams made several recommendations to improve the Blue TVAC. His main suggestions were to [4]:

- Establish a functional cooling system
- Upgrade the DAQ system to allow for a greater number of thermocouples to be used
- Refine the Thermal Desktop model to improve the geometries of the modeled system
- Simulate cold soaks
- Measure the temperature gradient across the platen to better understand how the chamber behaves

4.2 Additional Heating System Testing

In 2018, Cal Poly student Michael Caudill improved the Blue TVAC and performed additional hot soaks with test articles based on Williams' recommendations. The 12-channel temperature logger was implemented to record temperature data from twelve different locations in the chamber. This is the same temperature logger that was used for this thesis project. Caudill conducted a total of eight hot soak tests on two different test articles, a 1U CubeSat mass model and a 3U CubeSat mass model [18]. Refer to Appendix C for the results of Caudill's tests.

Results from Caudill's tests show similar trends to the results from Williams' tests. The lowest chamber pressure reached by Caudill was 1.10×10^{-4} Torr [18]. The copper shroud and test article consistently reach lower temperatures than the platen [18]. Caudill's test results are important because they reveal more detailed trends in the temperature response of various surfaces within the chamber, like the door shroud and the copper shroud. Caudill also developed a thermal model with SolidWorks Thermal tool to verify the test results. A steady-state analysis was performed to predict the final temperature of the 1U and 3U CubeSat mass models which correlated to the experimental results with an thermal uncertainty of 5°C [18].

Upon concluding his testing, Caudill made several recommendations to improve the Blue TVAC. He first recommended that the interior of the copper shroud and the top of the platen be painted with a high emissivity coating to allow more radiative heat transfer from these surfaces to the test articles during heating and to absorb more heat from the test article during cooling [18]. Caudill also recommended installing a new O-ring to improve the seal of the chamber door to eliminate any potential leaks at the door seal so lower pressures could be reached in the chamber [18]. Finally, he recommended the purchase of the LN_2 dewar and the installment of the external plumbing to operate and test the cooling system [18].

4.3 Cooling System Testing

In 2019, Cal Poly students Michael Caudill and Bennett Diamond implemented the cooling system for the Blue TVAC and conducted preliminary tests to characterize its performance. After ensuring that the cooling system operates in compliance with the Cal Poly Environmental Health and Safety standards, Caudill and Diamond tested the chamber to determine the lowest attainable temperatures in the chamber and the duration for which a minimum temperature can be maintained [19]. To characterize the performance, Caudill and Diamond measured the temperature in the chamber during a cold soak. Refer to Appendix C for results from Caudill and Diamond's tests.

Caudill and Diamond made some important observations during testing. It was observed that the dewar filled with LN₂ would lose pressure during operation, which would limit the flow rate of LN₂ [19]. This was resolved by decreasing the ramp rate to maintain a controller power of 30%-40%. They also observed that the temperature set by the PID controller consistently differed from the temperatures recorded by the DAQ thermocouples. This was resolved by setting temperatures with the controller that were lower than the desired platen temperature. Finally, they observed that the LN₂ was rapidly depleted and did not sustain cold soaks longer than approximately five hours [19]. The lowest chamber pressure achieved during testing was 20×10^{-5} Torr, which is an order of magnitude higher than the pressure reached during tests conducted by Williams [19].

Upon concluding the cooling system tests, Caudill and Diamond made various recommendations for future work. They recommended that the PID control system be calibrated to correct for the discrepancies observed between the controller temperature and temperatures measured by the DAQ thermocouples [19]. They also recommended a thermal model be developed to correlate the test data to the model predicted data for the cold soaks [19]. Finally,

they advised that testing with a CubeSat mass model be conducted to further characterize the system performance when a test article is included [19].

4.4 Thesis Motivation

The previous work completed by students on the Blue TVAC has increased the potential for it to be used for various thermal testing of spacecraft test articles for educational and research activities. The data collected and the observations made have provided a critical understanding of the Blue TVAC to all future researchers. The recommendations that have been made by past students as well as the status of the recommendations are shown in Table 2.

Table 2: Overview of Recommendations Made by Past Students [4, 18, 19]

Recommendation	Made By	Status
Refurbish the cooling system to allow for operation	Adrian Williams	Addressed by Caudill and Diamond
Install a switch for chamber venting control	Adrian Williams	Addressed by Caudill and Diamond
Upgrade the DAQ system	Adrian Williams	Addressed by Caudill Diamond
Refine Thermal Desktop Model	Adrian Williams	Addressed by this thesis
Measure the temperature distribution across the platen	Adrian Williams	Addressed by this thesis
Install a turbo pump revolution per minute (RPM) monitoring device	Adrian Williams	Not addressed
Investigate temperature profile of the copper shroud	Adrian Williams	Addressed by this thesis
Install a test stand for test articles	Adrian Williams	Not addressed
Add a high-emissivity coating to the copper shroud	Michael Caudill	Not addressed
Install a new O-ring for the chamber door	Michael Caudill	Partially addressed by this thesis

Recommendation	Made By	Status
Test cooling system with test article(s)	Michael Caudill and Bennett Diamond	Addressed by this thesis
Calibrate/tune cryogenic fluid control system	Michael Caudill and Bennett Diamond	Not addressed
Correlate thermal model to cryogenic tests	Michael Caudill and Bennett Diamond	Addressed by this thesis
Develop testing procedures for other students	Michael Caudill and Bennett Diamond	Addressed by this thesis
Generate report containing full system capabilities for industry use	Michael Caudill and Bennett Diamond	Not addressed

While the Blue TVAC performance has been characterized, the thermal vacuum test repeatability and validity must be determined before the Blue TVAC can be operated for future purposes. The key gap in the past work that motivated this thesis project is the lack of full thermal vacuum testing and modeling. This includes conducting repeatable thermal vacuum tests and verifying the thermal response of the chamber. This was done for this thesis project by conducting multiple thermal vacuum tests with and without a test article while collecting temperature data at various point in the chamber. These tests also revealed the most efficient operational procedure needed to conduct repeatable tests. The thermal model that was developed for this thesis will allow users to further analyze the predicted distribution of heat within the chamber. The model can also be used to simulate future tests with varying test articles to predict the temperature response of a test article during a test. Overall, the testing and modeling conducted for this thesis project will allow future students to gain valuable experience and knowledge of thermal analysis and testing of spacecraft.

PROJECT METHODOLOGY

5.1 General Methodology

A general methodology for this thesis project was developed prior to the start of the project to ensure that effective decisions were made throughout the testing and modeling processes. A diagram of the overall methodology of this project is shown in Figure 26.

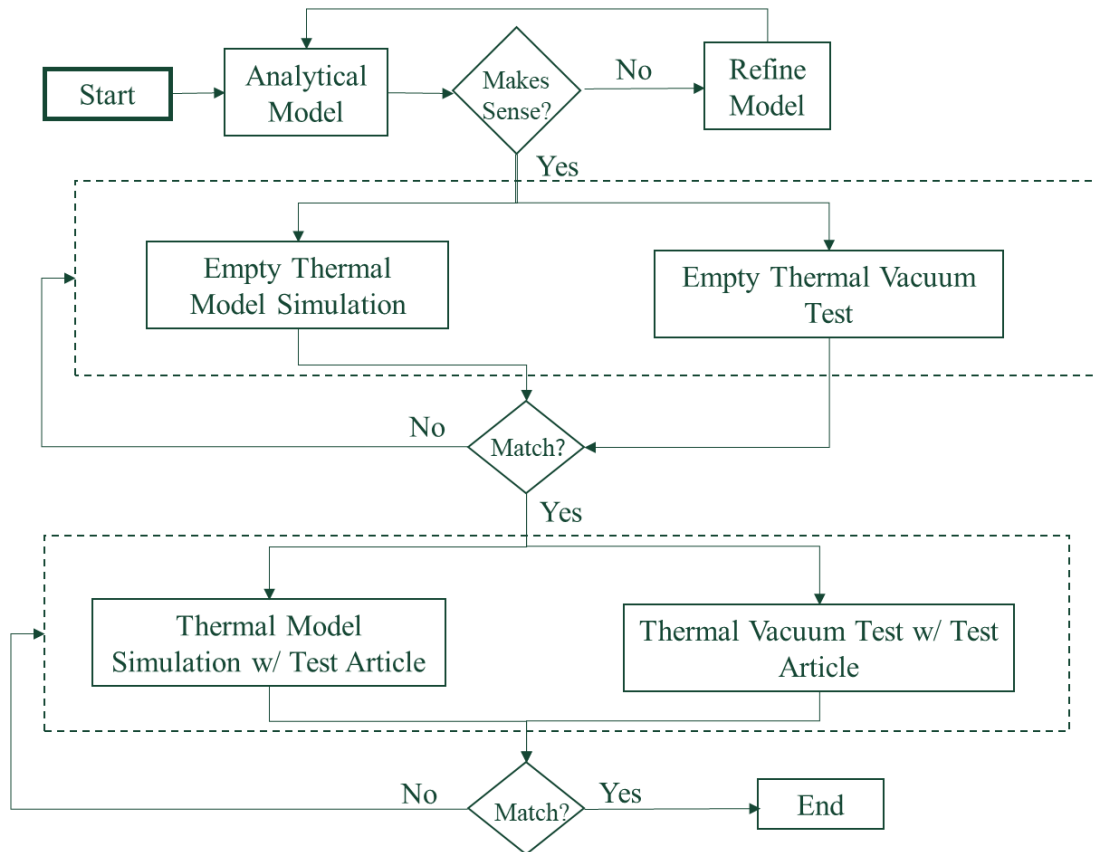


Figure 26: Project Methodology

To start, an analytical model was developed to predict the temperature response of the chamber using simplified system geometries and interfaces. This was done to determine the critical properties of the chamber such as the component geometries, component material properties, interface areas between components, and heat inputs to the system. When the results from this analysis were found to be reasonable, the physical testing and numerical modeling of

the system would begin. For the analytical model, a reasonable result was defined as a temperature with $\pm 15^{\circ}\text{C}$ of the expected temperature based on prior testing results. The analytical model was used mainly to ensure that before the start of testing and modeling, all system parameters were defined.

Once the system parameters were determined and the analytical model provided a baseline temperature response estimation of the platen, a thermal vacuum test was conducted to collect temperature data at specific points within the chamber. For the initial testing, no test article was used. These tests are referred to as empty tests. This experimental data would reveal the actual thermal response of the chamber during heating and cooling. In parallel to the initial testing of the chamber, a thermal model was developed using Thermal Desktop. After defining the chamber geometry, material properties, interfaces, and heat loads, the thermal vacuum test profile was simulated and numerical approximations of the thermal response of the chamber were made.

Once the initial tests and simulations were complete, a decision was made to determine the next step. First, it had to be decided if the thermal vacuum test conducted was repeatable. This means that it had to be proven that by following the same procedure, the same results would be obtained. If this was not proven, then more empty tests would be conducted. If repeatable experimental data was obtained, then another decision would need to be made. The experimental data would be compared to the numerical approximations and if the model predictions correlated to the test results with a thermal uncertainty margin of 15°C , then testing and modeling of the chamber with a test article would be performed. This margin is based on the thermal uncertainty margin that is recommended by the European Cooperation for Space Standardization (ECSS) [20]. Similar thermal uncertainty margins are used by NASA JPL, US Military standards and commercial businesses for qualification and protoflight thermal vacuum testing [2]. If the results

did not meet this correlation criteria, then additional empty tests would be conducted and the model would be refined to better match the temperature trends observed in the test data.

Once the test article was implemented in both the chamber and the Thermal Desktop model, repeatable experimental results would need to be obtained before valid comparisons of the testing data to the modeling data could be made. Once the repeatability of the test with the test article was proven, then the same correlation criteria was used to verify that the numerical model of the system predicted the experimental results with the required thermal uncertainty margin. If the uncertainty of the model predictions was greater than 15°C, more tests would need to be conducted and the model would be refined to achieve this required margin. Once this uncertainty margin in the model predictions of the test article was achieved, the project would be considered complete.

In summary, this general methodology ensures that the primary goals of this thesis project are accomplished. The computational thermal model of the Blue TVAC developed with and without a test article is verified with temperature data from repeatable thermal vacuum tests to predict the thermal response of the chamber with the defined thermal uncertainty margin.

5.2 Modeling Methodology

To begin modeling the Blue TVAC, the material properties of the system were defined. Table 3 below shows the thermophysical properties that were used for each of the elements in the thermal models. The thermal conductivity property is temperature dependent, but it was assumed to be a constant value during testing. For tests with more extreme variations in temperature, the temperature dependency of this property should be modeled as it may influence the uncertainty margin of the results. Table 3 includes the temperatures that the assumed thermal conductivity is accurate for.

Table 3: Blue TVAC Thermophysical Properties [21, 22, 23]

Material	Element	Thermal Conductivity k [W/m-K]	Specific Heat c_p [J/kg-K]	Density ρ [kg/m³]
Aluminum 6061-T6	Platen	167 @ 25°C	896	2700
Anodized Aluminum 6061-T6	3U CubeSat Mass Model	167 @ 25°C	896	2700
304 Stainless Steel	Heaters (3), Door, Inner Chamber Cylinder	16.3 @ 0°C-100°C	500	8030
Copper	Shroud	401 @ 0°C	386	8960
Teflon	Cylinders (4)	0.25 @ 25°C	1000	2200
Mylar	Outer Cylinder Insulation	0.16 @ 25°C-75°C	1172	1390

To model the radiative heat transfer between elements, the IR emissivity of the surfaces of the elements was also defined. Table 4 shows the IR emissivity that were used for each of the elements in the thermal models.

Table 4: Blue TVAC Optical Properties [21]

Material	Element	IR Emissivity
Aluminum 6061-T6	Platen	0.5
Anodized Aluminum 6061-T6	3U CubeSat Mass Model	0.9
304 Stainless Steel	Heaters (3), Door, Inner Chamber Cylinder	0.4
Copper	Shroud, LN ₂ Pipes	0.03
Teflon	Cylinders (4)	0.92
Mylar	Outer Cylinder Insulation	0.34
Black Surface Coating	Door Shroud	0.95

After determining the material properties of each element, the model was discretized into finite difference meshes that consist of individual nodes. Table 5 shows the total number of nodes used to model each element in the Blue TVAC.

Table 5: Discretization of the Blue TVAC Thermal Model

Element	Number of Nodes
Heaters	81
Platen	662
Teflon Cylinders	16
3U CubeSat Mass Model	108
Shroud	25
LN ₂ “Pipes”	15
Door Shroud	25
Inner Chamber Cylinder	50
Outer Insulative Chamber Cylinder	75
Total	1,057

Figure 27 shows the 3-D modeled platen and shroud meshes. The three strip heater meshes are not shown, but exist on the bottom side of the platen. The outer insulative chamber cylinder is also not shown. This element was modeled to have an insulative Mylar layer to minimize the radiation from the internal chamber to the external ambient air.

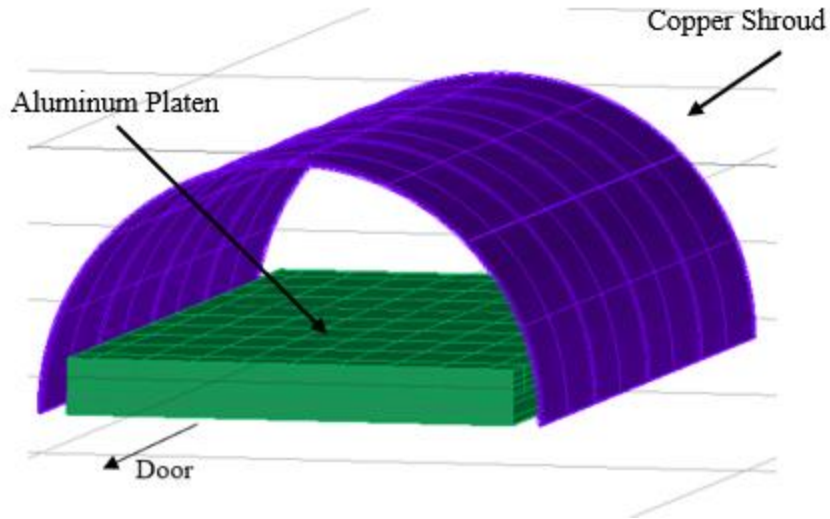


Figure 27: Platen and Shroud Meshes

For the cold soak simulations, the LN₂ plumbing was modeled as nodes with constant temperatures of -15°C. This assumption was made because the temperature of the LN₂ pipes during the experiments was not measured. The LN₂ flow required simplification for the simulations and it was assumed that the LN₂ pipes, which are in contact with the copper shroud and platen, are likely at a constant temperature while the LN₂ flows through them. The vaporization temperature of Nitrogen at sea level is approximately -195°C. While the Nitrogen is in a liquid state in the dewar, it is exhausted from the system as a gas, so the fluid undergoes a phase change at some point in the plumbing lines. In addition to the simulations presented in Chapter 6 of this thesis, a simulation was run with the LN₂ plumbing nodes set to -195°C. The results from this simulation are discussed in Chapter 6 as well. Recommendations for improving the LN₂ system thermal model is presented in Chapter 8.

Since the geometry of the plumbing through the platen is unknown, the pipes were assumed to be three parallel rectangular elements that extended longitudinally through the platen. This assumption was made because the inlet pipe is located in the middle of front center edge and there are two outlet pipes located on either side of the middle inlet pipe. The assumed geometries of the elements are shown in Figure 28.

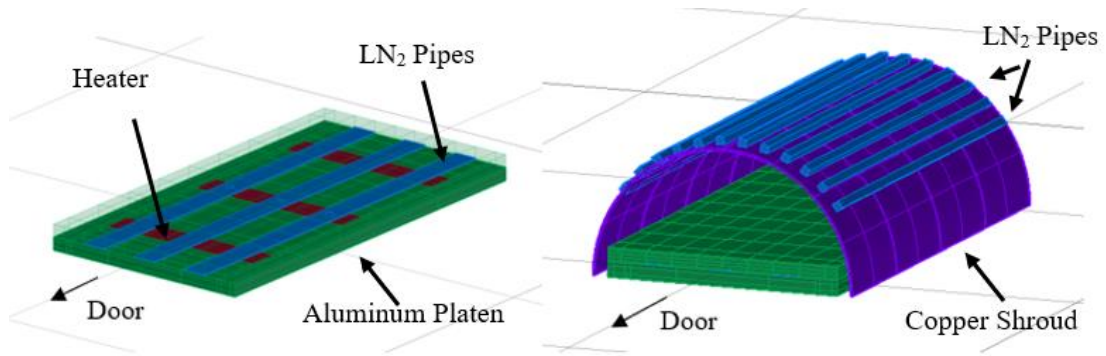


Figure 28: LN₂ Plumbing Meshes Through Platen (Left) and On Shroud (Right)

The image on the left of Figure 28 shows the assumed meshes of the LN₂ pipes that run through the platen in blue. The top surface of the platen is shown as transparent in this image to reveal the pipes. The image on the right shows the simplified geometry of the LN₂ pipes that run over the shroud in blue. The other elements of the chamber modeled were the chamber door, the inner chamber cylinder, and the outer chamber insulative cylinder. These modeled elements, excluding the outer chamber insulative cylinder, are shown in Figure 29.

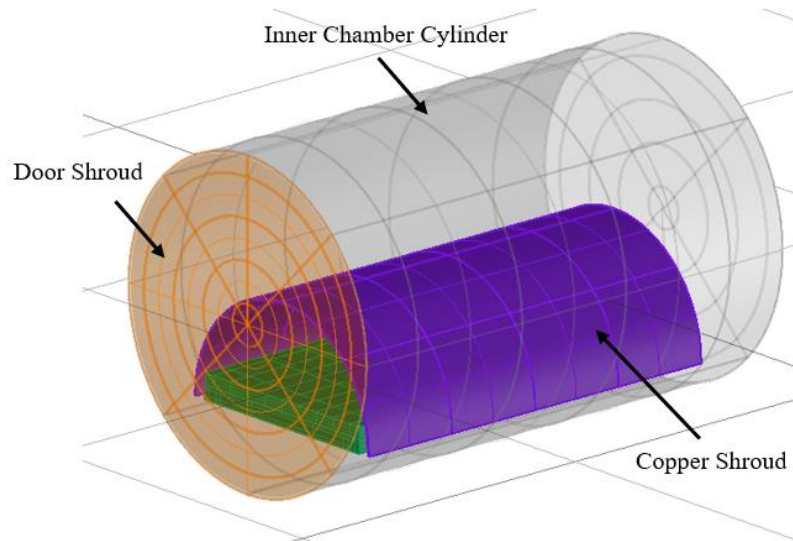


Figure 29: Chamber Door and Inner Cylinder Meshes

Finally, the 3U CubeSat mass model with Teflon cylinder supports were modeled to simulate the experiments that included this test article. The simplified geometry of this element

on the platen is shown in Figure 30. Note that while the Teflon cylinders are colored gray, this does not mean they have the same material properties as the mass model.

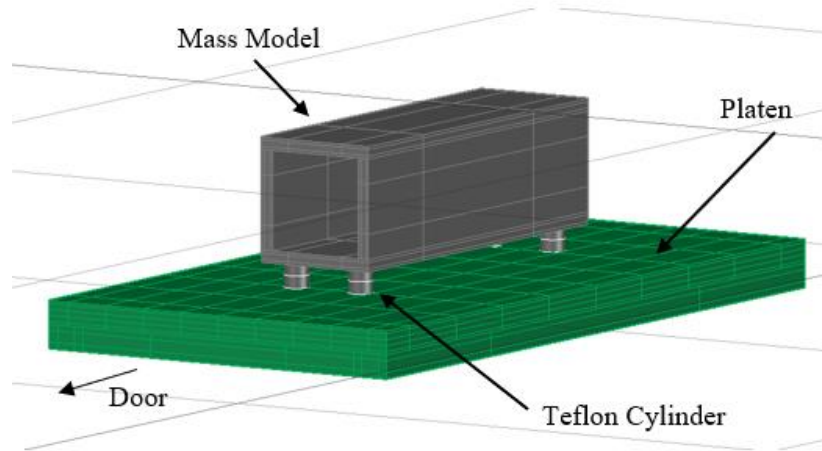


Figure 30: 3U CubeSat Mass Model Mesh

The next step in the modeling method was to define the interfaces between each of the elements. For each surface of every element, it was assumed that heat is transferred to other surfaces by radiation, conduction, or both. In Thermal Desktop, this was done by defining conductive “connectors” between the surfaces of elements and/or including a surface in a “radiation analysis group”. Figure 31 shows the defined interfaces between elements for the simulations that did not include the test article.

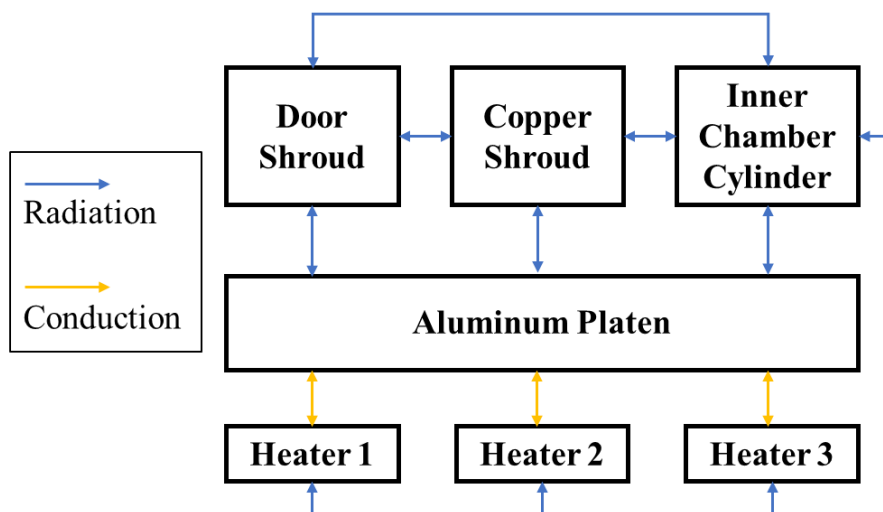


Figure 31: Model Interfaces Without the Test Article

For the model that includes the 3U CubeSat mass model, new interfaces had to be defined. These are shown in Figure 32.

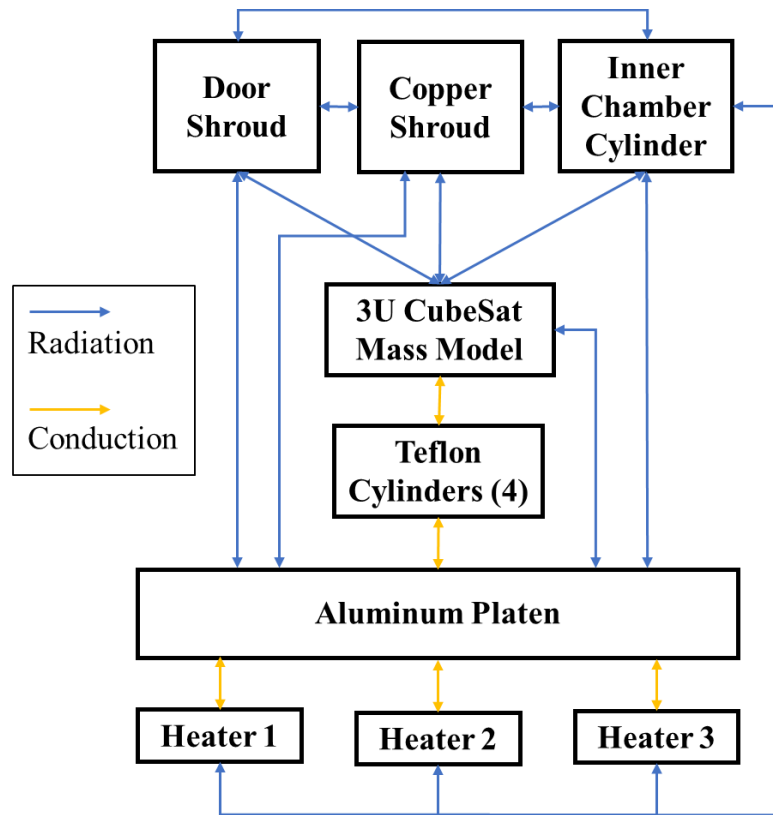


Figure 32: Model Interfaces with the Test Article

In these simulations, the heat conducted from the platen to the support structures of the platen were not modeled. Also not included are the electrical wires and the heat generated by the electrical resistance of these elements. The decision to omit these elements from the models was made because it was assumed that they would influence the simulation results by less than 5°C, but with a thermal uncertainty margin of 15°C, this would not be enough to influence the uncertainty of the predictions.

The next step in modeling the Blue TVAC was to define the heat loads from the heaters. In Thermal Desktop, these were modeled as “heaters”, which are thermostatically controlled heat loads to nodes or surfaces. The temperature used for the control of the heaters was defined to be

to top surface of the platen, since this is the temperature that is used by the PID temperature controller. Once activated, the heaters would output heat until the top surface of the platen reached a temperature of 50°C. The heater power was assumed to be 356 Watts which is approximately 75% of the maximum power of each heater, which is 475 Watts. This was decided because after testing, it was observed on the PID temperature controller display that about 60% to 80% of the maximum power was being output to the heaters during the heating phases.

After defining the heaters in the thermal model, the initial temperatures of each simulation were defined. For the cooling phase and cold soak phase simulations, all elements were set to an initial approximate ambient temperature of 22°C to 25°C. For the heating phase and hot soak phase simulations, the initial temperatures of each element were defined as the approximate final temperatures of that element that resulted from the cold soak simulations.

Once all model parameters were set, the times of the transient analysis simulations were defined for the heating, cooling, hot soak, and cold soak phases of the thermal vacuum test. This was done for both test configurations, with and without a test article. The simulations were then run and the results from these simulations are discussed in Chapter 6.

5.3 Testing Methodology

A total of 15 thermal vacuum tests were conducted with the Blue TVAC. Each test was performed for a unique purpose with the overall goal of determining the repeatability of a thermal vacuum test, the thermal response of the chamber and the temperature distribution within the chamber. This was all done to collect data that could be used to validate the developed thermal model. For each test, a thermal profile was programmed with the PID temperature controller to automatically control the heating and cooling systems. The PID temperature controller used temperature measurements from a thermocouple located on the platen surface to control the power output to the heating and cooling systems required to follow this profile. ISO Standard 19683 was used as a reference for the thermal profile parameters, although these parameters were

varied from test to test depending on the specific goals of the test. A nondimensionalized profile of the thermal vacuum tests conducted is shown in Figure 33.

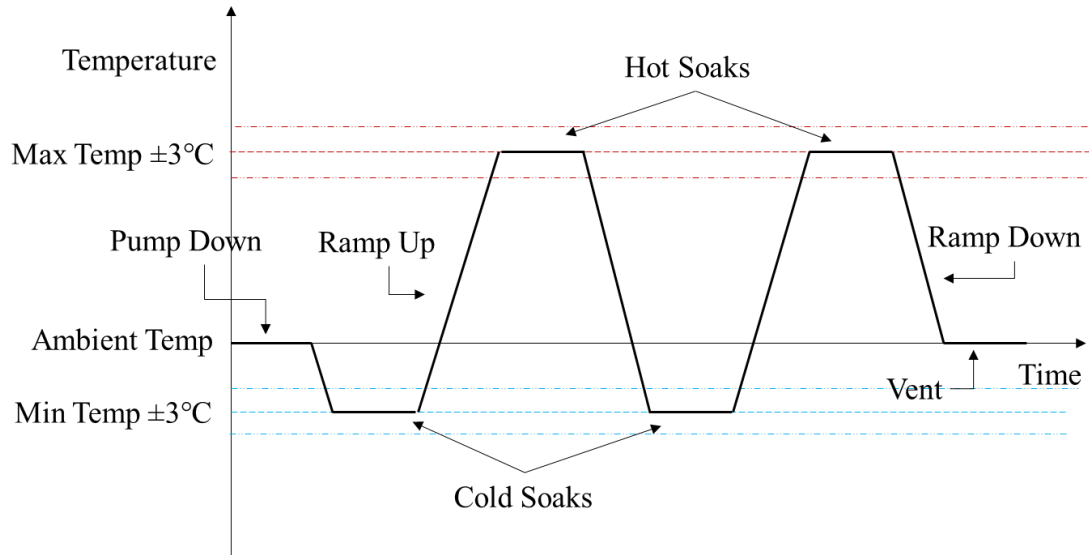


Figure 33: Nondimensionalized Thermal Vacuum Test Profile

During testing, the cooling system was activated after the chamber pressure dropped below approximately 10^{-3} Torr. The DAQ also began as soon as the cooling system was activated. Table 6 shows the testing parameters used for each thermal vacuum test.

Table 6: Thermal Vacuum Test Parameters

Test	Number of Cycles	Set Hot Soak Temperature (°C)	Set Cold Soak Temperature (°C)	Duration of Soak (min)	Set Ramp Rate (°C/min)	Measured Chamber Pressure (Torr)
1	<0.5	+50	n/a	<60	±5 or slower	27×10^{-5}
2	1	+50	-15	60	±5 or slower	26×10^{-5}
3	2	+50	-15	60	±5 or slower	19×10^{-5}
4	1	+60	-30	60	±5 or slower	24×10^{-5}
5	0.5	n/a	-30	90	±5 or slower	31×10^{-5}
6	1.5	+50	-15	60	±5 or slower	16×10^{-5}

Test	Number of Cycles	Set Hot Soak Temperature (°C)	Set Cold Soak Temperature (°C)	Duration of Soak (min)	Set Ramp Rate (°C/min)	Measured Chamber Pressure (Torr)
7	2	+60	-20	60	±5 or slower	16x10 ⁻⁵
8	1	+65	-25	60	±5 or slower	18x10 ⁻⁵
9	2	+65	-25	60	±5 or slower	17x10 ⁻⁵
10	2	+60	-20	60	±5 or slower	18x10 ⁻⁵
11	2	+60	-20	60	±5 or slower	16x10 ⁻⁵
12	1	+65	-22	60	±5 or slower	18x10 ⁻⁵
13	1.5	+50	-15	60	±5 or slower	21x10 ⁻⁵
14	2	+50	-15	60	±5 or slower	19x10 ⁻⁵
15	1	+50	-15	120	±5 or slower	20x10 ⁻⁵

Table 7 below shows a brief description for the purpose for each test that was conducted for this thesis. Some tests were conducted for a similar purpose.

Table 7: Purpose of Each Thermal Vacuum Test

Test	Purpose
1-3	Collect initial temperature data of various surfaces in the Blue TVAC
4-5	Collect temperature data of various surfaces in the Blue TVAC with more extreme target soak temperatures
6-7	Test new PID temperature controller thermocouple locations to resolve observed temperature discrepancy in readings
8-9	Test deeper bucket of water for exhaust hose to resolve LN ₂ dewar backpressure issues
10-11	Collect initial temperature data for tests with 3U CubeSat mass model
12-13	Verify new T type thermocouples with empty thermal vacuum tests
14-15	Conduct tests with 3U CubeSat mass model and verify thermocouple application method

The next step in testing was to decide where to position the thermocouples. There are twelve thermocouples that can be used to collect data during a test. Each of the twelve thermocouples is designated by a name of TC1 through TC12. For each thermal vacuum test, these thermocouples were applied to a surface inside the chamber with a piece of polyimide tape as shown in Figure 34. For Test 15, an additional piece of aluminum tape was added to cover the welded tip of the thermocouple. The rationale and results of this different application method are discussed in Section 6.5. Refer to Appendix B for the thermocouple application procedure.



Figure 34: Thermocouple Application Method

The locations of each thermocouple and number of thermocouples at each location is presented for each test in Table 8. The specific thermocouple configurations used for each test are shown in figures in Appendix D. The locations of each thermocouple were selected to collect temperature data for areas of the test section that may be influencing a test article the most when it included in a test. With only twelve available thermocouples, it was not possible to investigate the thermal profile of every surface in the chamber.

Table 8: Thermocouple Description and Locations During Testing

Test	Number of Thermocouples	Thermocouple Type	Thermocouple Locations [Number of thermocouples per location]
1	12	K	Platen [5] Copper Shroud [4] Door Shroud [2] Inner Chamber Cylinder [1]
2	12	K	Platen [5] Copper Shroud [4] Door Shroud [2] Inner Chamber Cylinder [1]
3	12	K	Platen [5] Copper Shroud [4] Door Shroud [2] Inner Chamber Cylinder [1]
4	12	K	Platen [5] Copper Shroud [4] Door Shroud [2] Inner Chamber Cylinder [1]
5	12	K	Platen [5] Copper Shroud [4] Door Shroud [2] Inner Chamber Cylinder [1]
6	12	K	Platen [6] Copper Shroud [4] Door Shroud [2]
7	11	K	Platen [6] Copper Shroud [4] Door Shroud [1]
8	12	K	Platen [7] Copper Shroud [4] Door Shroud [1]

Test	Number of Thermocouples	Thermocouple Type	Thermocouple Locations [Number of thermocouples per location]
9	12	K	Platen [7] Copper Shroud [4] Door Shroud [1]
10	11	K	Mass Model [9] Platen [2]
11	11	K	Mass Model [9] Platen [2]
12	12	T	Platen [7] Copper Shroud [4] Door Shroud [1]
13	12	T	Platen [12]
14	12	T	Mass Model [8] Platen [4]
15	12	T	Mass Model [8] Platen [4]

Note that after Test 11, T type thermocouples were installed and used to obtain more accurate temperature readings. The results from this change are discussed in detail in Chapter 6. Once the thermocouples were secured to the various surfaces and the profile parameters were programmed, the 12-channel temperature recorder was set to log the temperature measurement from each thermocouple with a sample rate of once every 60 seconds. The thermal vacuum test could then begin. The key results from the thermal vacuum tests are discussed in Chapter 6.

Chapter 6

RESULTS

6.1 Analytical Model Results

Before conducting numerical simulations of the thermal vacuum tests, an analytical model was developed to calculate the expected temperature changes of the platen during heating. The equations described in Section 2.1 were used for these calculations. For these calculations, assumptions were made to simplify the problem to make it solvable without numerical approximation techniques. The assumptions made for these initial calculations were:

- 1-D heat transfer from the 3 heaters to the platen
 - Assumed because heat primarily flows from the middle of the platen to the top
- Each heater outputs 75% of maximum 475 Watts
 - Assumed based on the average power output observed during testing
- Steady state analysis for 25 minutes of heating
 - Assumed based on the time of heating to approximately 57°C in prior tests
- Constant material properties
 - Assumed to avoid non-linearity in equations
- Constant temperature throughout elements
 - Assumed to simplify calculations for initial approximations
- Conduction only from heaters to platen, radiation only from platen to every other surface in view
 - Assumed to model the heat transfer for this chamber in a vacuum state

Results from the analytical calculations showed that after 25 minutes of conductive heating, the platen reaches a temperature of approximately 103°C. After 85 minutes of radiative heat transfer from the platen, it reaches a temperature of approximately 52°C. These results are shown in Figure 35.

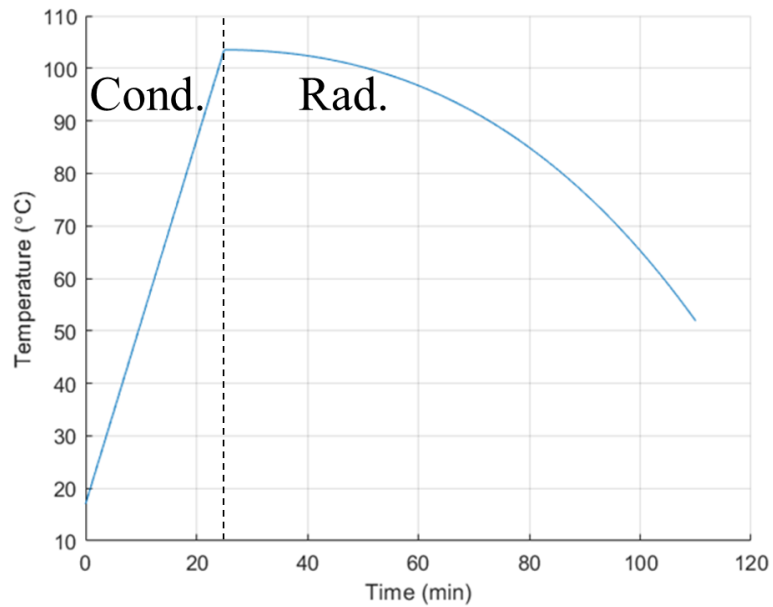


Figure 35: Analytical Platen Temperature Calculations

Calculation details are provided in Appendix E. Based on prior testing by Williams, it was expected that after 25 minutes of heating, the platen would reach a temperature of approximately 57°C and maintain this temperature after over one hour [4]. The error in this calculation is approximately 5°C, which is a result of the assumptions made to simplify the analysis. This thermal uncertainty margin is within the target margin of 15°C, so the decision was made to begin testing and making numerical approximations to predict the temperatures of other elements in the chamber during an empty thermal vacuum test.

6.2 Preliminary Test Results

The first eleven thermal vacuum tests were conducted with the goal of measuring the temperature distribution and thermal response of the chamber during heating and cooling. Before this data could be used to validate the thermal model being developed, the temperatures in the chamber had to be repeatably measured. A repeatable operating procedure for conducting thermal vacuum tests with the Blue TVAC was developed and can be found in [11].

In the first eleven tests, it was revealed that the repeatability of a test was mostly dependent on the availability of LN₂ in the dewar. Since the use of this fluid is automatically controlled by the PID temperature controller, the amount used during a test depends on the set temperatures, ramp rates, and soak durations. The LN₂ is used to reach the minimum temperatures and maintain both the hot and cold soak temperatures. It was common for the LN₂ to run out during the second ramp down phase of the thermal vacuum test, which resulted in a second cold soak at a temperature higher than desired. Currently, the 35 liter LN₂ dewar cannot repeatedly supply enough coolant for two complete empty thermal vacuum cycles. This was the only observed limitation to conducting repeatable thermal vacuum tests with the Blue TVAC.

Initial temperature distribution results showed a 2°C to 8°C temperature discrepancy between the temperature readings from the DAQ thermocouples placed on the platen and the PID temperature controller reading from the platen. The DAQ thermocouple configuration on the platen used for Test 3 is shown in Figure 36. These five thermocouples were taped to the surface of the platen with polyimide tape. The configuration of the other seven DAQ thermocouples can be found in Appendix D.

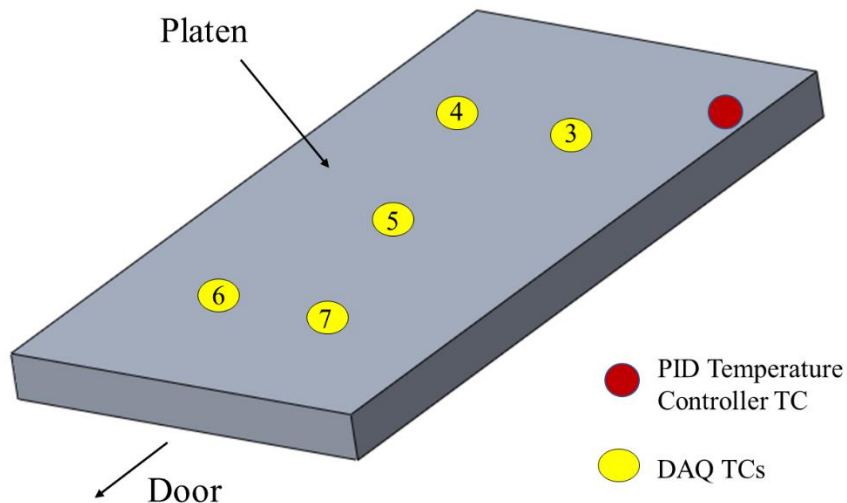


Figure 36: Thermocouple Configuration on Platen for Test 3

For Test 3, the PID controller thermocouple was installed on the right rear edge of the platen. This thermocouple was originally screwed into the platen with a washer made of an unknown material that was soldered to the ends of the thermocouple wires.

The temperature data collected by the DAQ thermocouples on the platen is shown in Figure 37. Data from the thermocouples located on the other surfaces in the chamber can be found in Appendix F. Note that data was not collected by the PID temperature controller. It was only observed from the display screen that the PID controller thermocouple measured a temperature of -15°C during the cold soak and 50°C during the hot soak.

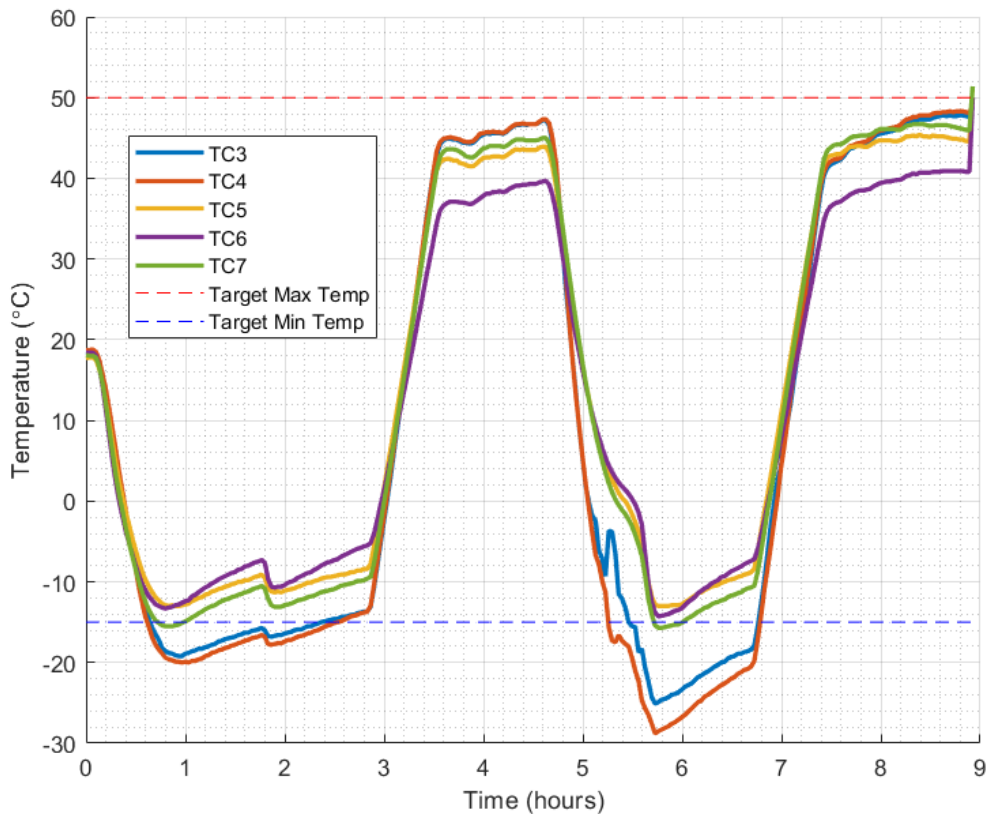


Figure 37: Thermal Response of Platen During Test 3

Figure 37 shows that when the PID temperature controller was set to reach a cold soak platen temperature of -15°C , TC3-TC7 located on the platen measured an average cold soak temperature of approximately -16°C to -10°C during the first cold soak and -19°C to -13°C during

the second cold soak. For the hot soaks, when the PID temperature controller measured a platen temperature of 50°C, the five thermocouples measured an average temperature of approximately 42°C to 45°C for the first hot soak and 42°C to 46°C for the second hot soak. This discrepancy was consistent throughout all eleven tests.

Another consistent trend in the data from the first eleven tests was a measured increase in platen temperatures during the hot and cold soaks. While the PID temperature controller measured a platen temperature within $\pm 1^\circ\text{C}$ of the set temperatures, the DAQ thermocouples on the platen measured an increasing temperature at a rate of approximately 4-8 °C/hr.

During the first eleven tests, hypotheses were made and tested to determine the root cause of the observed temperature discrepancies between the PID temperature controller thermocouple readings and the DAQ thermocouple readings. The first hypothesis was that the PID temperature controller thermocouple was taking measurements from a location on the platen that actually varied in temperature from the DAQ thermocouple locations. The PID temperature controller thermocouple was originally located on the right rear edge of the platen while the DAQ thermocouples were placed in the middle area of the platen. The hypothesis was that the edges of the platen may get colder than the middle of the platen since the copper shroud is approximately 1 mm from the left and right edges of the platen. This hypothesis was proven false after the PID temperature controller thermocouple was moved to a more central location and the temperature discrepancies were still observed in the data. Figures showing the new thermocouple configuration can be found in Appendix D. The results from the tests conducted with the new thermocouple configuration can be found in Appendix F.

The second hypothesis formed was that the thermocouples used for the DAQ were being influenced by temperature fluctuations around the junctions external to the chamber. Figure 38 shows one of the panel jacks that is on the outside of the chamber with the original K type thermocouples connected. There is also a similar panel jack to connect the thermocouple wires

inside the chamber. The junction for the PID temperature controller thermocouple is located on the back of the unit.

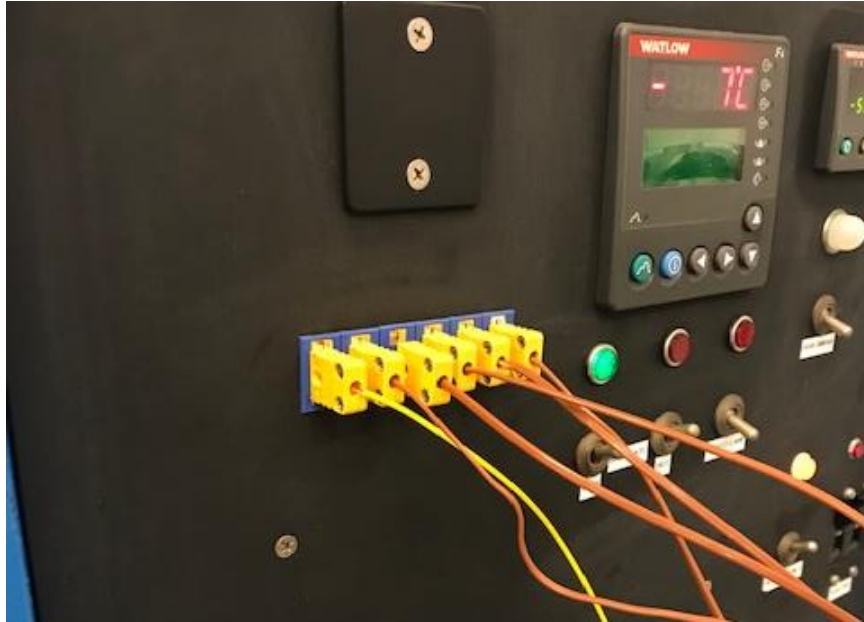


Figure 38: External T Type Thermocouple Panel Jack with K Type Thermocouples

It was hypothesized that the exposed wires at these junctions are sensitive to the changes in temperature around the junctions, which may result in inaccurate readings. This was tested by blowing hot air across the junctions with a hair blow dryer and observing the resulting temperature readings. When this was done, there was a measured change in temperature of about 40°C in both the DAQ system measurements and the PID temperature controller measurement. This proved that fluctuating temperature of the air surrounding the thermocouple junctions does influence the measurements, but it was assumed that the ambient air temperature is constant during testing. This result provided useful information but did not explain the temperature measurement discrepancies.

The final hypothesis was formed after observing that the panel jack shown in Figure 38 is colored blue. In general, thermocouples are color coded to indicate the thermocouple type. Figure

39 shows the various types of thermocouples with their associated color codes, sensitivity range, and standard limits of error.

Calibration	Tem Range	Std. Limits of Error
J	0°C to 750°C (32° F to 13382°F)	Greater of 2.2°C or 0.75%
K	-200°C to 1250°C (-328° F to 2282°F)	Greater of 2.2°C or 0.75%
E	-200°C to 900°C (-328° F to 1652°F)	Greater of 1.7°C or 0.5%
T	-250°C to 350°C (-328° F to 662°F)	Greater of 1.0°C or 0.75%

Figure 39: Omega Thermocouple Types [22]

For the first eleven tests, K type thermocouples were connected in series to T type thermocouple extension wires. The K type thermocouple wires are made of Nickel-Chromium and Nickel-Aluminum while the T type thermocouple wires are made of Copper and Copper-Nickel [17]. When wires of different materials are connected in series, the voltage potential across the wires that is converted to a temperature reading is disrupted and the temperature measurement is not accurate. When it was discovered that the Blue TVAC is equipped for T type thermocouples rather than K type, twelve new T type thermocouples were installed to test this hypothesis. Tests 12 and 13 were conducted to verify the new T type thermocouples.

6.3 Empty Thermal Vacuum Test Results

The new T type thermocouples were verified by Test 12 and 13. Temperature data was collected during these empty thermal vacuum tests that was then used to validate the thermal

model simulation of this test. In this section, the results from these two tests are discussed. The corresponding simulation results are presented in Section 6.4.

Twelve new T type thermocouples were built and installed in the Blue TVAC. Procedures for building and repairing the thermocouples in use can be found in Appendix G. Seven of these thermocouples were secured to the platen in the same configuration that was used for Test 7 as shown in Figure 40. The thermocouples on the platen are labeled TC2-TC6 and TC12. The same configuration was used to compare the results from these two tests. Four of the thermocouples were attached to the copper shroud surface and one was attached to the door shroud surface as shown in Figure 41 and Figure 42. The installation method of the PID temperature controller thermocouple was also changed for this test. During test preparation, the soldered connection of the washer tip to the thermocouple wires failed and the washer tip separated from the wires. The exposed wires of the PID temperature controller thermocouple were twisted to touch and covered with aluminum tape. These ends were then taped to the surface of the platen with polyimide tape in the location shown in Figure 40.

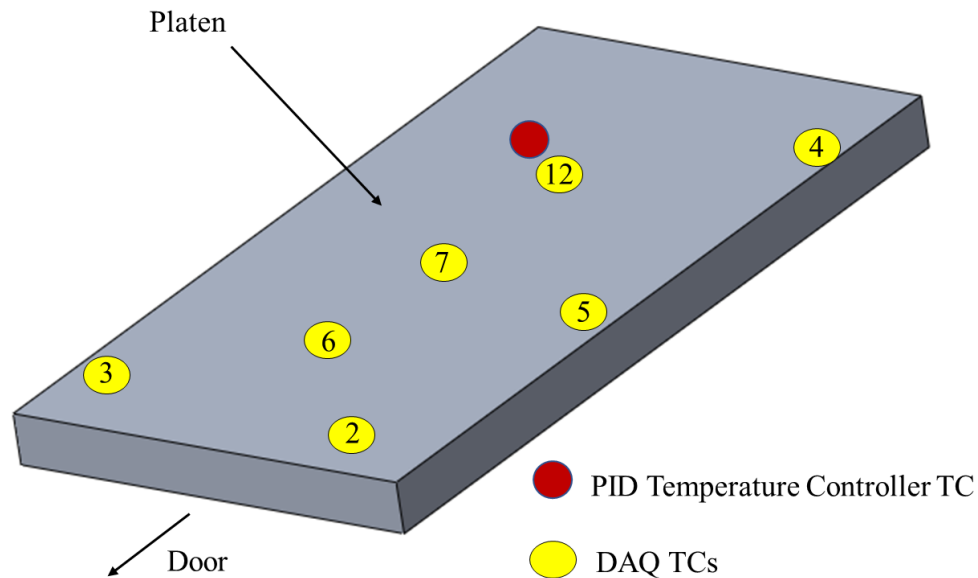


Figure 40: Thermocouple Configuration on Platen for Test 12

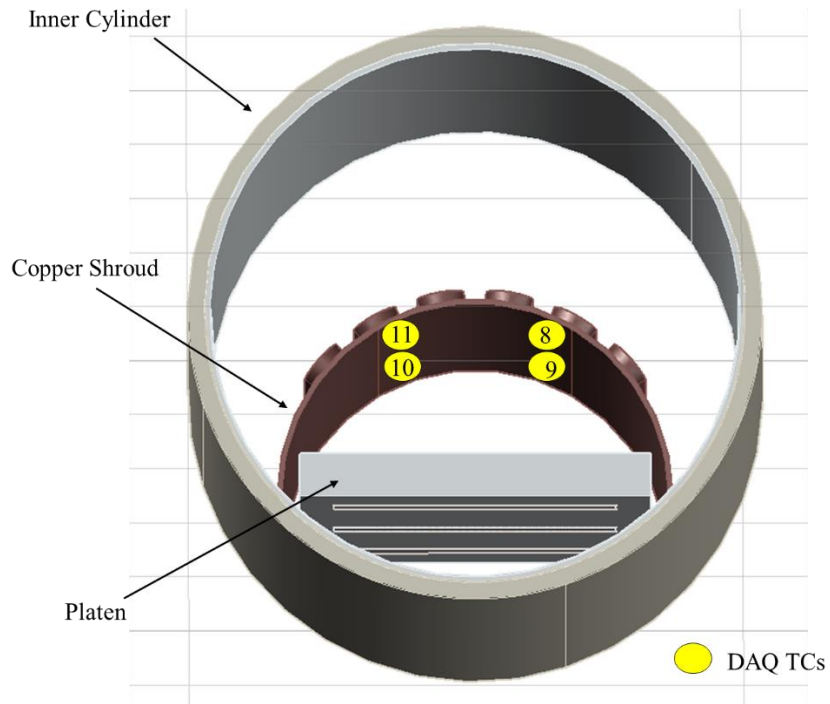


Figure 41: Thermocouple Configuration on Copper Shroud for Test 12

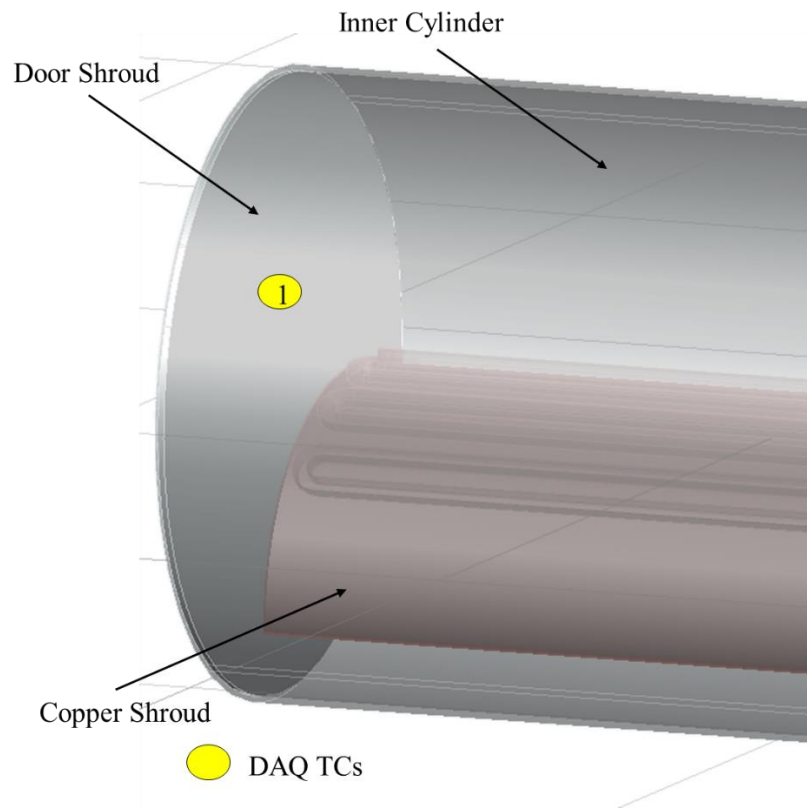


Figure 42: Thermocouple Configuration on Door Shroud for Test 12

The hypothesis that the temperature measurement discrepancies were caused by inconsistent thermocouple types was proven true as the results showed agreement between the PID temperature controller temperature readings and the new T type thermocouple readings. The temperature of the platen surface during Test 12 is shown in Figure 43. Note that the readings from the PID temperature controller thermocouple were not recorded, but the display screen showed that the platen was at a temperature of -22°C during the cold soak and 65°C during the hot soak. The cold soak was also abbreviated by approximately 15 minutes due to an operational error made. The temperature of the copper shroud surface and door shroud during Test 12 are shown in Figure 44.

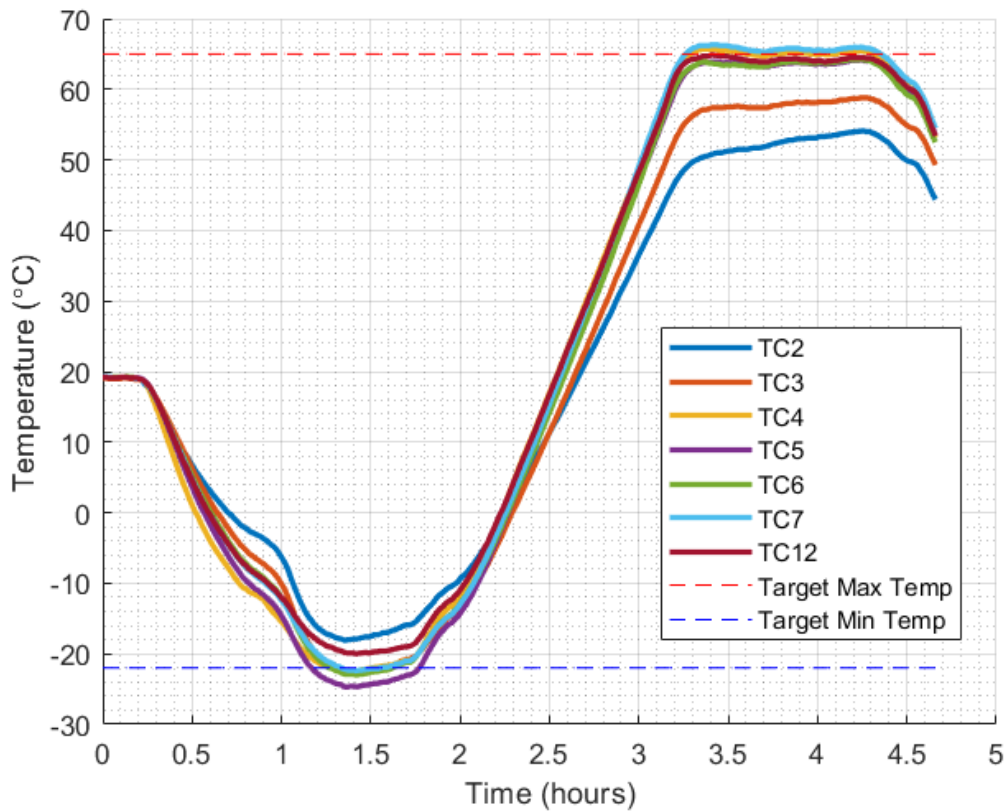


Figure 43: Thermal Response of Platen During Test 12

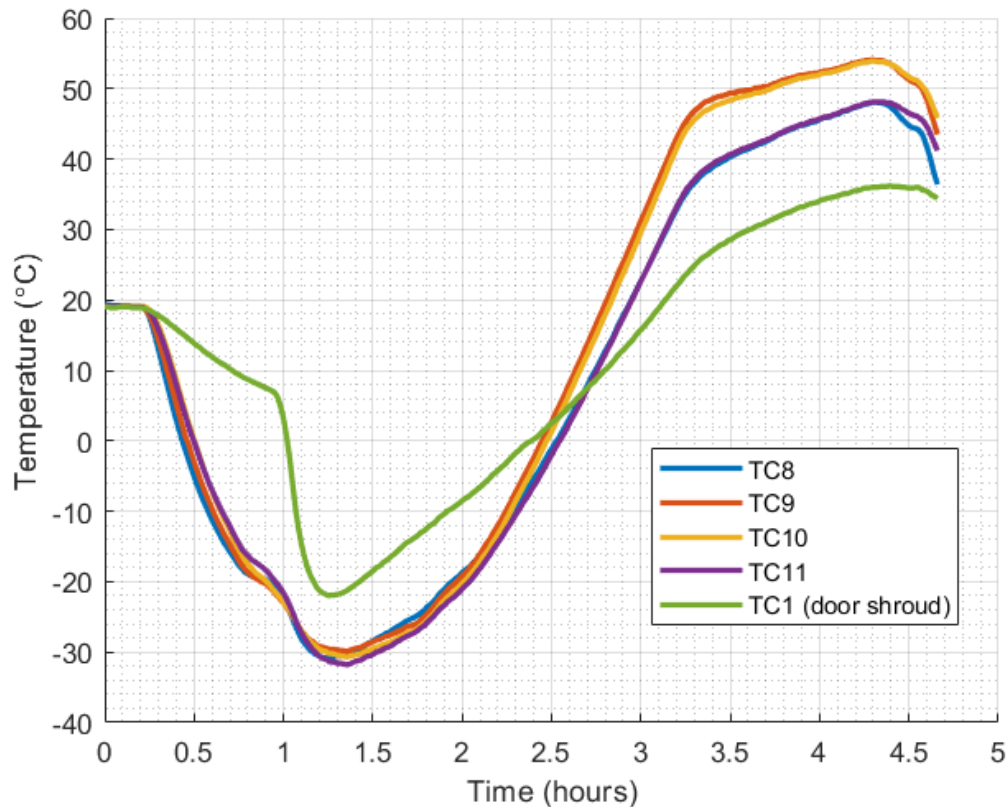


Figure 44: Thermal Response of Copper Shroud and Door Shroud During Test 12

Figure 43 shows that during the cold soak, the average temperature of the seven DAQ thermocouples on the platen was approximately 1°C greater than the PID temperature controller measurement. During the hot soak, the average temperature of the platen varied by approximately 3°C from the PID temperature controller measurement. It was also observed that the previous rate of increase in temperature during the cold soak and hot soak was decreased in this test. This variation conforms with the temperature tolerance of $\pm 3^{\circ}\text{C}$ required by the ISO Standard 19683. Data from TC2 and TC3 shows that the front area of the platen was warmer during the cold soak and cooler during the hot soak than the rest of the platen.

As shown in Figure 44, the rear end of the copper shroud tended to be about 7°C warmer than the front end of the shroud during the hot soak. The sudden decrease in temperature observed by all thermocouples after about one hour is when the door shroud LN₂ valve was

opened and allowed LN₂ to flow to the door shroud for about five minutes before it was closed for the remainder of the test. This operation followed a brief period of time that the set ramp rate was decreased to allow the LN₂ dewar to regain sufficient pressure, which is why the copper shroud and platen experience a decreased cooling rate at approximately 45 minutes.

Test 13 was conducted to verify these results and establish a repeatable trend in the observed temperature distribution across the platen surface. For Test 13, the thermocouples were repositioned to collect more data from the surface of the platen. The thermocouple configuration used for this test is shown in Figure 45.

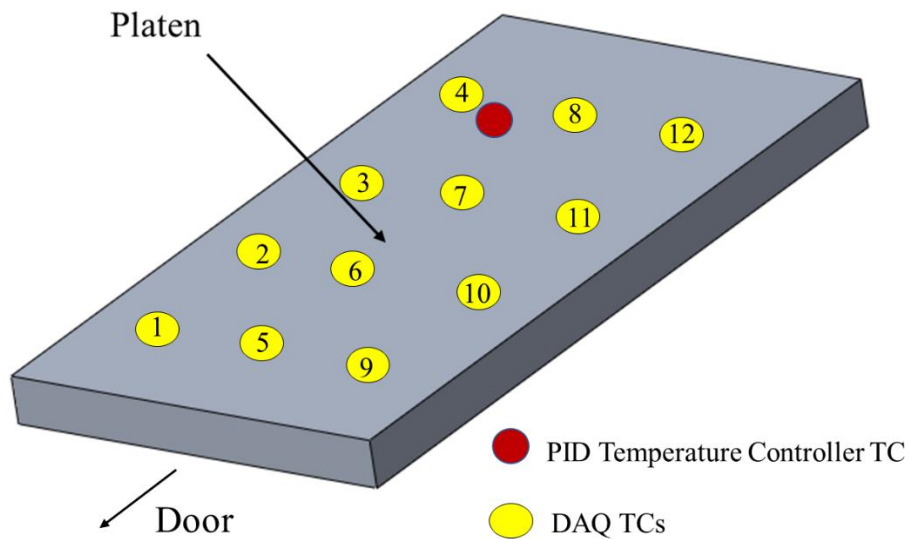


Figure 45: Thermocouple Configuration for Test 13

This test verified that the new T type thermocouples did reduce the discrepancy in temperature readings. Figure 46 shows the temperatures of the platen during this test. Note that the second cold soak at -15°C was not completed because the LN₂ supply was expended during the second cooling phase.

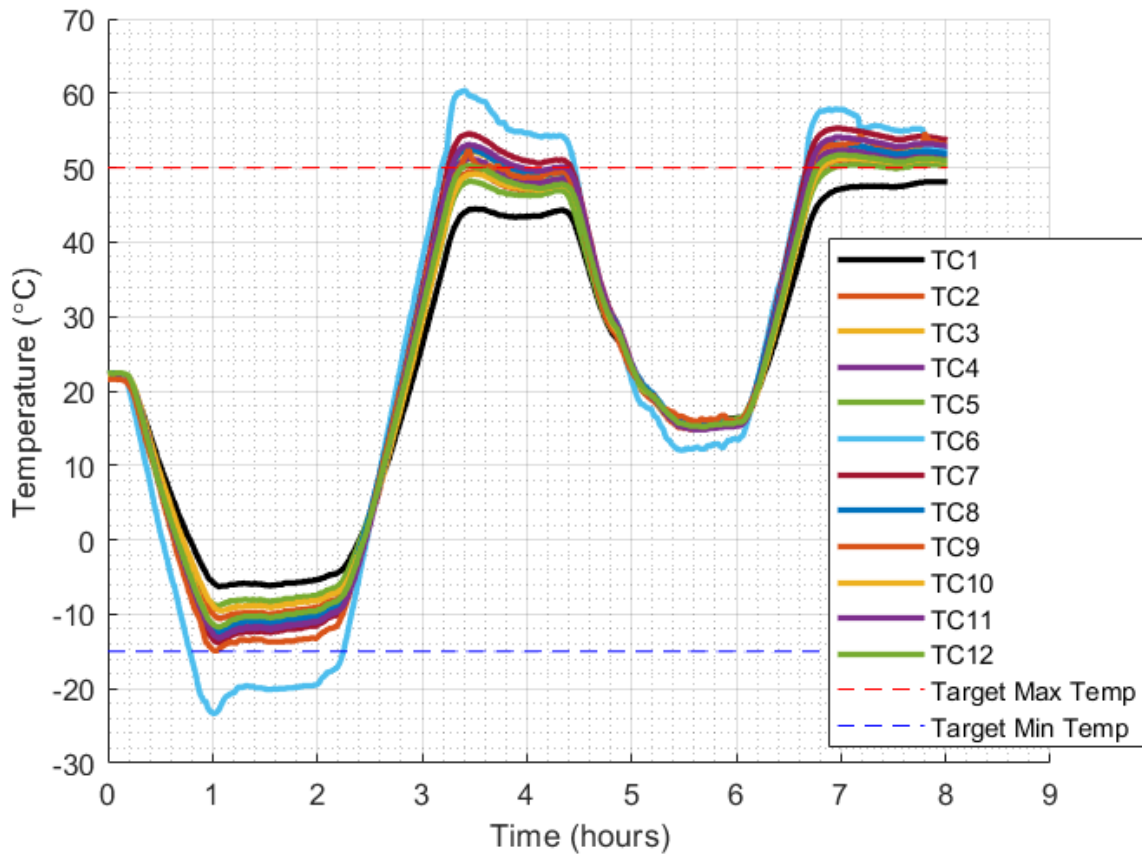


Figure 46: Thermal Response of Platen During Test 13

This test revealed a trend in the temperature distribution across the platen. The front left area of the platen, measured by TC1, was measured to be over 2°C colder than the other areas during the first cold soak and both hot soaks, which is greater than the standard limit of error of $\pm 1^\circ\text{C}$ in the measurement. TC6, which was positioned on the middle front area of the platen, also measured temperatures that varied significantly from the rest of the thermocouples. This thermal response was not observed in Test 12 and indicates a potentially poor connection between this thermocouple and the platen surface. While the temperature during the first cold soak was observed to have increased by approximately 2°C, this increase was also measured by the PID temperature controller, which displayed a temperature of -13°C for the majority of the first cold

soak. The decrease of approximately 4°C during the first hot soak was also measured by both the PID temperature controller and the twelve DAQ thermocouples.

As shown, during the first cold soak, the measured temperatures were still approximately 4°C greater than the target temperature of -15°C. This is due to a consistently observed issue with the cooling system. The PID temperature controller allows $\pm 1^\circ\text{C}$ of variance in temperature from the target temperature during a soak. When the platen temperature is greater than $\pm 1^\circ\text{C}$ from the target temperature, the PID temperature controller outputs power to either heat or cool the platen to maintain the target temperature. During this cold soak, it was observed that the PID temperature controller measured a temperature of -13°C, which was greater than the target temperature of $-15 \pm 1^\circ\text{C}$, so the LN₂ flow rate was increased in an attempt to lower the platen temperature again. This flow rate was not high enough to cool the chamber during the one hour cold soak, which is why the DAQ thermocouples also measured temperatures of -13°C to -10°C, on average during the first cold soak. This phenomenon of insufficient LN₂ flow occurred throughout testing and will be discussed in more detail in Chapter 7.

During Test 13, the LN₂ flow to the door shroud was not activated in an attempt to conserve the LN₂ supply. In preliminary testing, it was observed that manually activating LN₂ flow to the door shroud did not significantly influence the temperature of the platen. Since the LN₂ flow to the door shroud must be manually controlled, it is difficult to reach and maintain the target temperatures with $\pm 3^\circ\text{C}$ margin due to the delayed thermal response of the door shroud and the delay in the thermocouple reading of the door shroud temperature that is displayed on the chamber. For these reasons, it was decided to leave the door shroud LN₂ valve closed for the entirety of the test.

6.4 Empty Thermal Vacuum Simulation Results

The data from Tests 12 and 13 was used to verify the thermal model results. After setting up the numerical model in Thermal Desktop as described in Section 5.2, an empty cold soak

simulation was conducted to predict the temperature of the platen and other surfaces in the chamber during the cooling phases of the thermal vacuum test. Figure 47-49 show the temperatures of the various modeled elements after the one hour cooling phase from an initial ambient temperature of 22°C. This simulates the initial one hour cooling phase that was measured in Test 13.

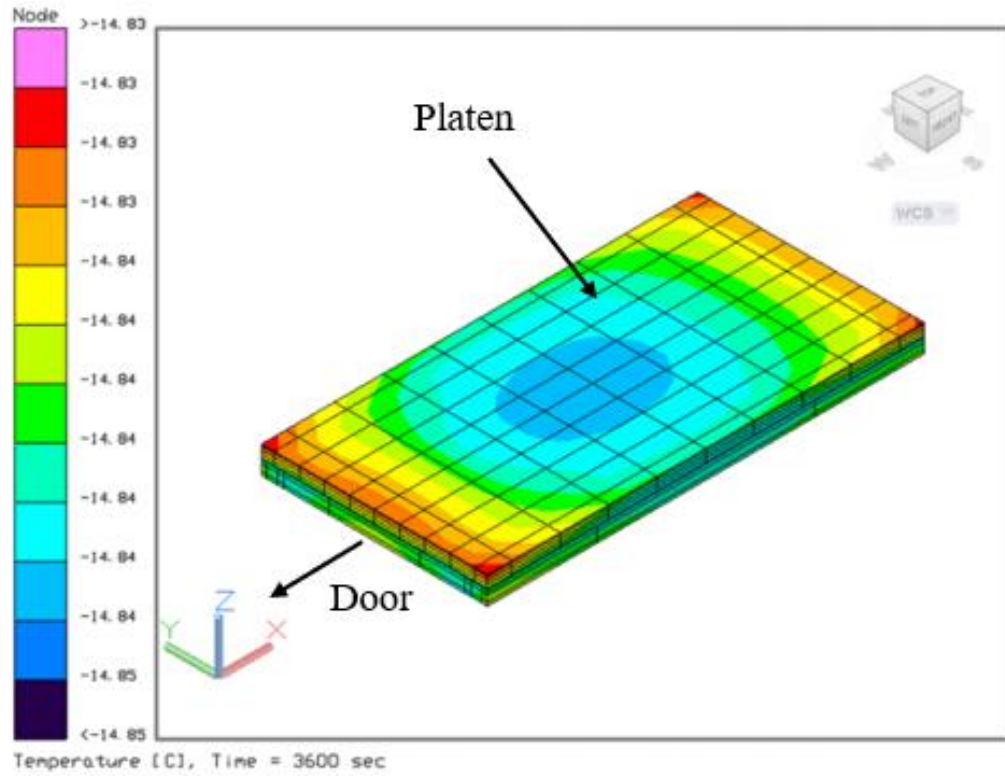


Figure 47: Predicted Temperature of Platen After Empty Cooling Phase

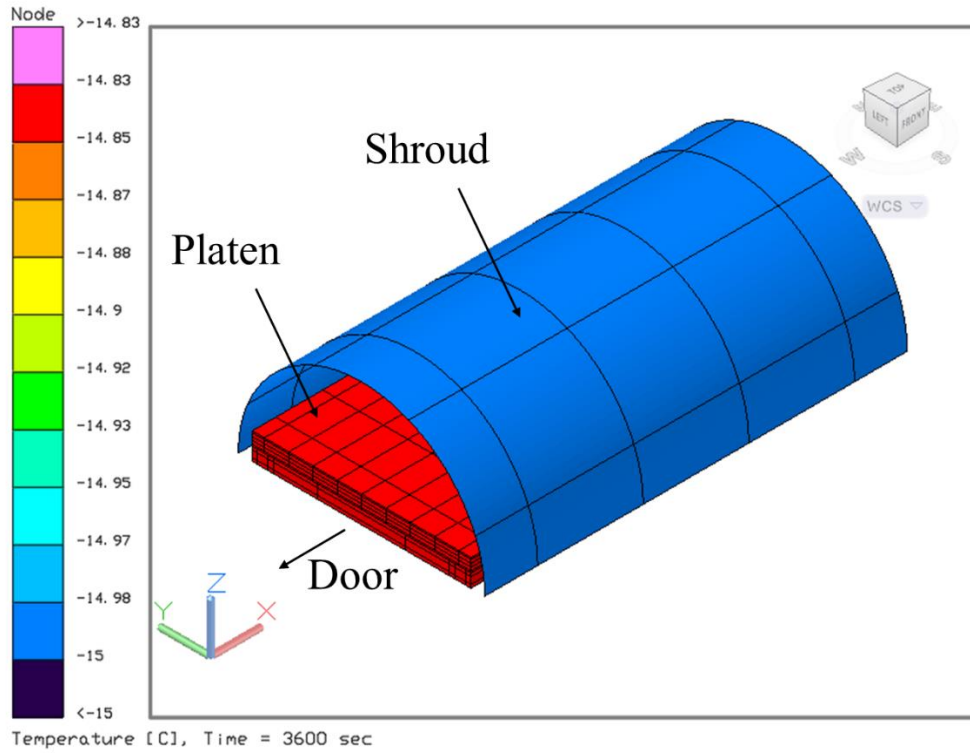


Figure 48: Predicted Temperature of Shroud After Empty Cooling Phase

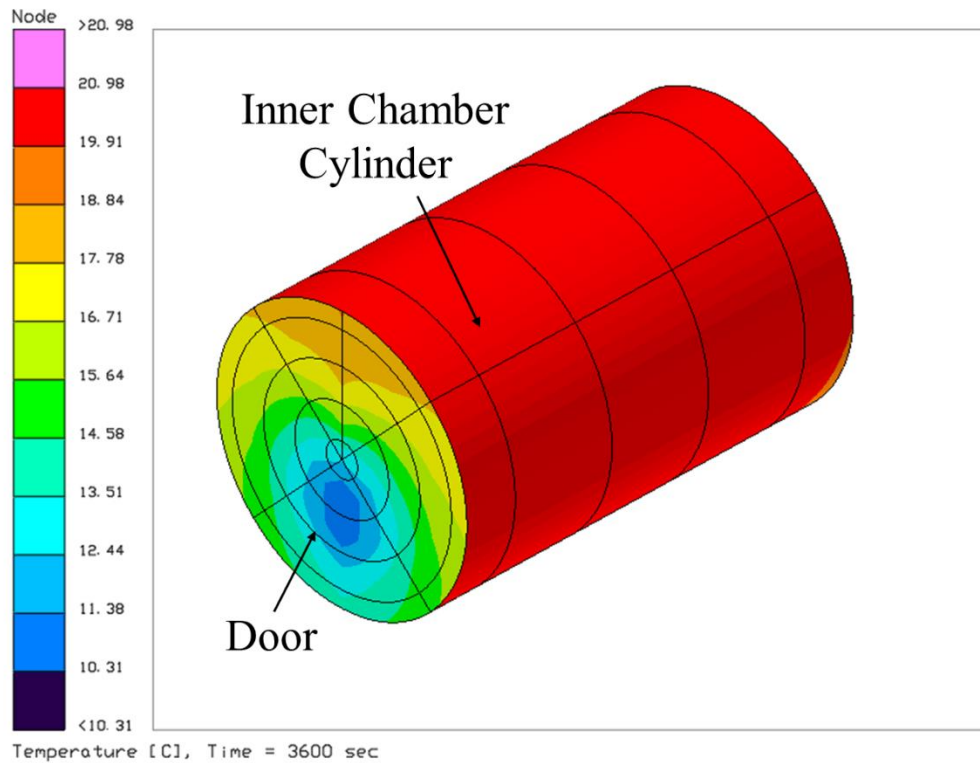


Figure 49: Predicted Temperature of Inner Cylinder and Door After Empty Cooling Phase

As shown in Figure 47, the platen reaches a temperature of approximately -14.8°C after one hour of cooling from the surfaces modeling the LN₂ flow in the platen and across the copper shroud. The simulation results show a variation of approximately 0.02°C in temperature across the surface of the platen after one hour. As shown in Figure 48, the copper shroud reaches a temperature of -15°C. Figure 49 shows that the inner chamber cylinder cools to a temperature of approximately 20°C while the door shroud ranges in temperatures of approximately 10°C to 21°C.

The results from the simulations of the cooling phase of the empty thermal vacuum test were compared to the results from Tests 12 and 13. The average temperature presented from the test results used for comparison is the instantaneous average DAQ thermocouple reading after one hour of cooling. Since these readings are changing during the test, the comparisons are approximate and are dependent on the defined time duration of the cooling phase used for comparisons. The comparison between the test data and the model predictions of the approximate surface temperatures of the various elements in the chamber after one hour of cooling are shown in Table 9.

Table 9: Empty Cooling Phase Temperature Comparison

Element	Simulation Temperature (°C)	Test 12 Average Temperature (°C)	Test 13 Average Temperature (°C)	Difference (°C)
Platen	-14.8	-12.5	-12.3	2.3-2.5
Copper Shroud	-15	-22	n/a	7
Door Shroud	10-21	4.8	n/a	5.2-16.2
Inner Chamber Cylinder	20	n/a	n/a	n/a

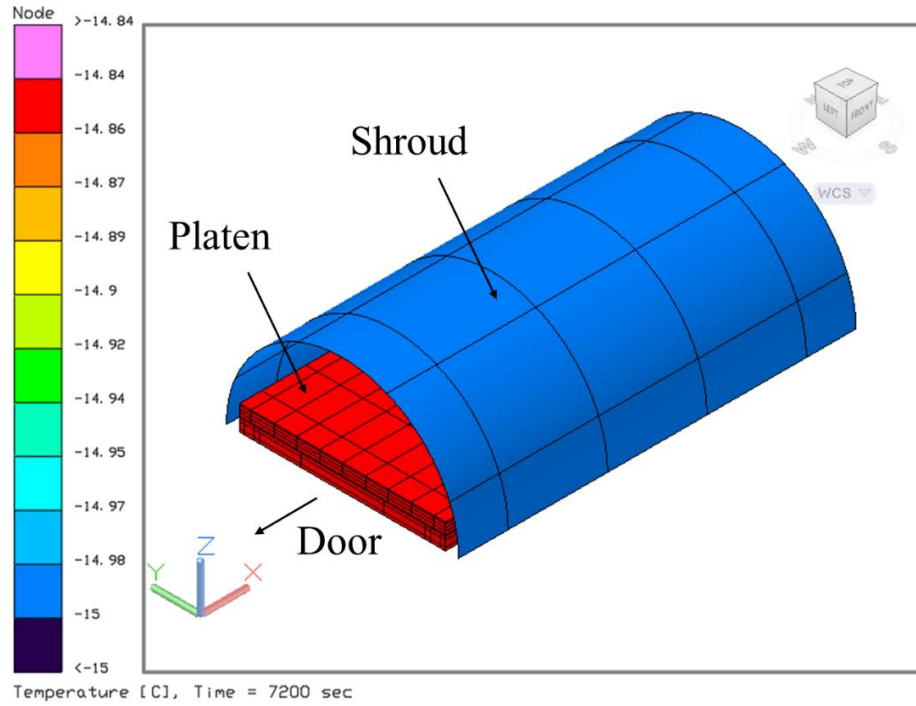


Figure 51: Predicted Temperature of Shroud After Empty Cold Soak

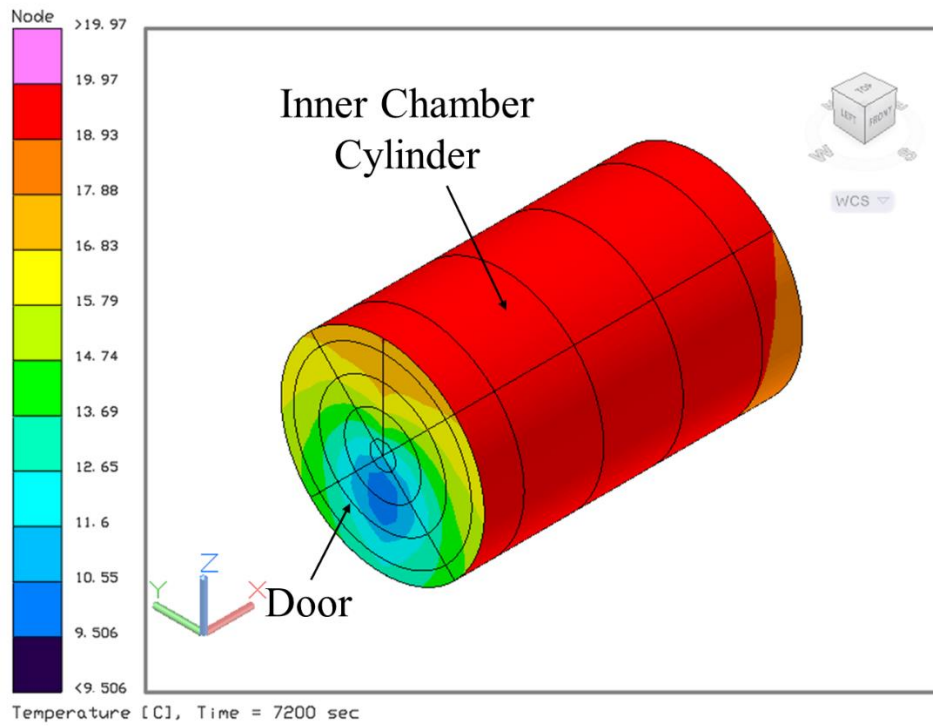


Figure 52: Predicted Temperature of Inner Cylinder and Door After Empty Cold Soak

As shown in Figure 50, the platen maintains a temperature of approximately -14.8°C after the one hour cold soak. The simulation results now show a variation of approximately 0.01°C in temperature across the surface of the platen after a total of 120 minutes. As shown in Figure 51, the copper shroud maintains a temperature of -15°C . Figure 52 shows that the inner chamber cylinder cools to a temperature of approximately 19°C while the door shroud ranges in temperatures of approximately 9°C to 17°C .

The results from the simulations of the cold soak of the empty thermal vacuum test were compared to the results from Tests 12 and 13. The average temperature presented from the test results used for comparison is the instantaneous average DAQ thermocouple reading after one hour cold soak. Since these readings are changing during the test, the comparisons are approximate and are dependent on the defined time duration of the cold soak used for comparisons. The comparison between the test data and the model predictions of the approximate surface temperatures of the various elements in the chamber after the one hour cold soak are shown in Table 10. Note that for Test 12, the cold soak temperature was set to -20°C so the data from this test are shown but not used for comparison to the simulation.

Table 10: Empty Cold Soak Temperature Comparison

Element	Simulation Temperature ($^{\circ}\text{C}$)	Test 12 Average Temperature ($^{\circ}\text{C}$)	Test 13 Average Temperature ($^{\circ}\text{C}$)	Difference ($^{\circ}\text{C}$)
Platen	-14.8	-20	-10	4.8
Copper Shroud	-15	-27	n/a	n/a
Door Shroud	9-17	-15	n/a	n/a
Inner Chamber Cylinder	19	n/a	n/a	n/a

As shown in the right most column of Table 10, the difference in the temperatures predicted by the simulation and the test results for the platen is within the acceptable 15°C thermal uncertainty margin.

After simulating the cold soak phase of the empty thermal vacuum test, the heating phase and hot soak phase were simulated. For the heating phase, the initial temperatures of each element were assumed to be the respective final temperatures from the cold soak simulation. The assumed duration of the heating phase was based on the duration of heating observed in Test 13, which was approximately 1.3 hours. Figure 53-55 show the resulting surface temperature at the end of the heating phase.

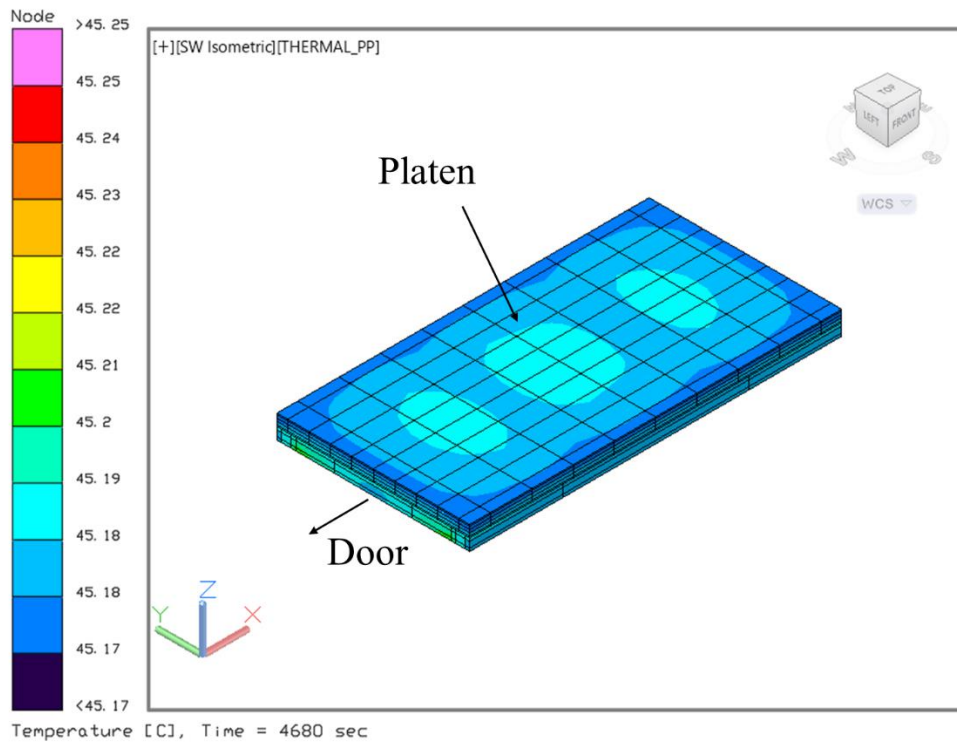


Figure 53: Predicted Temperature of Platen After Empty Heating Phase

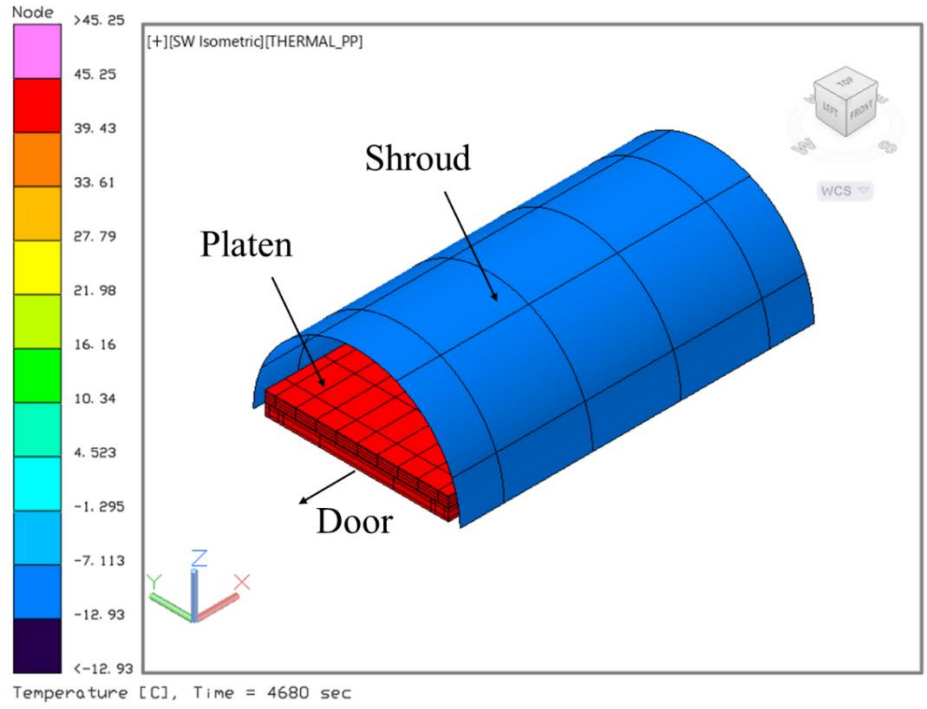


Figure 54: Predicted Temperature of Shroud After Empty Heating Phase

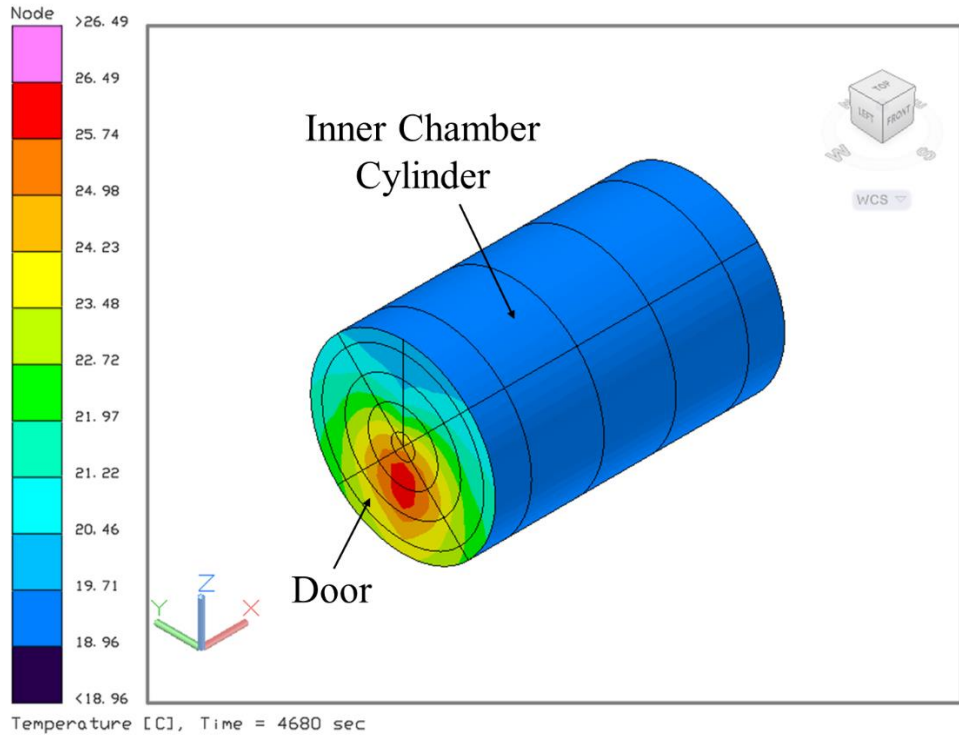


Figure 55: Predicted Temperature of Inner Cylinder and Door After Empty Heating Phase

As shown in Figure 53, the platen reaches a temperature of approximately 45°C after the 1.3 hour heating phase. The simulation results show a variation of approximately 0.02°C in temperature across the surface of the platen with the edges being slightly cooler than the middle regions. As shown in Figure 54, the copper shroud warms to a temperature of approximately -13°C. Figure 55 shows that the inner chamber cylinder heats to a temperature of approximately 19°C while the door shroud ranges in temperatures of approximately 20°C to 26°C with the bottom half being warmer than the top half.

The results from the simulations of the 1.3 hour heating phase of the empty thermal vacuum test were compared to the results from Tests 12 and 13. The average temperature presented from the test results used for comparison is the instantaneous average DAQ thermocouple reading after 1.3 hours of heating. Since these readings are changing during the test, the comparisons are approximate and are dependent on the defined time duration of the heating phase used for comparisons. The comparison between the test data and the model predictions of the approximate surface temperatures of the various elements in the chamber after 1.3 hours of heating are shown in Table 11. Note that for Test 12, the hot soak temperature was set to 65°C so the data from this test is shown but is not used for comparison to the simulation.

Table 11: Empty Heating Phase Temperature Comparison

Element	Simulation Temperature (°C)	Test 12 Average Temperature (°C)	Test 13 Average Temperature (°C)	Difference (°C)
Platen	45.2	61	51.4	6.2
Copper Shroud	-13	41	n/a	n/a
Door Shroud	20-26	25	n/a	n/a
Inner Chamber Cylinder	19	n/a	n/a	n/a

As shown in the right most column of Table 11, the difference in the temperatures predicted by the simulation and the test results for the platen is within the acceptable 15°C thermal uncertainty margin. The simulation predicts that the copper shroud only warms by about 2°C during the heating phase while the results from Test 12 show that the copper shroud heats by about 60°C during the heating phase. This indicates that the copper shroud may have a higher emissivity than what is modeled.

The one hour hot soak was then simulated by running this simulation for a total of 2.3 hours with the same initial temperatures. Figure 56-58 show the resulting surface temperatures at the end of the hot soak phase.

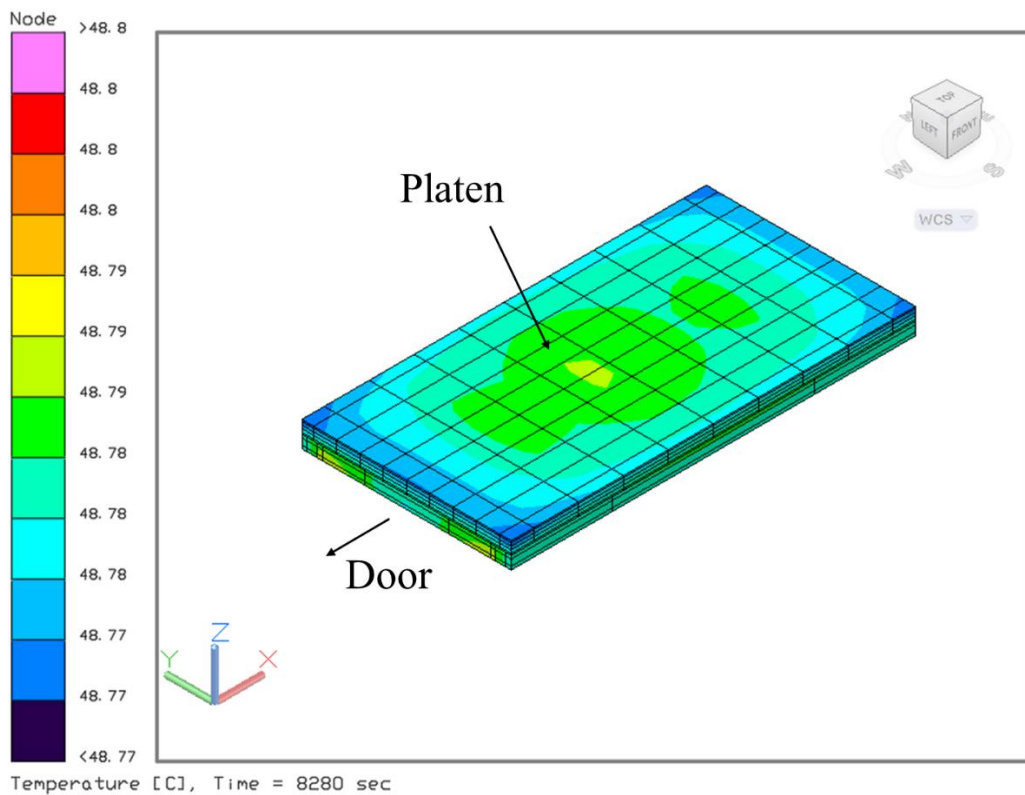


Figure 56: Predicted Temperature of Platen After Empty Hot Soak

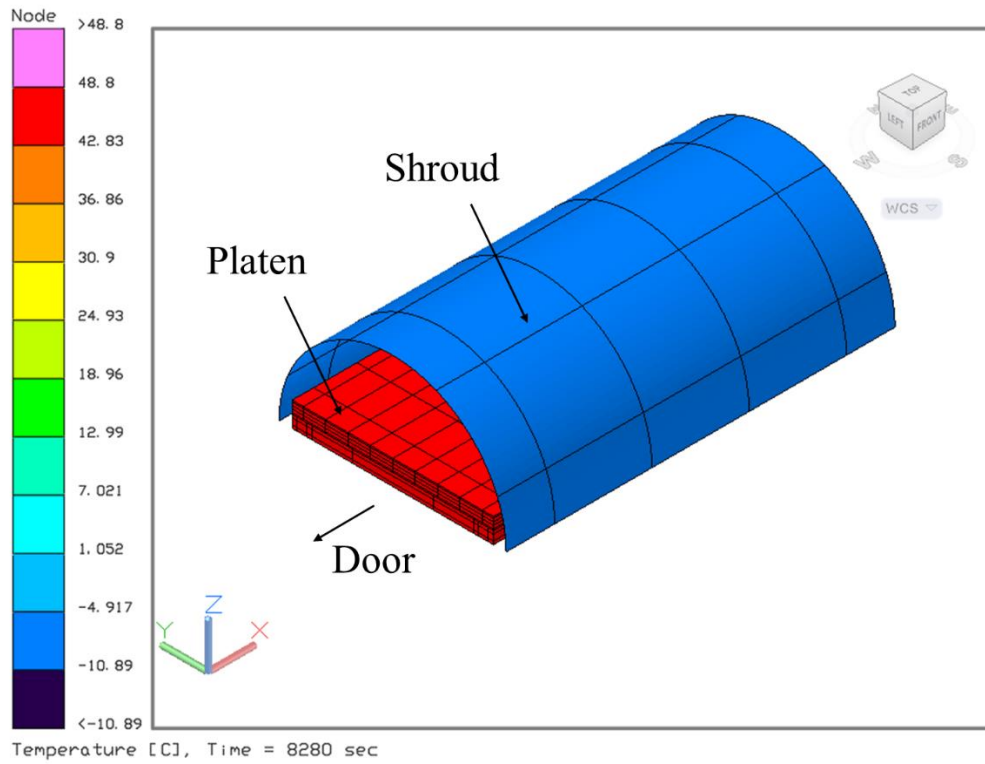


Figure 57: Predicted Temperature of Shroud After Empty Hot Soak

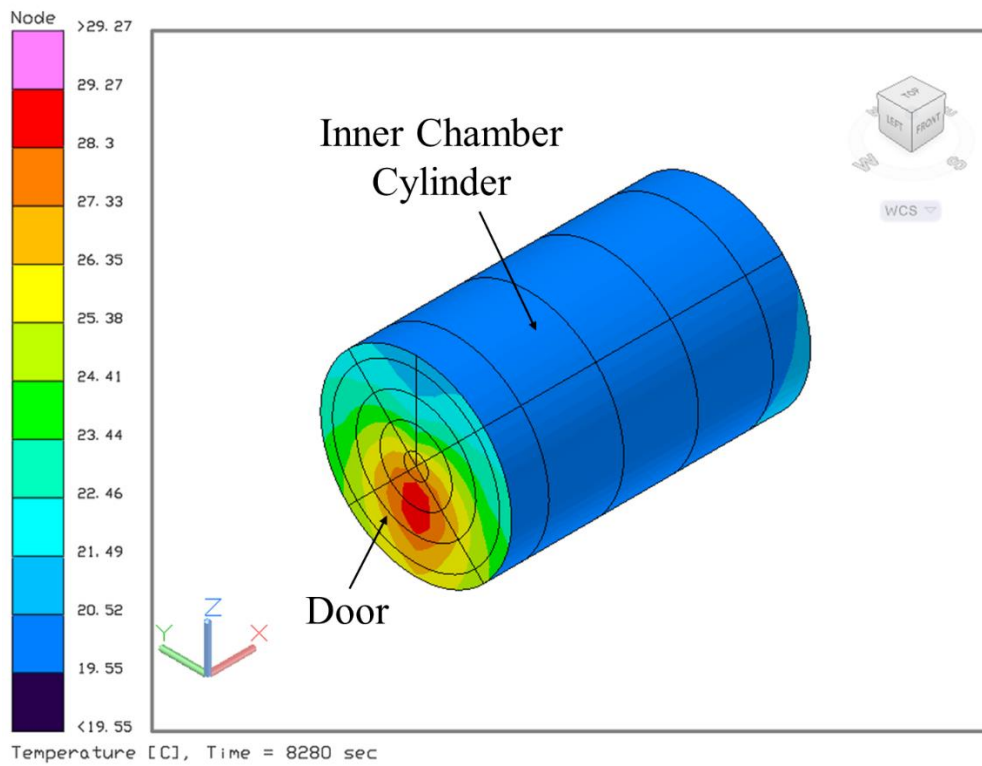


Figure 58: Predicted Temperature of Inner Cylinder and Door After Empty Hot Soak

As shown in Figure 56, the platen reaches a temperature of approximately 48.8°C after the one hour hot soak. The simulation results show a variation of approximately 0.03°C in temperature across the surface of the platen with the edges being slightly cooler than the middle regions. As shown in Figure 57, the copper shroud warms to a temperature of approximately -11°C. Figure 58 shows that the inner chamber cylinder heats to a temperature of approximately 19.5°C while the door shroud ranges in temperatures of approximately 21°C to 29°C with the bottom half being warmer than the top half.

The results from the simulations of the one hour hot soak phase of the empty thermal vacuum test were compared to the results from Tests 12 and 13. The average temperature presented from the test results used for comparison is the instantaneous average DAQ thermocouple reading after the one hour hot soak. Since these readings are changing during the test, the comparisons are approximate and are dependent on the defined time duration of the hot soak phase used for comparisons. The comparison between the test data and the model predictions of the approximate surface temperatures of the various elements in the chamber after the one hour hot soak are shown in Table 12. Note that for Test 12, the hot soak temperature was set to 65°C so the data from this test is shown but is not used for comparison to the simulation.

Table 12: Empty Hot Soak Temperature Comparison

Element	Simulation Temperature (°C)	Test 12 Average Temperature (°C)	Test 13 Average Temperature (°C)	Difference (°C)
Platen	48.8	62	48.8 (1 st cycle) 51.6 (2 nd cycle)	0 (1 st cycle) 2.8 (2 nd cycle)
Copper Shroud	-11	51	n/a	n/a
Door Shroud	20-28	36	n/a	n/a
Inner Chamber Cylinder	19	n/a	n/a	n/a

As shown in the right most column of Table 12, the difference in the temperatures predicted by the simulation and the test results for the platen is within the acceptable 15°C thermal uncertainty margin. Since the platen temperature predicted by the simulation was validated by the thermal vacuum test results, a test article was integrated into the test and simulation to further validate the thermal model.

6.5 Test Article Thermal Vacuum Test Results

Tests 14 and 15 were conducted with a 3U CubeSat mass model to establish a trend in thermal response of the chamber when a test article is included in the thermal vacuum test. The data from these tests was then used to validate the thermal simulations of the thermal vacuum test with the test article. The results from these simulations are presented in Section 6.6. The test article was placed on four Teflon cylinder supports of radius 2.4 cm and height of 1.4 cm to minimize conductive heat transfer from the platen to the mass model. The thermocouple configuration on the mass model is shown in Figure 59 and Figure 60.

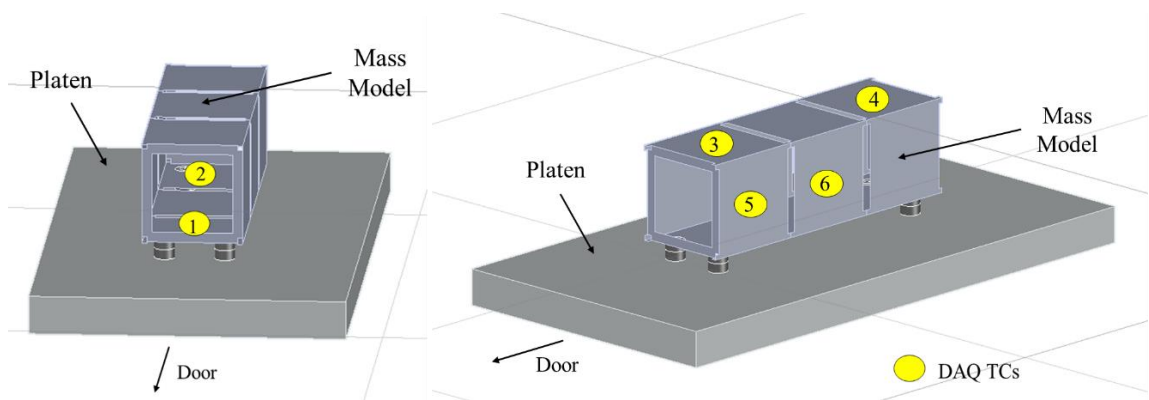


Figure 59: Thermocouple Configuration on Mass Model for Tests 14 and 15 (Right, Top and Bottom Sides)

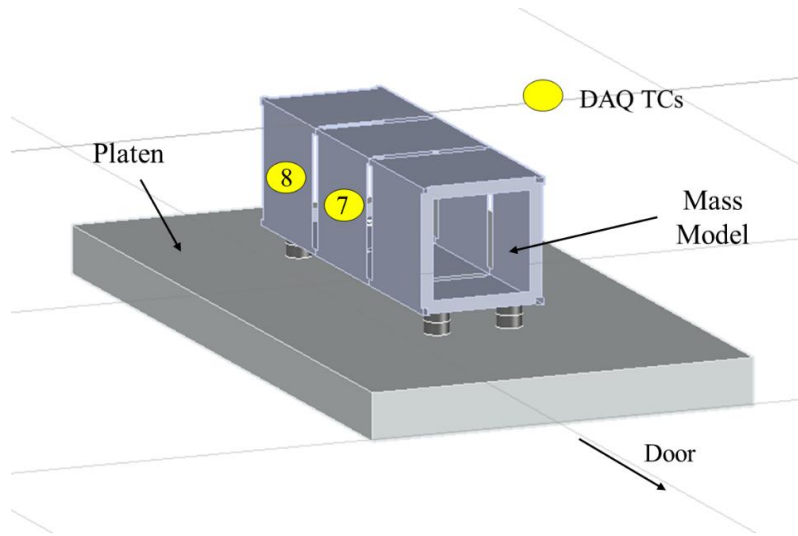


Figure 60: Thermocouple Configuration on Mass Model for Tests 14 and 15 (Left Side)

Figure 59 and Figure 60 shows three views of the mass model on the platen supported by the Teflon cylinders. As shown in the top left image, TC1 and TC2 were secured to the interior faces of the bottom panels. All other thermocouples were secured to the exterior faces of the panels. The thermocouple configuration on the surface of the platen is shown in Figure 61. In this figure, the mass model is represented by a dashed black line.

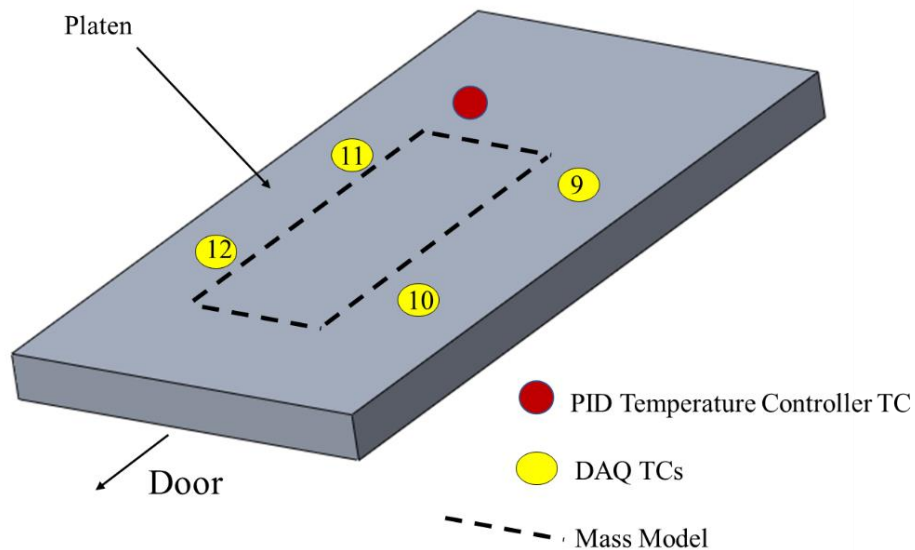


Figure 61: Thermocouple Configuration on Platen for Tests 14 and 15

6.5.1 Test 14 Results

For Test 14, the DAQ thermocouples were secured to the surface of the platen and the mass model surfaces with polyimide tape. The twisted wires on the end of the PID temperature controller thermocouple were covered with aluminum tape and secured to the surface of the platen with polyimide tape. The temperatures measured by the DAQ thermocouples are shown in Figure 62.

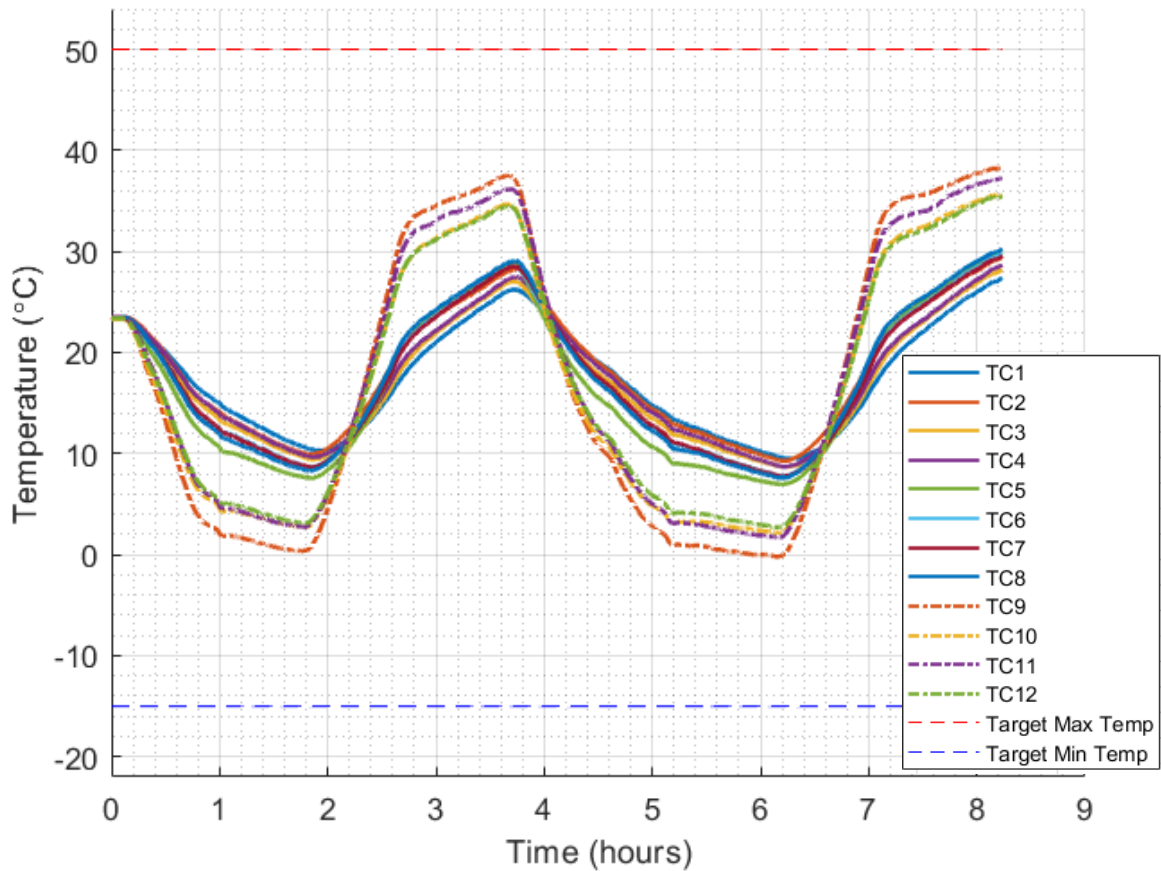


Figure 62: Thermal Response of Platen and Mass Model During Test 14

In Figure 62, the measurements of the mass model are shown as solid lines while the measurements of the platen are shown as dashed lines. New observations were made from the data collected during Test 14. As shown in Figure 62, the DAQ thermocouple measurements of the platen surface show that the platen does not reach the set soak temperatures of -15°C and 50°C. In contrast, during the soaks, the PID temperature controller did display readings of -15°C

and 50°C at these times. Similar to Tests 1-11, there was an observed discrepancy between the DAQ thermocouple readings and the PID temperature controller thermocouple readings of the platen temperature. During the cold soaks, this discrepancy was approximately 17°C to 21°C while during the hot soaks it was approximately 14°C to 19°C.

The four DAQ thermocouples on the platen also measured a decreasing temperature during the cold soak and an increasing temperature during the hot soak. This change of approximately 2-4 °C/min during the hot and cold soaks would be investigated further during Test 15.

Figure 62 shows that the change in temperature across the mass model was less than that of the platen surface, which was expected as the primary mode of heat transfer to the mass model was radiation. During the test, the measured temperature difference between the mass model and the platen was approximately 7°C to 10°C during the cold and hot soak phases.

Before Test 15 was conducted, the root cause of the discrepancy in temperature measurements between the DAQ thermocouples and the PID temperature controller that was only observed with the addition of the mass model was investigated. Several hypotheses were made to explain this phenomenon. It was initially suspected that there was a hardware malfunction with the PID temperature controller thermocouple. After inspecting the connections of the thermocouple to the controller unit and noticing no faults with this connection, this hypothesis was ruled out. Note that further examination of the PID temperature controller wires would involve invasive operations to remove the wires from the feedthrough to the chamber, which may risk the integrity of the vacuum seal at the feedthrough port.

Another hypothesis was made that the PID temperature controller was not configured correctly for the thermocouple it uses. After reviewing the configuration settings of the PID temperature controller, it was discovered that the PID temperature controller is configured for a T type thermocouple. It is assumed that the thermocouple currently in use is a T type since this

thermocouple has no color coding or labeling. It is also assumed that the PID temperature controller is configured correctly for this thermocouple.

Finally, it was theorized that the root cause of the discrepancy in the measurements was due to an inconsistency in the application method of the thermocouples on the platen. The PID temperature controller thermocouple wires were connected with aluminum tape before being secured to the surface of the platen with polyimide tape while the DAQ thermocouples were secured to the surfaces with only polyimide tape. With the aluminum tape addition, the PID temperature controller thermocouples were measuring the temperature of a material that was in direct contact with the platen material which has similar thermo-optical properties. The DAQ thermocouples likely had greater area specific contact resistance with the surface of the platen as it was observed that sometimes, a small gap would remain between the platen surface and the beaded end of the thermocouple, even with the polyimide tape applied.

The hypothesis was that the difference in the thermocouple application methods used resulted in a difference in the contact resistance between the thermocouples and the platen for the PID temperature controller thermocouple versus the DAQ thermocouples. While the PID controller thermocouple was predominantly influenced by the conductive heat transfer from the platen, the DAQ thermocouples were influenced by this, but also by the radiative heat transfer to and from the surfaces of the mass model. According to [23], thermocouples should be applied with tape of similar thermo-optical properties as the surface it is to be attached to. Test 15 would be conducted with consistent thermocouple application methods in an attempt to decrease the temperature discrepancy observed in Test 14.

6.5.2 Test 15 Results

For Test 15, the hypothesis that the temperature discrepancy between the platen measurements observed in Test 14 was caused by inconsistent application methods was tested. It was decided that the DAQ thermocouple beaded ends would also be covered by aluminum tape

before being attached to the surface of the platen and mass model. Figure 63 shows how the aluminum tape was attached to the end of the thermocouples.



Figure 63: DAQ Thermocouple with Aluminum Tape Attached

The consistent application method would ensure that all thermocouples had approximately equal contact resistances between the thermocouple and the surface of the platen. The thermocouples were positioned in the same locations as Test 14, shown in Figure 59-61 above. One cycle was conducted with two hour hot and cold soaks to verify the temperature trends observed during the soaks of Test 14. The results from Test 15 are shown in Figure 64.

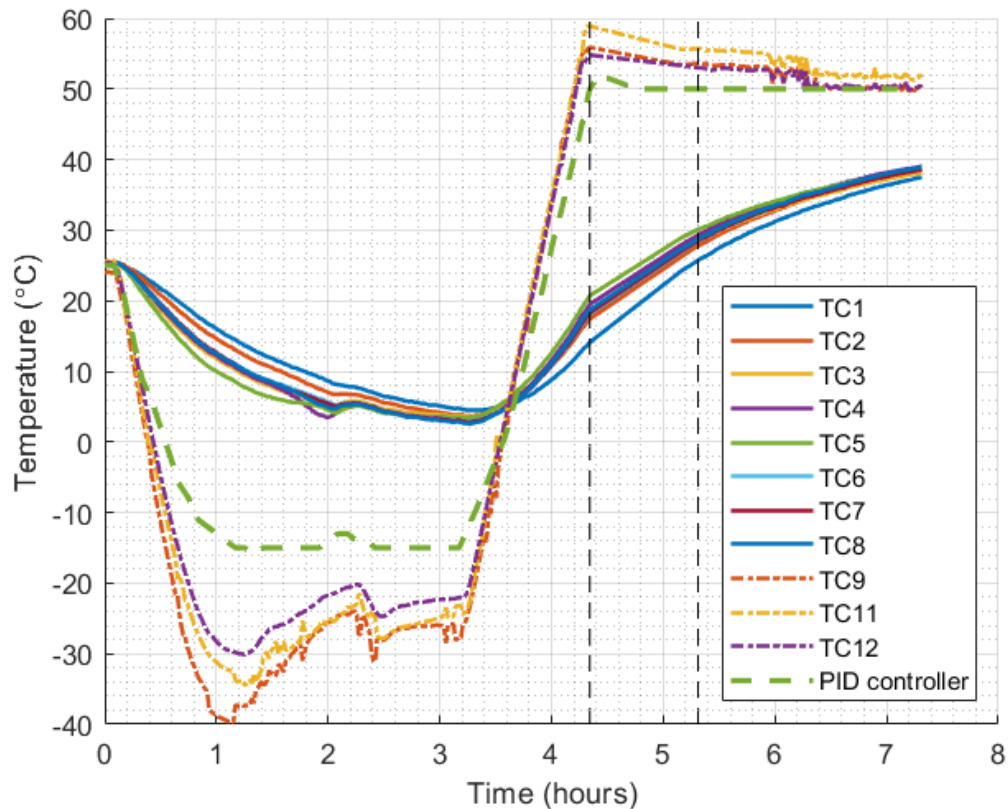


Figure 64: Thermal Response of Platen and Mass Model During Test 15

For Test 15, the temperature displayed by the PID temperature controller was recorded by hand approximately once every five minutes. These measurements are shown by the green dashed line in Figure 64. During Test 15, the DAQ temperature recorder batteries died, and it ceased data collection after approximately 4.3 hours. The lack of data collection was noticed after about an hour at which time the batteries were replaced, and the data collection resumed. The dashed vertical lines shown in Figure 64 at approximately 4.3 hours and 5.3 hours represent the start and end time of no data collection. Between these dashed lines, the DAQ data is linearly interpolated. It was also observed that the taped connection of TC10 to the platen surface failed during the test so the data from this thermocouple is not shown as it did not measure the platen surface temperature.

As shown, after approximately one hour of cooling, the average temperature of the platen was approximately -33°C . After the two hour cold soak, the average platen temperature increased to approximately -24°C . This was approximately 9°C to 18°C less than the recorded PID temperature controller measurement. After one hour of heating, the average temperature of the platen was approximately 56°C . After the two hour hot soak, the average platen temperature decreased to approximately 51°C . This was approximately 1°C to 4°C greater than the PID recorded PID temperature controller measurement. The new discrepancies in the measured temperatures indicate that the application method of the thermocouples does have an effect on the temperature measurement. Recommendations for further decreasing this discrepancy are presented in Chapter 8.

As shown in Figure 64, the surfaces of the mass model vary in temperature by approximately 2°C to 6°C during the test. The bottom interior surfaces measured by TC1 and TC2 tend to stay warmer than the other surfaces during the cold soak and cooler than the other surfaces during the hot soak. This indicates that the 3U CubeSat mass model walls provide insulation to the interior section of the mass model. Recommendations for testing the insulative properties of the mass model are presented in Chapter 8.

Since the results from Test 15 showed a decreased discrepancy between the average platen temperature readings from the DAQ thermocouples and the PID controller thermocouple, this test data was primarily used to validate the thermal model with the test article.

6.6 Test Article Thermal Vacuum Simulation Results

The data from Test 15 was used verify the thermal model results. After setting up the numerical model in Thermal Desktop as described in Section 5.2, an empty cold soak simulation was conducted to predict the temperature of the platen and other surfaces in the chamber during the cooling phase and cold soak phase of the thermal vacuum test. Figure 65-66 show the temperatures of the platen and the mass model after the 1.2 hour cooling phase from an initial

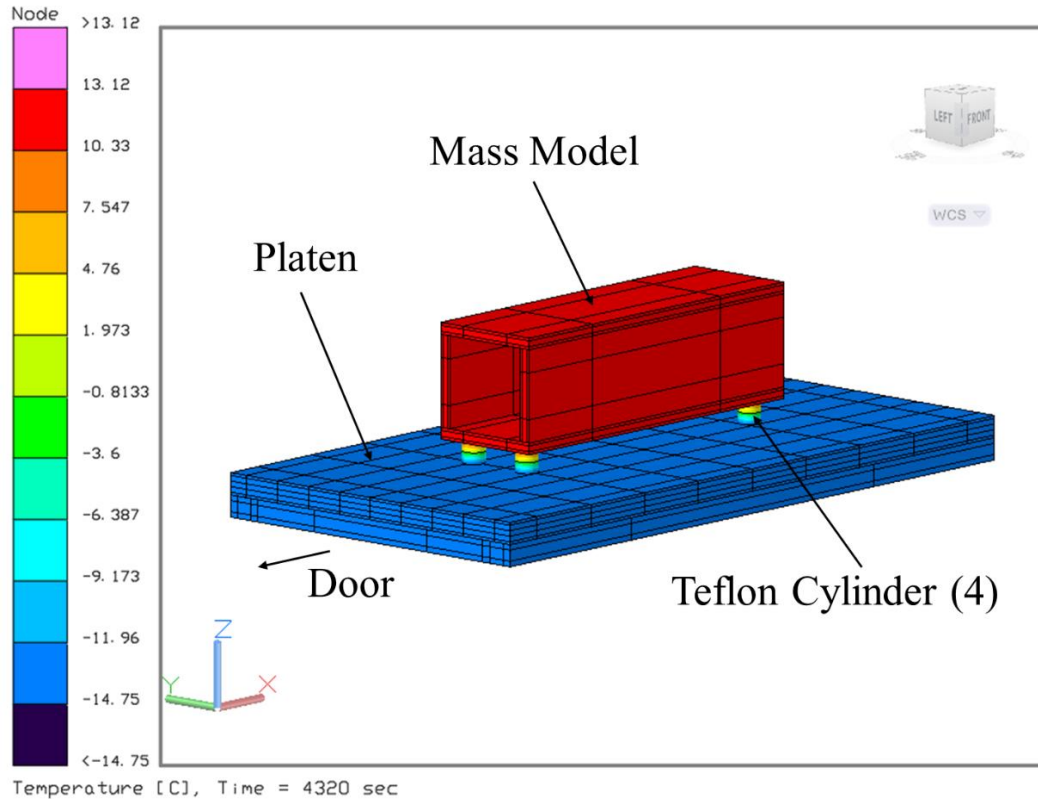


Figure 66: Predicted Temperature of Mass Model After Cooling Phase

As shown in Figure 65, the platen reaches a temperature of approximately -14.7°C after 1.2 hours of cooling from the surfaces modeling the LN_2 flow in the platen and across the copper shroud. The simulation results show a variation of approximately 0.02°C in temperature across the surface of the platen after 1.2 hours. As shown in Figure 66, the mass model reaches a temperature of 13°C while the Teflon support cylinders vary in temperatures of -14.7°C to 13°C as they store the heat from the mass model and reduce the conductive heat transfer from the mass model to the platen. The temperature of the copper shroud reached a temperature of -15°C , the inner cylinder reached a temperature of approximately 23°C and the chamber door ranged in temperatures of 13°C to 20°C after 1.2 hours. The resulting color maps of these elements can be found in Appendix H.

The results from the simulations of the cooling phase of the thermal vacuum test were compared to the results from Test 15. The average temperature presented from the test results

used for comparison is the instantaneous average DAQ thermocouple reading after 1.2 hours of cooling. Since these readings are changing during the test, the comparisons are approximate and are dependent on the defined time duration of the cooling phase used for comparisons. The comparison between the test data and the model predictions of the approximate surface temperatures of the platen and the mass model in the chamber after 1.2 hours of cooling are shown in Table 13.

Table 13: Cooling Phase with Mass Model Temperature Comparison

Element	Simulation Temperature (°C)	Test 15 Average DAQ Temperature (°C)	Test 15 PID TC Temperature (°C)	Difference (°C)
Platen	-14.7	-33.5	-15	18.8/0.3
Mass Model	13	10	n/a	3

As shown in the right most column of Table 13, the difference in the temperatures predicted by the simulation is 18.8°C greater than the average platen temperature from the DAQ thermocouples, but only 0.2°C greater than the temperature recorded by the PID temperature controller thermocouple. The predicted temperature of the mass model is 3°C greater than the measured average temperature of the platen after the 1.2 hour cooling phase.

The two hour cold soak was then simulated by running this simulation for a total of 3.2 hours with the same initial temperatures of 25°C. Figure 67-68 show the resulting surface temperatures at the end of the cold soak phase.

As shown in Figure 67, the platen maintains a temperature of approximately -14.8°C after the 2 hour cold soak. The simulation results show a variation of approximately 0.01°C in temperature across the surface of the platen after 3.2 hours. As shown in Figure 68, the mass model reaches a temperature of approximately 2°C while the Teflon support cylinders vary in temperatures of -14.8°C to 2°C as they store the heat from the mass model and reduce the conductive heat transfer from the mass model to the platen. The temperature of the copper shroud reached a temperature of -15°C , the inner cylinder reached a temperature of approximately 20°C and the chamber door ranged in temperatures of 10°C to 18°C after 3.2 hours. The resulting color maps of these elements can be found in Appendix H.

The results from the simulations of the cold soak of the thermal vacuum test were compared to the results from Test 15. The average temperature presented from the test results used for comparison is the instantaneous average DAQ thermocouple reading after the two hour cold soak. Since these readings are changing during the test, the comparisons are approximate and are dependent on the defined time duration of the cold soak phase used for comparisons. The comparison between the test data and the model predictions of the approximate surface temperatures of the platen and the mass model in the chamber after 1.2 hours of cooling are shown in Table 14.

Table 14: Cold Soak with Mass Model Temperature Comparison

Element	Simulation Temperature ($^{\circ}\text{C}$)	Test 15 Average DAQ Temperature ($^{\circ}\text{C}$)	Test 15 PID TC Temperature ($^{\circ}\text{C}$)	Difference ($^{\circ}\text{C}$)
Platen	-14.8	-24.3	-15	9.5/0.2
Mass Model	2	3	n/a	1

As shown in the right most column of Table 14, the difference in the temperatures predicted by the simulation is 9.5°C greater than the average platen temperature from the DAQ thermocouples, but only 0.2°C greater than the temperature recorded by the PID temperature

controller thermocouple. The predicted temperature of the mass model is 1°C less than the measured average temperature of the platen after the two hour cold soak.

After simulating the cold soak of the thermal vacuum test with the mass model, the heating phase and hot soak phase were simulated. For the heating phase, the initial temperatures of each element were assumed to be the respective final temperatures from the cold soak simulation. The assumed duration of the heating phase was based on the duration of heating observed in Test 15, which was approximately one hour. Figure 69-70 show the resulting surface temperatures at the end of the heating phase.

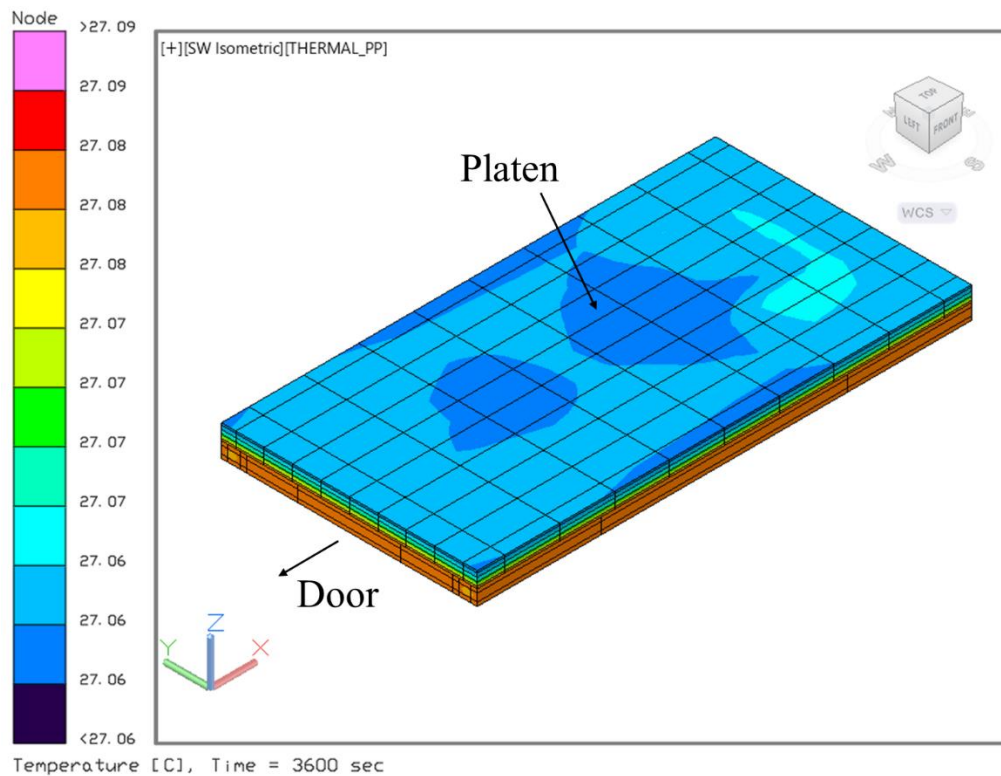


Figure 69: Predicted Temperature of Platen After Heating Phase with Mass Model

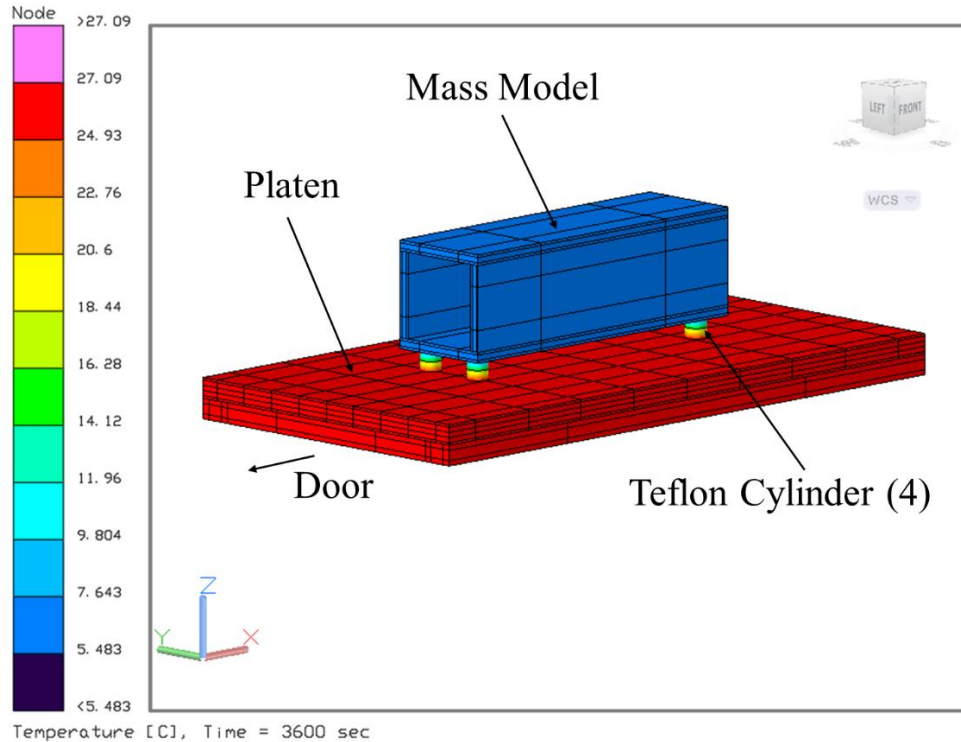


Figure 70: Predicted Temperature of Mass Model After Heating Phase

As shown in Figure 69, the platen reaches a temperature of approximately 27°C after the one hour heating phase. The simulation results show a variation of approximately 0.03°C in temperature across the surface of the platen. As shown in Figure 70, the mass model warms to a temperature of approximately 5°C while the Teflon support cylinders vary in temperatures of 5°C to 27°C as they store the heat from the platen and reduce the conductive heat transfer from the platen to the mass model. The temperature of the copper shroud reached a temperature of -13°C, the inner cylinder reached a temperature of approximately 17°C and the chamber door ranged in temperatures of 17°C to 18°C after one hour. The resulting color maps of these elements can be found in Appendix H.

The results from the simulations of the one hour heating phase of the thermal vacuum test with the mass model were compared to the results from Tests 15. The average temperature presented from the test results used for comparison is the instantaneous average DAQ

thermocouple reading after one hour of heating. Since these readings are changing during the test, the comparisons are approximate and are dependent on the defined time duration of the heating phase used for comparisons. The comparison between the test data and the model predictions of the approximate surface temperatures of the platen and the mass model after one hour of heating are shown in Table 15.

Table 15: Heating Phase with Mass Model Temperature Comparison

Element	Simulation Temperature (°C)	Test 15 Average DAQ Temperature (°C)	Test 15 PID TC Temperature (°C)	Difference (°C)
Platen	27	56	52	29/25
Mass Model	5	18	n/a	13

As shown in the right most column of Table 15, the difference in the temperatures predicted by the simulation is 29°C less than the average platen temperature from the DAQ thermocouples and 25°C less than the temperature recorded by the PID temperature controller thermocouple. The predicted temperature of the mass model is 13°C less than the measured average temperature of the platen after the one hour heating phase.

The two hour hot soak was then simulated by running this simulation for a total of three hours with the same initial temperatures. Figure 71-72 show the resulting surface temperatures at the end of the hot soak phase.

As shown in Figure 71, the platen reaches a temperature of approximately 43.9°C after the two hour hot soak. The simulation results show a variation of approximately 0.01°C in temperature across the surface of the platen. As shown in Figure 72, the mass model warms to a temperature of approximately 24°C while the Teflon support cylinders vary in temperatures of 24°C to 44°C as they store the heat from the platen and reduce the conductive heat transfer from the platen to the mass model. The temperature of the copper shroud reached a temperature of -8°C, the inner cylinder reached a temperature of approximately 18°C and the chamber door ranged in temperatures of 19°C to 27°C after three hours. The resulting color maps of these elements can be found in Appendix H.

The results from the simulations of the two hour hot soak phase of the empty thermal vacuum test were compared to the results from Test 15. The average temperature presented from the test results used for comparison is the instantaneous average DAQ thermocouple reading after the two hour hot soak. Since these readings are changing during the test, the comparisons are approximate and are dependent on the defined time duration of the hot soak phase used for comparisons. The comparison between the test data and the model predictions of the average temperatures of the platen and mass model after the two hour hot soak are shown in Table 16.

Table 16: Hot Soak with Mass Model Temperature Comparison

Element	Simulation Temperature (°C)	Test 12 Average DAQ Temperature (°C)	Test 15 PID TC Temperature (°C)	Difference (°C)
Platen	43.9	51.1	50	7.2/6.1
Mass Model	24	35	n/a	11

As shown in the right most column of Table 16, the difference in the temperatures predicted by the simulation is 7.2°C less than the average platen temperature from the DAQ thermocouples and 6.1°C less than the temperature recorded by the PID temperature controller

thermocouple. The predicted temperature of the mass model is 11°C less than the measured average temperature of the platen after the two hour hot soak.

Simulations were also run with additional nodes on the surface of the platen to represent the thermocouples placed on the platen. This was done in an attempt to measure the thermal response observed by the thermocouples measured during Test 15. These thermocouples were modeled to be 1 cm by 1 cm surfaces of Aluminum 6061 that were separated from the platen by 1 mm. With these implemented into the simulations, the results showed no noticeable variation in temperature from the platen surface to the surfaces modeling the thermocouples. In Chapter 8, recommendations are made for improving this model in an attempt to accurately predict the measurements that the thermocouples record during tests.

The implications of the thermal model correlation to the test results are presented in Chapter 7. The thermal uncertainty margin of 15°C was exceeded for the cooling phase and heating phase thermal vacuum simulations that included the test article. Recommendations for improving the thermal model to better predict thermal vacuum test results with a test article are presented in Chapter 8.

Chapter 7

CONCLUSION

7.1 General Results

A thermal model of the Blue TVAC was developed and used to predict the thermal response inside the chamber during an empty thermal vacuum test and a thermal vacuum test with a 3U CubeSat Mass Model. These thermal vacuum tests were conducted with the Blue TVAC as per the ISO Standard 19683. Improvements to the DAQ system of the Blue TVAC were made to increase the repeatability of a thermal vacuum test. The subsequent sections in this chapter describe the conclusions made and present the various lessons learned throughout the thesis work.

7.2 Empty Thermal Vacuum Tests

A total of eleven empty thermal vacuum tests were conducted with the Blue TVAC. The primary conclusions were made from Test 12 and Test 13. These two empty thermal vacuum tests revealed the following important characteristics about the Blue TVAC:

- The Blue TVAC must be operated with T type thermocouples for data collection
- The DAQ thermocouples measure temperatures that vary by approximately 4°C to 14°C across the surface of the platen
- The front left area of the platen tends to be warmer than the rest of the platen during the cold soaks and cooler than the rest of the platen during the hot soaks.
 - Other than this, there is no repeatable trend in the temperature distribution across the surface of the platen
- The target soak temperatures of -15°C and 50°C can be reached and maintained repeatably for only one cycle with one hour soak durations

Conclusions are also drawn from the comparison of the thermal model results to the empty thermal vacuum test results. It is concluded that the empty thermal vacuum simulations

can predict the temperatures of the platen surface in the chamber with the thermal uncertainty margins shown in Table 17. It is also concluded that the thermal model does not predict the temperature variations across the platen surface that is observed in the test data.

Table 17: Thermal Uncertainty Margin for Empty Thermal Vacuum Simulations

Phase of Thermal Vacuum Test	Thermal Uncertainty Margin (°C)
Cooling	2.3-2.5
Cold Soak	4.8
Heating	6.2
Hot Soak	0/2.8

The thermal simulation predictions for the platen temperature have a thermal uncertainty margin of less than 15°C for all phases of the thermal vacuum test.

7.3 Thermal Vacuum Tests with Test Article

A total of four thermal vacuum tests with the 3U CubeSat mass model were conducted with the Blue TVAC. The primary conclusions were made from Test 14 and Test 15. These two empty thermal vacuum tests revealed the following important characteristics about the Blue TVAC:

- The same application method must be used for installing the DAQ thermocouples and the PID temperature controller thermocouple in the chamber
- The DAQ thermocouples measure temperatures that vary by approximately 1°C to 10°C across the surface of the platen
- The DAQ thermocouples measure temperatures that vary by approximately 2°C to 6°C across the surfaces of the mass model
- The bottom internal surfaces of the mass model tend to be cooler than the external surfaces during the cold soak and warmer than the external surfaces during the hot soak

- The target soak temperatures of -15°C and 50°C can be reached and maintained by the PID temperature controller repeatably for at least two cycles with at least one hour soak durations

Conclusions are also drawn from the comparison of the thermal model results to the thermal vacuum test results. It is concluded that the thermal vacuum simulations with the mass model can predict the temperatures of the platen surface and the mass model surfaces with the thermal uncertainty margins shown in Table 18. It is also concluded that the thermal model does not predict the temperature variations across the platen surface that is observed in the test data.

Table 18: Thermal Uncertainty Margin for Thermal Vacuum Simulations with Mass Model

Phase of Thermal Vacuum Test	Platen Temperature Thermal Uncertainty Margin (°C)	Mass Model Temperature Thermal Uncertainty Margin (°C)
Cooling	18.8	3
Cold Soak	9.5	1
Heating	29	13
Hot Soak	7.2	11

The platen thermal uncertainty margins presented in Table 18 are based on the temperatures measured by the DAQ thermocouples, not the PID temperature controller measurements. The thermal simulation predictions for the platen temperatures have a thermal uncertainty margin of less than 15°C for the cold soak and hot soak phases of the thermal vacuum test. The thermal model must be modified to accurately predict the platen temperature during the cooling and heating phases of the test. Recommendations for improving the thermal model are presented in Chapter 8. The simulation predictions for the mass model temperatures during the thermal vacuum test is within the acceptable 15°C thermal uncertainty margin for all phases.

7.4 Thermal Vacuum Test Repeatability

The repeatability of a thermal vacuum test with the Blue TVAC was verified as per ISO Standard 19683 during the testing process. The repeatable aspects of the thermal vacuum test include:

- Minimum chamber pressure
- Chamber pump down time
- Ramp rate of ± 5 °C/min or slower
- Empty hot soak platen temperature of 50 ± 3 °C for one hour
- One complete thermal vacuum cycle

These parts of the thermal vacuum test were consistently completed and can be expected to continue to be repeatable when following the thermal vacuum test procedure [11]. Other aspects of the thermal vacuum test were not consistently completed during every test. These nonrepeatable aspects of the thermal vacuum test include:

- Cold soak platen temperature of -15 ± 3 °C for one hour
- Two complete thermal vacuum cycles

It is hypothesized that the cold soak platen temperature did not repeatably reach -15 ± 3 °C during testing due to a fault in the PID temperature controller control laws. Since the PID temperature controller controls the solenoid valves that periodically release LN₂ into the chamber, if the valves do not open and stay open with sufficient frequency, then the platen will not cool as desired. It is expected that with an improved control law, the PID temperature controller would regulate the LN₂ flow to allow the platen to consistently cool to the desired cold soak temperature. Recommendations for modifying the PID temperature controller parameters are presented in Chapter 8.

Two complete empty thermal vacuum cycles were not consistently completed during testing due to an insufficient supply of LN₂. The amount of LN₂ used during a test depends on the testing parameters and the presence of a test article. It is expected that the most LN₂ is used during the cooling phases of the thermal vacuum tests, but it is also used to maintain the hot soak and cold soak temperatures. The LN₂ is also continuously expended when the chamber door shroud valve is manually opened. Since the LN₂ use is dependent on many varying test parameters, the number of thermal vacuum cycles completed in each test was inconsistent. Occasionally, the LN₂ supply lasted for two full cycles of the empty thermal vacuum test, but more often it would run out at some point during the second cooling phase. This did not occur when the 3U CubeSat mass model was tested. For these tests, the current LN₂ dewar provided enough coolant for two thermal vacuum cycles. It is possible that it would not be sufficient for more than two cycles with the mass model. It is predicted that a larger LN₂ dewar of at least 50 liters would provide enough coolant to complete two empty thermal vacuum cycles with the test parameters used for this thesis project. A larger tank would also ensure that over two cycles with a test article could be completed if needed.

7.5 Lessons Learned

Throughout the testing and modeling process, many valuable lessons were learned that may be beneficial for future students who do work with the Blue TVAC. These lessons learned can be divided into three different categories: thermal analysis lessons, operational lessons, and personal lessons.

7.5.1 Thermal Analysis Lessons

During the thermal modeling process of this project, it was quickly learned that familiarity with a new software must be established before any analytical tasks are completed. Approximately thirty hours of completing Thermal Desktop tutorials and creating simple models are necessary to gain the experience needed to become familiar with the software. If the software is familiar to the user, the process of setting up the model and running simulations is more efficient and less

frustrating. The Thermal Desktop software includes many features and while not every feature is used in a model, it is helpful to know the general purpose and necessary inputs of each one. It was also learned that the Aerospace Engineering IT specialist is a valuable resource when it comes to troubleshooting any licensing or remote desktop server. It is never a bad idea to reach out for help as soon as possible with these problems.

While modeling the Blue TVAC, it was also learned that time can be saved by referencing preexisting models. While prior thermal models of the Blue TVAC included simplifications and limitations that needed to be improved for this thesis project, it was helpful to use various aspects of these models rather than starting from nothing. For this reason, the thermal model developed for this thesis project can be modified and improved for future analytical purposes. Preexisting thermal model results can also be used for comparison when developing a new model. Past simulation results can be reproduced to verify the newly developed model.

7.5.2 Operational Lessons

It was initially learned that before any valid tests can be conducted with the Blue TVAC, it is important to confirm that all subsystems of the chamber are operating as expected from past tests. It is likely that long durations of time will pass between tests, so before conducting a full thermal vacuum test, the vacuum system, heating and cooling systems, DAQ system, and PID temperature controller system functionality must be verified. It was learned that at least five system tests should be performed to verify the system performance before changes are made to the system to ensure that the system is performing nominally.

The Blue TVAC is a system that operates as desired if and only if every subsystem of the machine is functioning properly. Before expecting to be able to conduct repeatable tests, the operating procedure as well as the inputs and outputs for each subsystem should be understood. This is especially relevant for the vacuum pump system, the DAQ system, the PID temperature controller, the temperature limit controllers, and the cooling system. It was quickly learned that

each of these subsystems must function independently of each other before the Blue TVAC as a whole can perform as desired. For example, the results from the thermal vacuum tests only made sense after it was discovered that the DAQ system for this chamber is designed to operate with T type thermocouples. Without understanding how the individual DAQ system operates, the entire Blue TVAC system did not operate as expected.

It was also quickly learned that patience is required during thermal vacuum tests. On average, these tests lasted approximately 8 hours from the start of the thermal profile to the end. This does not include the time required for setting up the test, pumping down the chamber, and venting the chamber after the test. While it is not necessary to be present in the lab for the entirety of the test, it was discovered that being present during the entire test resulted in a better understanding of the behavior of the chamber. Manual operations are currently required for the cooling phases of the thermal vacuum test, so it is necessary to be present during these times.

It was also learned that the LN₂ dewar must be consistently monitored during testing, especially during the cooling phases. The LN₂ flow is sufficient for cooling when the dewar pressure is 4-6 psi, but during continuous use, such as the during the cooling phases, the pressure often decreased below 4 psi, which is insufficient for pumping the LN₂ through the chamber. To increase the dewar pressure, the LN₂ flow rate must be manually decreased by setting a slower ramp rate with the PID temperature controller. Once the dewar pressure recovered to >4psi, the ramp rate could be increased by manually setting a temperature on the PID temperature controller without specifying a ramp rate. Since the rate of cooling the chamber is dependent on the LN₂ dewar pressure, the pressure gauge must be checked at least once every ten minutes during testing to ensure it is operating in the effective range.

7.5.3 Personal Lessons

Throughout this process, one of the most valuable lessons learned was the importance of communication. More often than not, an advisor, professor, lab technician, or IT specialist will

have an answer to a question that may take hours of personal investigation. It is never a bad idea to ask for help and there is never a question that should not be asked. As for any project that involves many resources and stakeholders, it is important to communicate any changes to the system or relevant results to the involved parties. Documentation and communication of changes to the system must be maintained to ensure that all involved parties and future parties are aware of new developments.

Chapter 8

FUTURE WORK

8.1 LN₂ Supply

The main limiting factor in the completion of a thermal vacuum test is the LN₂ supply. Currently, the 35 liter dewar of LN₂ does not provide enough coolant to repeatably conduct two cycles of an empty thermal vacuum test. While it does provide enough coolant to complete two full thermal vacuum cycles with the mass model according to the ISO Standard 19683, it likely will not provide for more than two cycles or for a test with more extreme temperature range requirements. Future potential customers may need to conduct longer tests to verify their system. There are three potential recommendations made to upgrade the current LN₂ supply.

8.1.1 Purchase of Worthington 50 Liter Dewar

The current dewar in use is a Worthington 35 liter dewar. It is expected that an additional 15 liters of LN₂ would allow for two complete thermal vacuum cycles to be completed. A cost estimate was received by Worthington Industries, which amounted to \$1,448.06 for the 50 liter dewar. No additional plumbing equipment would be required to integrate this dewar into the Blue TVAC system. Although this larger dewar would allow for extended testing time, the 50 liter would likely not provide enough LN₂ more than about three thermal vacuum cycles. Praxair Technology delivers the LN₂ to Cal Poly one time per week so to run more than one thermal vacuum test each week, an alternative source of LN₂ is necessary. If the Blue TVAC is to be used for extended thermal vacuum testing, or for multiple tests per week, it is recommended that an even larger LN₂ dewar is purchased.

8.1.2 Purchase of 250 lbs LN₂ Dewar

To run more than one thermal vacuum test per week or to run thermal vacuum tests with over two cycles, it is recommended that a 250 lb LN₂ dewar be purchased by Praxair. This is the

same dewar that is purchased by the MATE department for their lab activities that involve the use of LN₂. It costs approximately \$80.00 to replace this dewar and would provide approximately four times the current amount of LN₂. To measure the amount of LN₂ in the tank, the dewar is placed and stationed on a scale, which would also be a necessary purchase for determining when the dewar is empty. A scale for this purpose costs approximately \$200 to \$400. Further investigation is required to determine if additional plumbing equipment would need to be purchased to integrate this tank into the Blue TVAC system.

8.2 PID Temperature Controller Analysis

In the final two tests, it was observed that despite consistent thermocouple application methods, the PID temperature controller thermocouple measures platen temperatures that consistently vary from the twelve DAQ thermocouple readings. These observations indicate that the PID temperature controller may need to be recalibrated to provide valid measurements used for the temperature control of the platen. This can be done by changing the calibration offset parameter of the input thermocouple. Currently, the calibration offset parameter is set to the default value of 0°C. Refer to [14] for complete instructions for changing this parameter. If this parameter is changed, tests must be conducted following the modification to verify the effects of each change.

During testing, it was consistently observed that the PID temperature controller did not control the temperature in the chamber as programmed. When a ramp rate of -5 °C/min was programmed, the chamber would cool at a rate of approximately -0.2 °C/min. At this rate, it would take approximately three hours for the platen to cool from 20°C to -15°C. To reduce this cooling time during tests, the programmed profile step was paused and the target temperature was manually set, which allowed the chamber to output maximum power to the cooling system. When this was done, the ramp rate increased to approximately -0.5 to -0.9 °C/min and the platen cooled to -15°C in approximately one hour. It was also observed during testing that during the cold

soaks, the PID controller measured temperature of the platen would often rise above the tolerance of $\pm 1^{\circ}\text{C}$ allowed by the controller. When this would occur, the PID temperature controller would periodically open and close the solenoid valves to cool the platen, but the automated flow of LN_2 was insufficient in cooling the platen.

These observations indicate that the output power to the cooling system may need to be modified to increase the amount of LN_2 released during cooling phases. Potentially the “Cycle Time” parameter of the output power to the cooling system may need to be changed to accomplish this. Currently, this parameter is set to a fixed time of 5.0 seconds. Complete instructions for changing this parameter can be found in [14]. If this parameter is changed, tests must be conducted following the modification to verify the effects of the change.

8.3 Testing

It is recommended that further testing is conducted with the Blue TVAC to increase the repeatability of thermal vacuum tests. For all future testing, it is recommended that the PID temperature controller readout of the platen temperature is recorded once every five to ten minutes in order to better compare this reading to the temperature readings from the DAQ thermocouples.

Next, it is recommended that empty thermal vacuum tests with the modified PID temperature controller parameters be conducted to measure the thermal response of the chamber when different parameters are used. It is important that any changes to the PID parameters are documented to determine which parameters affect the thermal response of the chamber.

It is also recommended that the 3U CubeSat mass model is tested with a thermally sensitive component included within the mass model structure. This could be done to measure the insulative properties of the mass model structure as well as to determine if the temperature requirements of a component can be satisfied during a thermal vacuum test. It is also

recommended that a test article with an internal heat source be tested to measure the thermal behavior of the test article when it is in an environment more similar to its operating thermal environment in orbit.

If the LN₂ dewar is upgraded and/or the PID temperature controller control laws are edited, it is recommended that additional empty thermal vacuum tests are conducted to determine the effect of these changes on the system. If and when a change is introduced to the system or operating procedure, it is recommended that a test be conducted at least two times to ensure the repeatability of the test results.

Lastly, it is recommended that more thermal vacuum tests be conducted to collect the temperature response data across more surfaces in the chamber. The validity of the thermal model may be improved if more comparisons can be made for the thermal response of other surfaces in the chamber, specifically the copper shroud, LN₂ pipes, the door shroud, and the inner chamber cylinder. This may require installing more thermocouples and the addition of a DAQ system to allow for more thermocouples to be used for data collection during testing.

8.4 Thermal Modeling

It is recommended that the thermal model be improved by reducing the amount of simplifications made in modeling the cooling system of the chamber. If the flow rate of LN₂ during the cooling phases of the thermal vacuum test are measured or approximated, the LN₂ pipes in the model can be modeled as actual fluid pipes using the FloCAD model in Thermal Desktop. The geometry of the pipes through the platen would still have to be approximated without disassembling the chamber to determine this. Another method of improving the cooling system model would be to measure the temperature of the LN₂ pipes across the copper shroud during a thermal vacuum test. The nodes of the pipes in the thermal model could then be set to these temperatures.

To reduce the thermal uncertainty margin of the thermal model predictions, it is also recommended that the material properties of the elements in the model be refined. Since the emissivity of the platen, the mass model, and the copper shroud were assumed values, it is likely that these parameters can be changed to better approximate the radiative heat transfer that occurs within the chamber. It is also likely that the material properties of the elements do not remain constant during testing, so the temperature dependent nature of these properties should be accounted for.

The model could also be improved by including more elements such as the electrical wires, the platen support structure, and the thermocouple panel jack. The conduction and radiation to and from these elements can be modeled and the thermal uncertainty margin of the predicted platen temperature may be decreased.

For the thermal model that includes the 3U CubeSat mass model, the predictions from these simulations could be improved by refining the geometry of the mass model. Currently, it is modeled as one solid, thin walled rectangular prism, but in reality, it is composed of 3 1U CubeSat units that are connected by small features at the corners of each unit. The mass model also has support beams that extend longitudinally on the interior of the model that are screwed into the mass model surfaces. These material properties of these features as well as the associated torques of the tightened screws are unknown and were not incorporated in the thermal model. These complexities in the material geometries and properties likely influence the thermal response of this test article during thermal vacuum tests.

8.5 Chamber Vacuum Leak Investigation

It is recommended that the pressure leak in the Blue TVAC be further investigated to determine the root cause for the increased chamber pressure that has been observed in the last two years. Appendix A provides information on the analysis that has been done to resolve this issue for this thesis. More sophisticated methods of leak detection are necessary to mitigate the current

leak. This may involve using the Helium leak detector that is in the Cal Poly Space Environments Lab to detect where the leak is originating from. If the leak is mitigated, the time duration of a thermal vacuum test will be decreased as the chamber will pump down faster. Industry requirements for thermal vacuum testing will also be satisfied with a lower chamber pressure during testing.

REFERENCES

- [1] J. Wertz, D. Everett and J. Puschell, *Space Mission Engineering: The New SMAD*, Microcosm Inc, 2011.
- [2] D. G. Gilmore, *Spacecraft Thermal Control Hand Book*, American Institute of Aeronautics and Astronautics, Inc, 2002.
- [3] R. D. Karam, *Satellite Thermal Control for Systems Engineers*, American Institute of Aeronautics and Astronautics, 1998.
- [4] A. Williams, "Thermal Vacuum Chamber Refurbishment and Analysis," San Luis Obispo: California Polytechnic State University, 2018.
- [5] "Low Earth Orbit Spacecraft Charging Design Handbook," 2007.
- [6] V. L. Pisacane, *The Space Environment and its Effects on Space Systems*, American Institute of Aeronautics and Astronautics, Inc., 2008.
- [7] S. Yan, J. Li and R. Cai, "Thermal Analysis of Composite Solar Array Subjected to Space Heat Flux," *Aerospace Science and Technology*, vol. 27, no. 1, p. 85.
- [8] International Organization for Standardization, *Space Systems: Design Qualification and Acceptance Tests of Small Spacecraft and Units*.
- [9] J. Holman, *Heat Transfer*, 10 ed., McGraw-Hill, 2009.
- [10] C&R Technologies, "User's Manual Thermal Desktop Version 6.0," 2017.
- [11] M. R. Jensma, *Thermal Vacuum Test Procedure for the Blue Thermal Vacuum Chamber*, California Polytechnic State University, San Luis Obispo, 2020.
- [12] Leybold Vacuum, "Turbovac Operating Instructions," 2006.
- [13] Granville-Phillips, *Granville-Phillips Series 307 Vacuum Measurements Controller Instruction Manual*, 2014.
- [14] Watlow Winona, *Series F4S/D User's Manual*, 2011.
- [15] Watlow Winona, *Series 97 User's Manual*, 2007.
- [16] General, *12-Channel Temperature Recorder with Excel-Formatted Data Logging SD Card User's Manual*, 2013.
- [17] Omega, *Revised Thermocouple Reference Table*, pp. Z-204 - Z-2017.
- [18] M. Caudill, *Cal Poly TVAC SubContract*, 2018.

- [19] M. Caudill and B. Diamond, *Cal Poly TVAC Chamber: Cryogenics*, 2019.
- [20] European Cooperation for Space Standardization, *Space Engineering Testing*, 2002, pp. 138-141.
- [21] J. H. Henninger, "Solar Absorptance and Thermal Emittance of Some Common Spacecraft Thermal Control Coatings," NASA Reference Publication 1121, 1984.
- [22] "Thermocouple Types," Omega, [Online]. Available: <https://www.omega.com/en-us/resources/thermocouple-types>. [Accessed 28 April 2020].
- [23] N. A. Fishwick, K. A. Smith and J. A. Romera Perez, "Lessons Learned from Thermal Vacuum Testing of LISA Pathfinder over three system level Thermal Tests," in *International Conference on Environmental Systems*, 2015.
- [24] GSFC-STD-7000A, *General Environment Verification Standards (GEVS) for GSFC Flight Programs and Projects*, Greenbelt, Maryland: NASA Goddard Space Flight Center, 2013.
- [25] "Mylar Polyester Film Product Information," DuPont Teijin Films. [Online].
- [26] "Properties for Molded PTFE," Trebor, [Online]. Available: <https://trborintl.com/content/properties-molded-ptfe>. [Accessed 28 April 2020].
- [27] Engineers Edge, "Thermal Properties of Metals, Conductivity, Thermal Expansion, Specific Heat," [Online]. Available: <http://engineersedge.com/properties-of-metals.htm>. [Accessed 28 April 2020].

APPENDICES

Appendix A

VACUUM SYSTEM ANALYSIS

A.1 Initial Observations

Prior to running thermal vacuum tests with the Blue TVAC for this thesis, it was observed by past operators that the vacuum system performance may be insufficient for bringing the chamber to a pressure low enough for valid thermal vacuum tests according to industry standards, such as the NASA GEVS or the ISO Standard 19683 [27, 8]. It was also observed that the chamber pump down time had increased since Adrian Williams conducted tests in 2017 [4]. Table 19 below shows the comparison of chamber pump down times for Williams' tests versus the tests conducted for this thesis.

Table 19: Comparison of Chamber Pump Down Time

Chamber Pressure (Torr)	Average Time Recorded by Williams (hour) [4]	Average Time Recorded by Jensma (hour)
<50x10 ⁻³ (mechanical pump only)	<1	0.75
<20x10 ⁻³ (mechanical pump only)	<2	~18
<20x10 ⁻⁵ (mechanical and turbo pumps)	<7	~18
<50x10 ⁻⁶ (mechanical and turbo pumps)	~7	n/a

While the chamber was capable of maintaining a lower pressure during Williams' tests, the minimum pressure attained was still higher than the chamber pressure required by the NASA GEVS and ISO Standard 19683 for thermal vacuum testing.

A.2 Initial Hypothesis

Given the initial observations, it was hypothesized that a leak in the chamber is responsible for the increase in the minimum possible chamber pressure. The chamber can leak from any ports connected to the chamber. This includes the following:

- Chamber door O-ring seal
- Chamber viewing window seal
- Thermocouple feedthrough
- Pump lines
- Chamber vent valve
- Convectron and ion gauge ports
- LN₂ plumbing ports
- Electrical feedthrough for heaters

Each of these ports must be sealed properly to prohibit ambient air from seeping into the chamber and raising the chamber pressure.

After ensuring the fasteners used to seal each of the ports was tightened, it was predicted that the leak was originating at the chamber door O-ring seal. The O-ring had visible wear and did not sit properly in the gland in the door. After taking measurements of the gland in the door, new O-rings were ordered in attempt to create a better seal at the door. After testing the new O-rings, it was determined that the vacuum seal was not improved by either of these O-rings. The original O-ring was replaced before a new adjustment was made to the chamber door.

With the original O-ring in place, it was then predicted that the seal at the door could be improved by increasing the clamping force of the door onto the face of the chamber. This was accomplished by removing a small washer that was positioned between the chamber face and the door latch hook that is screwed to the chamber face. With the washer removed, the chamber door

would be pulled closer to the chamber face when the latch is secured to the hook. When this adjustment to the latching mechanism did not noticeably decrease the minimum attainable chamber pressure, approximately 1 mm of material was machined off the flat face of the chamber door latch mating surface. With the removal of the washer and the material from the latch, the chamber still did not pump down at a rate similar to that recorded by Williams. Furthermore, with the greater latching force applied, the latch could not be easily secured. To reduce the force needed to turn the latching mechanism, the washer plate was repositioned in its original place. It is assumed that a sufficient clamping force is currently being applied to the chamber door to seal the vacuum with the current O-ring in place.

A.3 Current Vacuum Status

After replacing the washer and removing material from the door latch mating surface, no further efforts were made to reduce the suspected leak in the Blue TVAC. Since the chamber could reach pressures that allow for the assumption that convective heat transfer is negligible, it was decided that time and resources would be used to develop a thermal model of the chamber rather than find and fix a possible leak in the chamber. Even if the chamber pressure was decreased to the pressures measured by Williams, the ISO Standard 19683 still would not be satisfied. For these reasons, it is determined that should any future customers request for thermal vacuum tests to be conducted with the Blue TVAC according to the ISO Standard 19683, it should be made known to the customer that the maximum chamber pressure requirement would not be satisfied unless further leak investigation is conducted and further testing verifies that the leak is mitigated.

Appendix B

THERMOCOUPLE APPLICATION PROCEDURE

The following thermocouple application procedure should be followed once the thermocouple configuration in the Blue TVAC has been determined. The equipment required for applying the thermocouples is listed in Table 20.

Table 20: Thermocouple Application Equipment

Equipment Description	Qty	Make	Details
DAQ Thermocouples	12	Omega	Type T
Polyimide Tape	1 roll	Kapton	1 in width
Aluminum Tape	1 roll	Nashua	2 in width
Scissors	1 pair	n/a	n/a
Thermocouple Reader	1	General	12 Channel
Isopropyl Alcohol	1 bottle	n/a	n/a
Cleaning napkins	10	Kimwipe	n/a

1. Prior to applying the thermocouples, ensure that each thermocouple is functioning properly by turning on the Thermocouple Reader and pinching the end of the thermocouple. Observe an increase in the temperature reading due to body heat.
2. Open the chamber door
3. Apply a few drops of isopropyl alcohol to a Kimwipe and wipe the surfaces that the thermocouples will be applied to
4. Cut a 1cm x 1cm piece of aluminum tape
5. Cover the beaded end of the thermocouple with the piece of aluminum tape
6. Cut a piece of Kapton tape about 1 square inch in size

7. With the piece of tape, tape the end of the thermocouple to the specified location in the chamber. Additional tape may be needed to secure the thermocouple.
8. Repeat steps 4-7 until all thermocouples are securely attached to the surfaces
9. Close the chamber door, making sure to not interfere with any thermocouple wires
10. Ensure that the Thermocouple Reader is displaying ambient temperatures for each of the thermocouples. If a thermocouple does not give a reading, open the chamber door and ensure the thermocouple is still making contact with the surface
11. Turn the Thermocouple Reader off

Appendix C

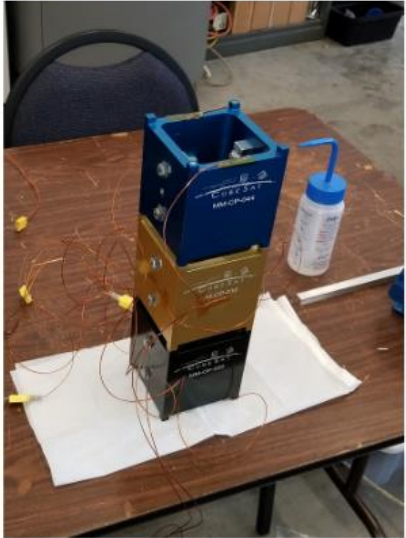
PRIOR TEST RESULTS

This appendix provides the test results from tests conducted by Cal Poly students Michael Caudill and Bennett Diamond in 2018 and 2019. These are the results referenced to in Chapter 4 of this thesis.

C.1 Test Results by Caudill

6.1 Test Results - 3U Mass Model

- **3U Aluminum Mass Model Test**
 - Low emissivity: 0.04 - 0.06
 - 8 temperature measurements
 - 3 bottom, 3 top, 2 sides
- **Results**
 - Shroud radiation temperatures do not well approximate platen temperatures
 - Equilibrium temperatures take 3-8 hours to achieve
 - Dependent on initial **delta-T**
 - Dependent on test subject
 - Test subjects approach shroud temp., then push shroud temp. further.



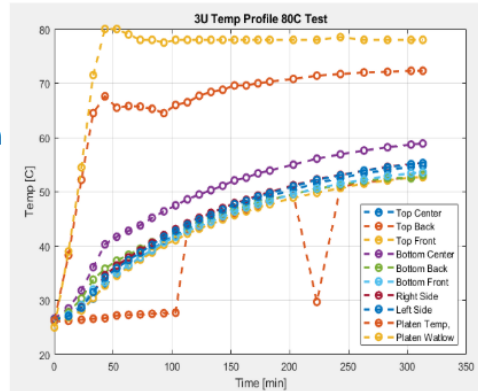
3U Polished Aluminum Mass Model

15

Figure 73: Caudill Presentation Slide 15

6.2 Test Results - 3U Mass Model: Raw Data

- **Temperature Ranges**
 - Average test subject temp.
 - Temp. difference approaches some true value
 - Dependent on set platen temp.
- **Set Temp. vs. Shroud Temp.**
 - Shroud temp. much less than platen temp.
 - Test subject pushes shroud temp. up.
 - Temp. gap is constant as platen temp. increases.



3U Temp Profile Test: Raw Data

16

Figure 74: Caudill Presentation Slide 16

6.3 Test Results - 3U Mass Model

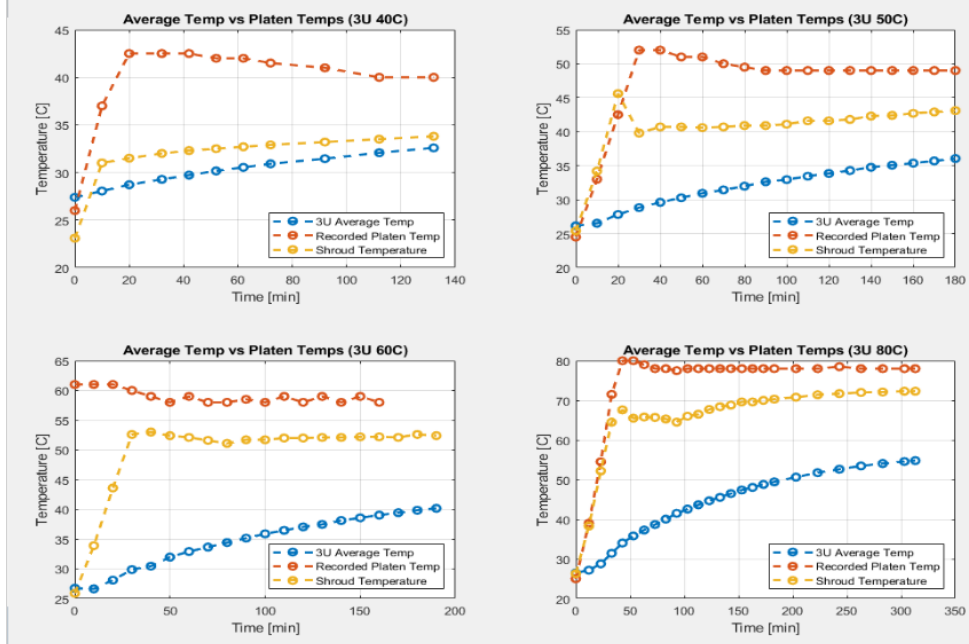


Figure 75: Caudill Presentation Slide 17

123

6.4 Test Results - 3U Mass Model

Platen Temp. [C]	Shroud Temp. [C]	Avg. Subject Temp. [C]	Platen/Amb Diff.	Amb/Subject Diff.
40 (40.0) °C	33.8 °C	32.6 °C	6.2 °C	1.2 °C
50 (49.3)°C	43.8 °C	36.1 °C	6.2 °C	7.7 °C
60 (58.7)°C	53.5 °C	40.2 °C	6.5 °C	13.4 °C
80 (78.7)°C	73.6 °C	54.8 °C	6.4 °C	18.8 °C

Platen Temperatures approximated set temperatures well, with larger temperature differences at higher settings.

Shroud radiation temperature did not reach platen setting, and in each case was: **6.317 +/- 0.12 °C** lower than platen setting.

Tests must be conducted from anywhere between 3-8 hours depending on initial temperature difference to achieve dependable data.

No true thermal equilibrium was reached, most tests were concluded after a rate of ~0.1 °C every 10 or 20 minutes. (Also dependent on time/lab limitations)

18

Figure 76: Caudill Presentation Slide 18

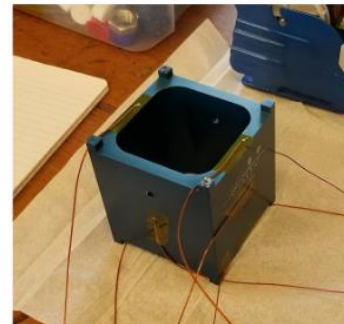
6.5 Test Results - 1U Mass Model

• 1U Anodized Aluminum Mass Model Test

- High Emissivity: 0.77 - 0.90
- 8 temperature measurements
 - 3 bottom, 3 top, 2 side

• Results

- Different relationship between platen and shroud radiation temperatures
 - Increasing difference between platen and shroud temperatures
- Different thermal profile vs. time
 - Faster increase in temperature
 - Less increase in shroud temperature from test subject



1U Anodized Aluminum Mass Model

19

Figure 77: Caudill Presentation Slide 19

6.6 Test Results - 1U Mass Model

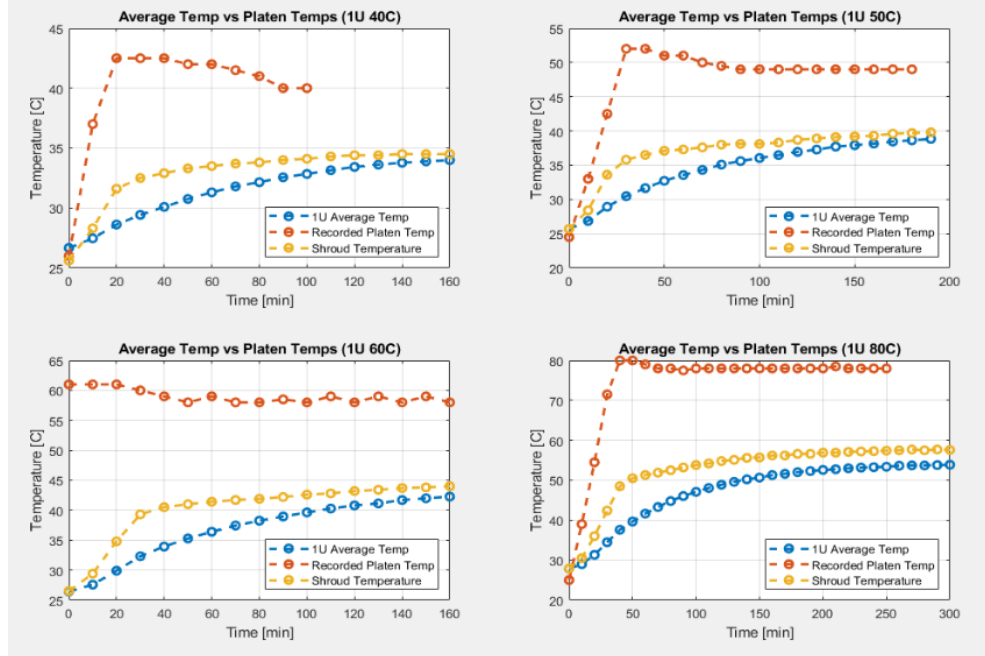
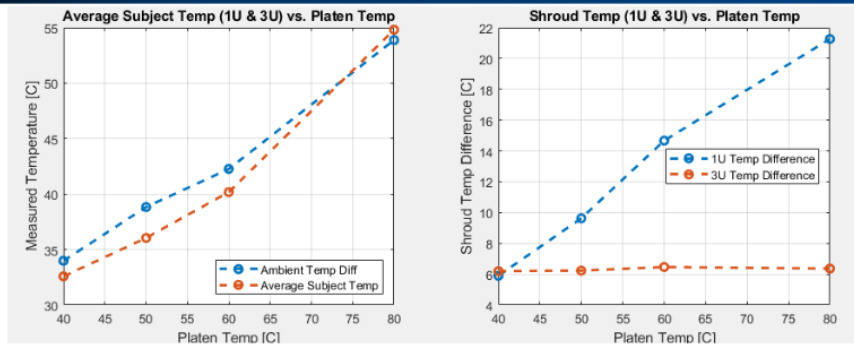


Figure 78: Caudill Presentation Slide 20

6.7 Test Results - Relationships Across Tests



- **Temperature Changes**
 - 'Linear' relationship between achieved test subject temp. and set platen temp.
 - 1U temperature is typically higher than 3U
 - Interaction between size and set platen temperature
- **Shroud Temperatures**
 - Difference between shroud temp. and platen temp.
 - 3U Difference is constant
 - 1U Difference is positive linear
 - Due to vastly different subject emissivities

21

Figure 79: Caudill Presentation Slide 21

6.8 Test Results - 1U Mass Model

Platen Temp. [C]	Shroud Temp. [C]	Avg. Subject Temp. [C]	Platen/Amb Diff.	Amb/Subject Diff.
40 (40.0) °C	34.1 °C	34.0 °C	5.9 °C	0.1 °C
50 (49.7)°C	40.4 °C	38.8 °C	9.6 °C	1.5 °C
60 (58.7)°C	44.1 °C	42.3 °C	14.7 °C	3.1 °C
80 (79.7)°C	58.7 °C	53.9 °C	21.3 °C	4.8 °C

Platen temperatures continue to approximate set temperatures very well

Shroud radiation temperatures are significantly lower than set platen temperatures, unlike the previous 3U mass model test. This is most likely due to the vastly different emissivities of each test subject, where the 1U absorbs more thermal radiation, and thus the shroud temperature is much lower.

This can also be confirmed by how closely the 1U average temperature approximates the shroud temperature.

Higher set temperatures correlate with higher gap between platen temperature and radiation temperature within test volume

Test subjects well approximated radiation temperatures, with larger temperature differences at higher set temperatures.

Test subjects never appear to achieve ambient radiation temperatures, yet lower temperatures come significantly closer to doing so.

22

Figure 80: Caudill Presentation Slide 22

C.2 Test Results by Caudill and Diamond

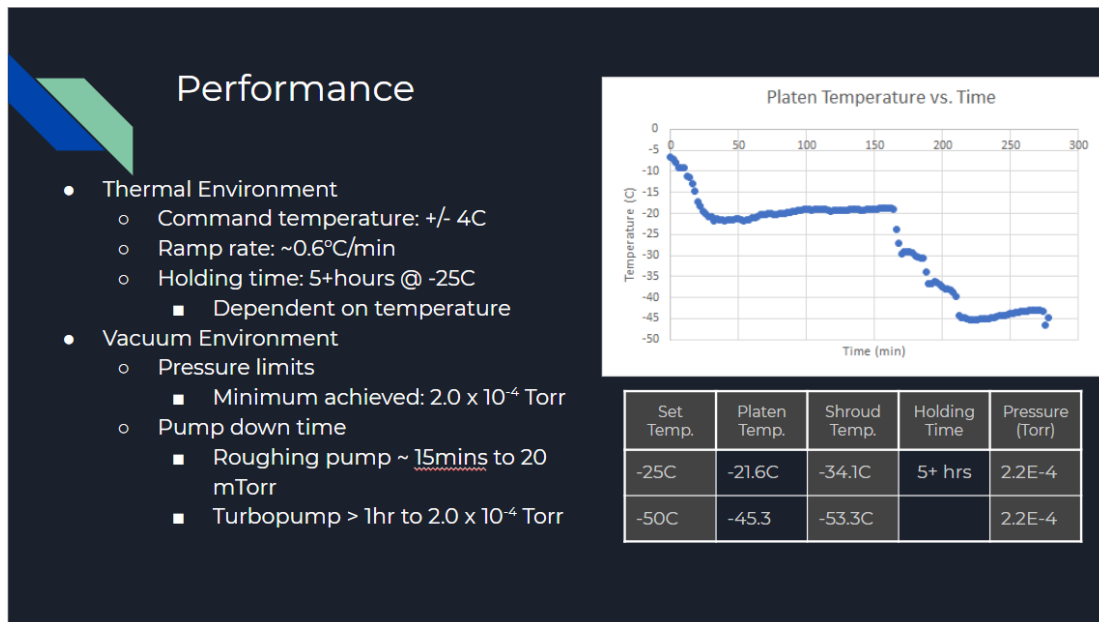


Figure 81: Caudill and Diamond Slide 10

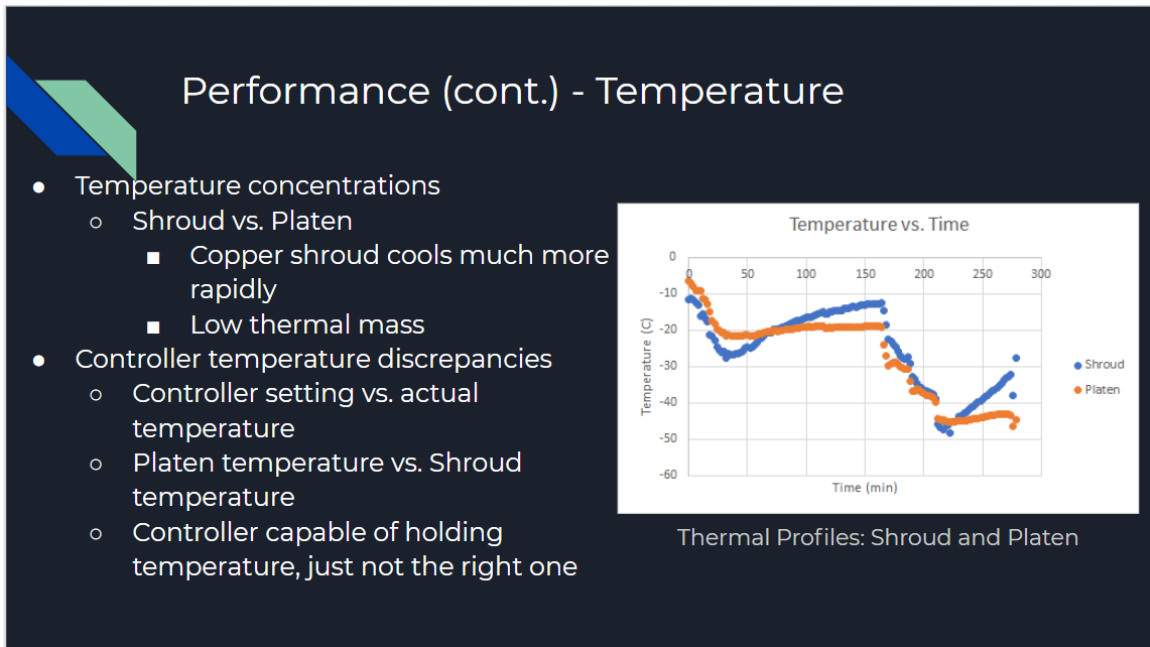


Figure 82: Caudill and Diamond Slide 11

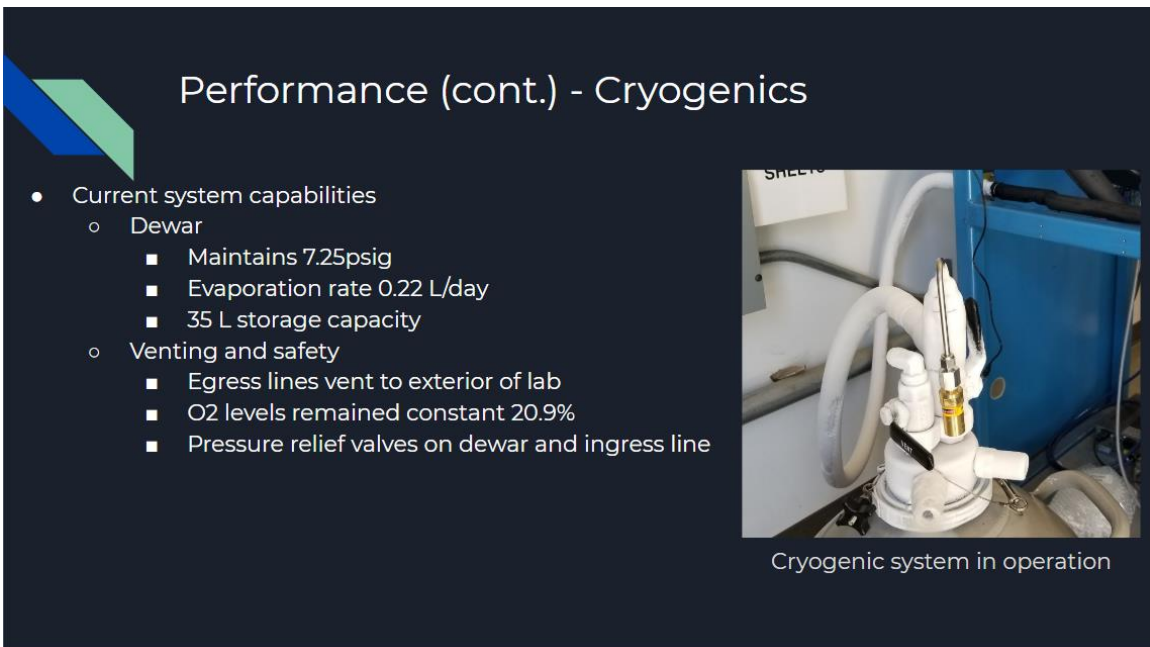


Figure 83: Caudill and Diamond Slide 12

Appendix D

THERMAL VACUUM TEST SETUPS

This appendix provides figures showing the various thermocouple configurations used for each thermal vacuum test conducted.

D.1 Tests 1-5 Setup

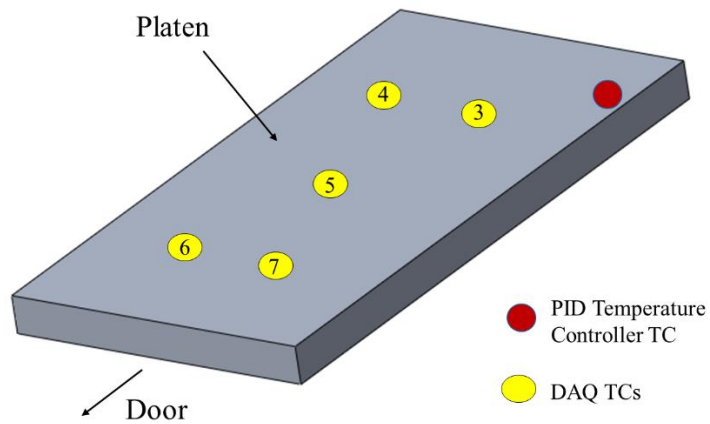


Figure 84: Tests 1-5 Thermocouple Configuration on Platen

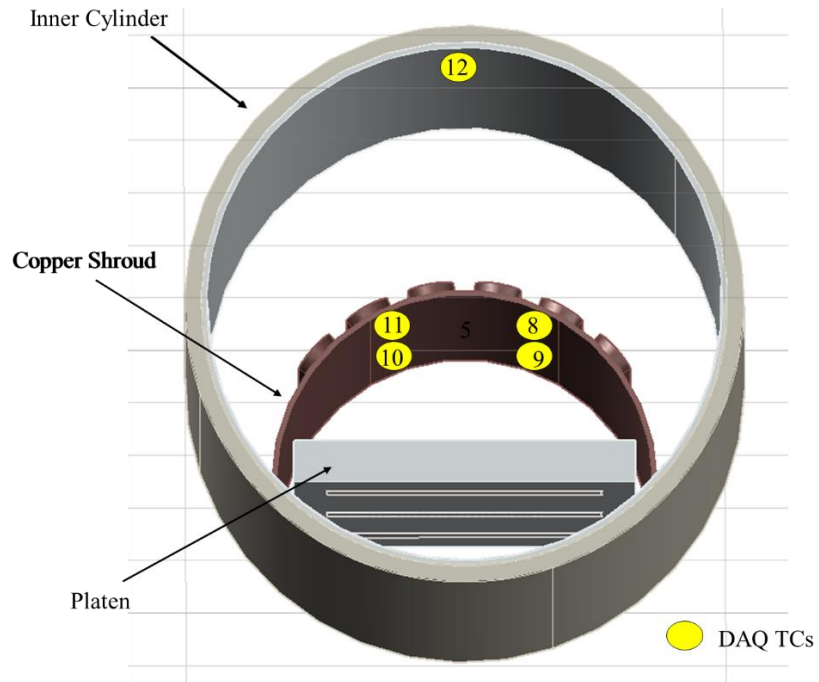


Figure 85: Tests 1-5 Thermocouple Configuration in Chamber

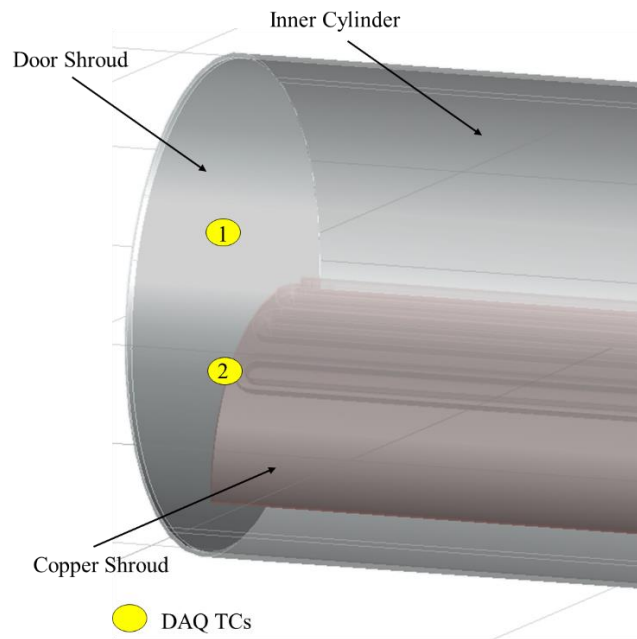


Figure 86: Tests 1-5 Thermocouple Configuration on Door Shroud

D.2 Test 6 Setup

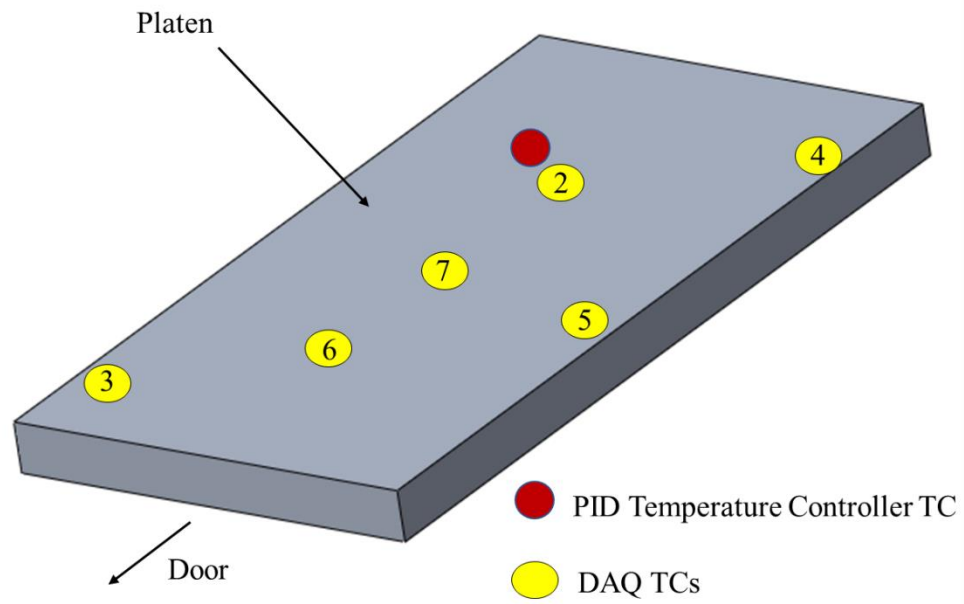


Figure 87: Test 6 Thermocouple Configuration on Platen

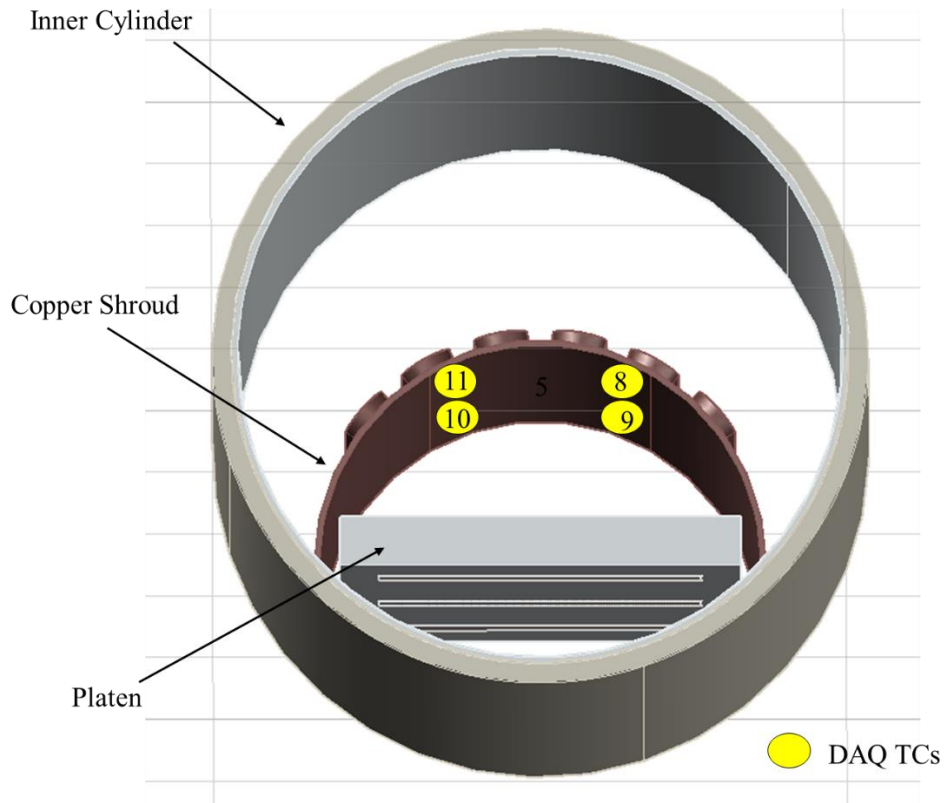


Figure 88: Test 6 Thermocouple Configuration in Chamber

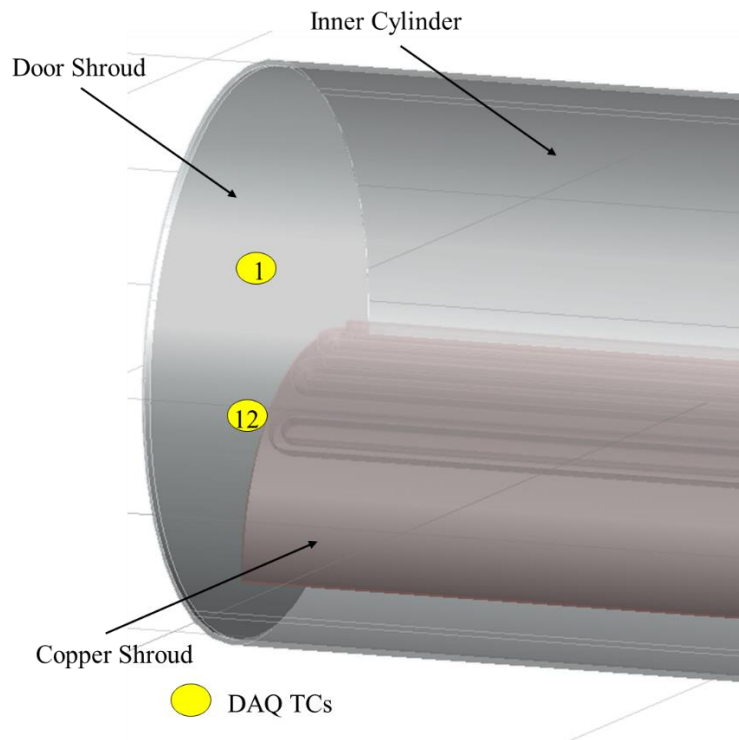


Figure 89: Test 6 Thermocouple Configuration on Door Shroud

D.3 Test 7 Setup

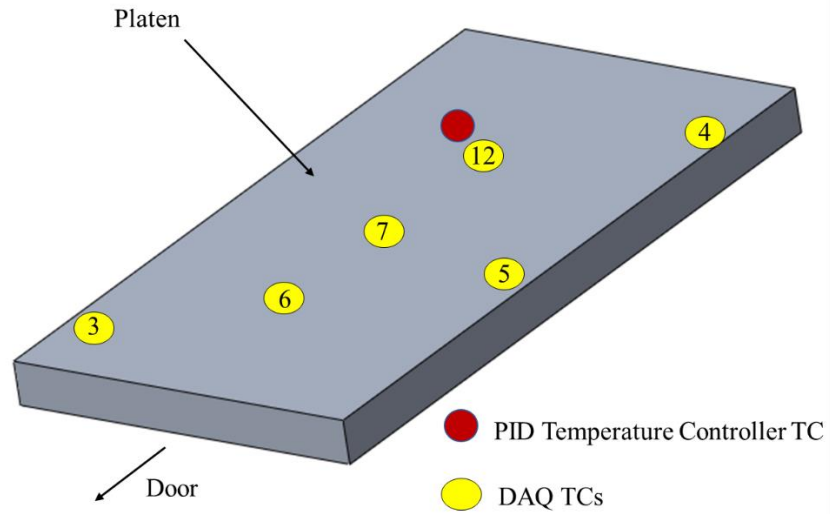


Figure 90: Test 7 Thermocouple Configuration on Platen

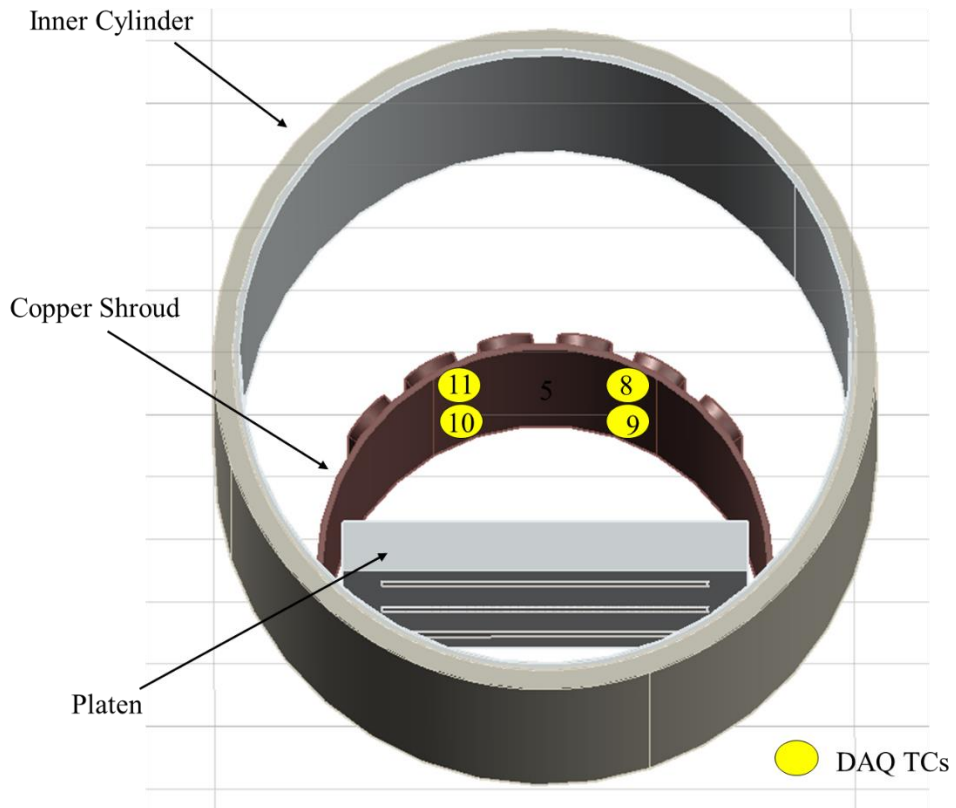


Figure 91: Test 7 Thermocouple Configuration in Chamber

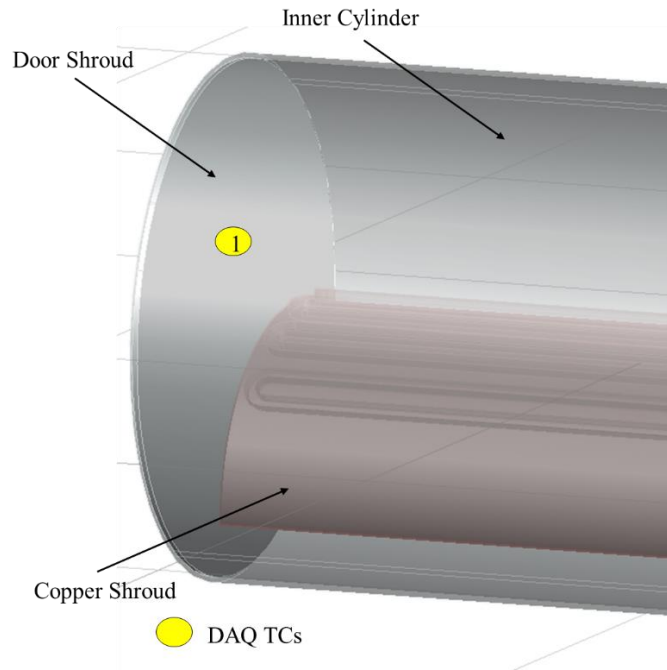


Figure 92: Test 7 Thermocouple Configuration on Door Shroud

D.4 Test 8-9 Setup

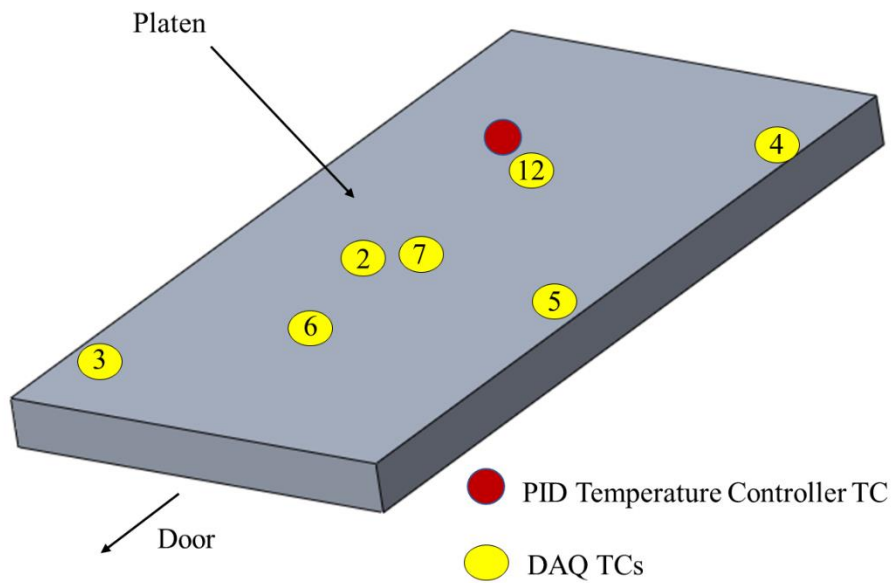


Figure 93: Tests 8-9 Thermocouple Configuration on Platen

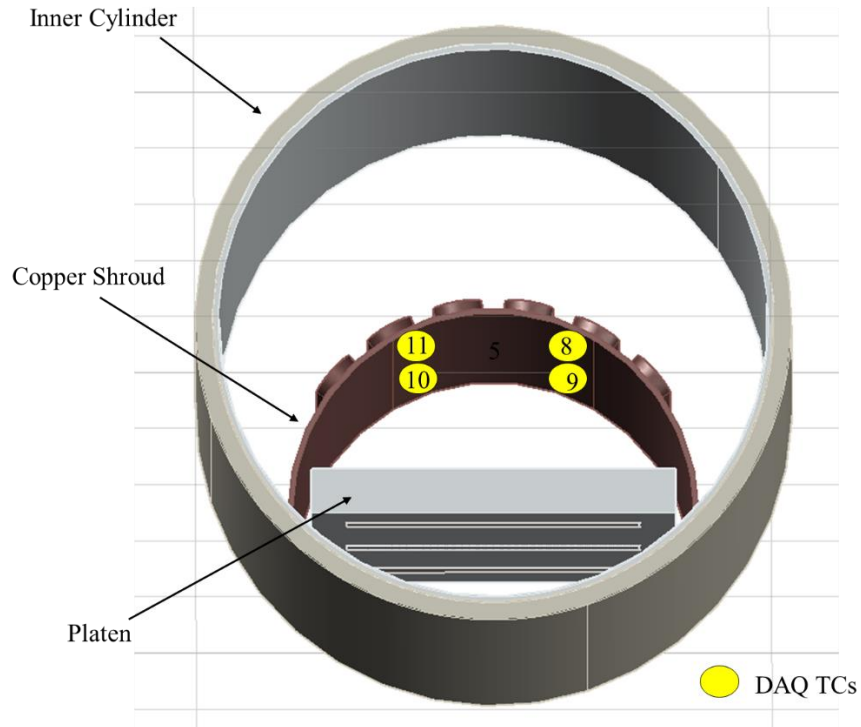


Figure 94: Tests 8-9 Thermocouple Configuration in Chamber

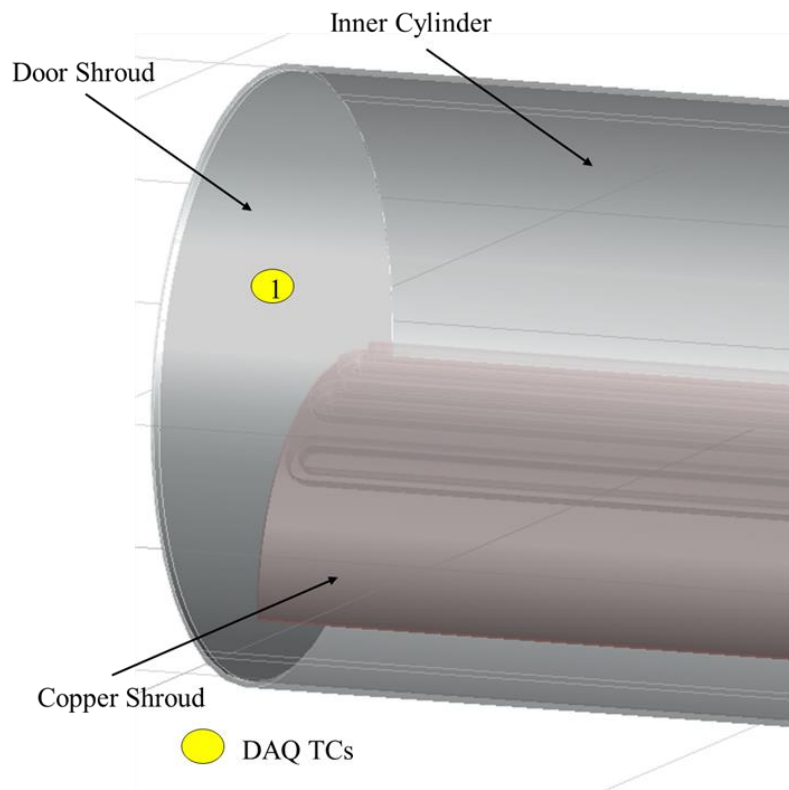


Figure 95: Tests 8-9 Thermocouple Configuration on Door Shroud

D.5 Test 10-11 Setup

Note that for Test 10, the Teflon support cylinders were not used to separate the mass model from the platen surface. Instead, the mass model made direct contact with the platen surface.

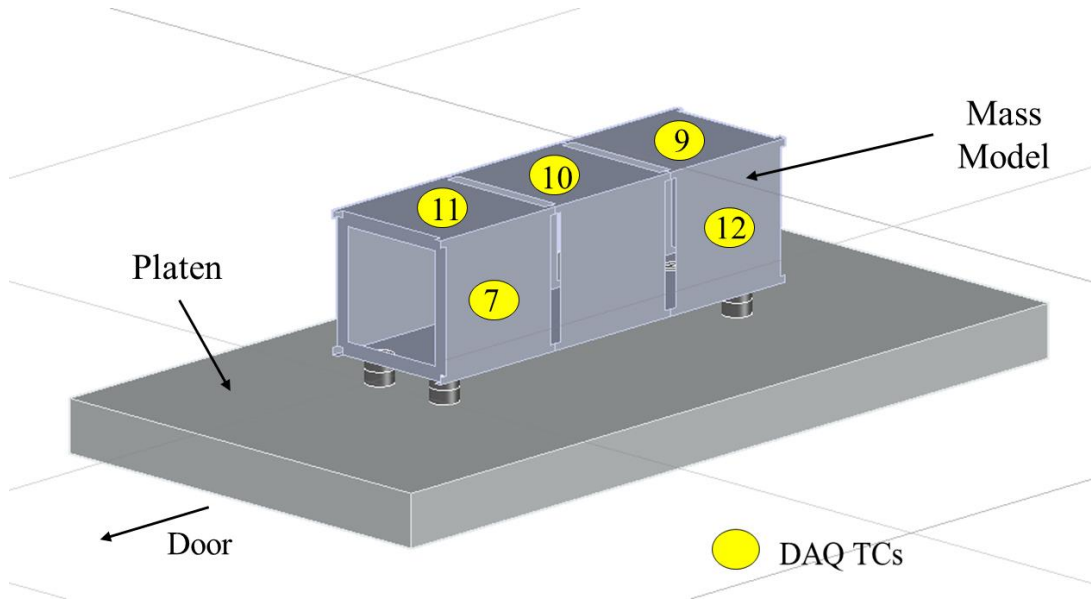


Figure 96: Tests 10-11 Thermocouple Configuration Mass Model (Right and Top)

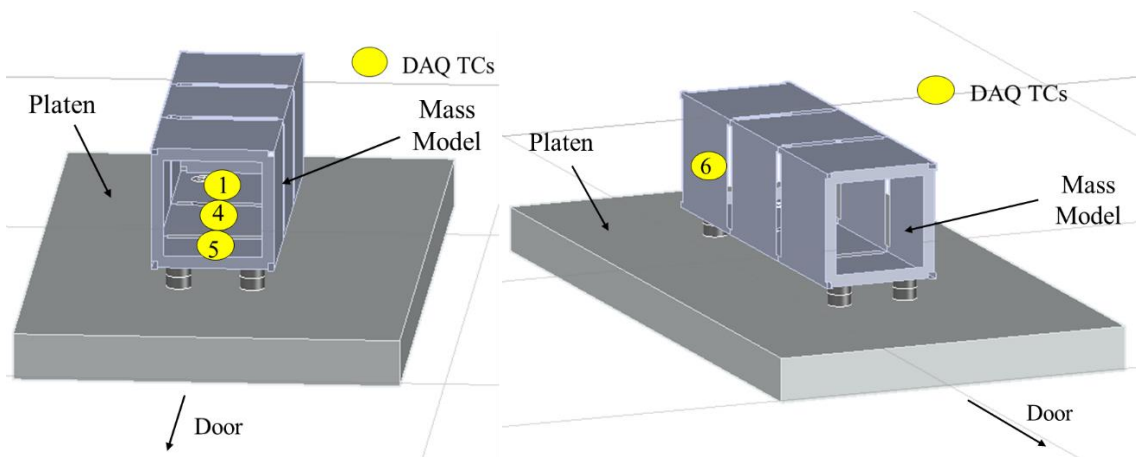


Figure 97: Tests 10-11 Thermocouple Configuration Mass Model (Bottom and Left)

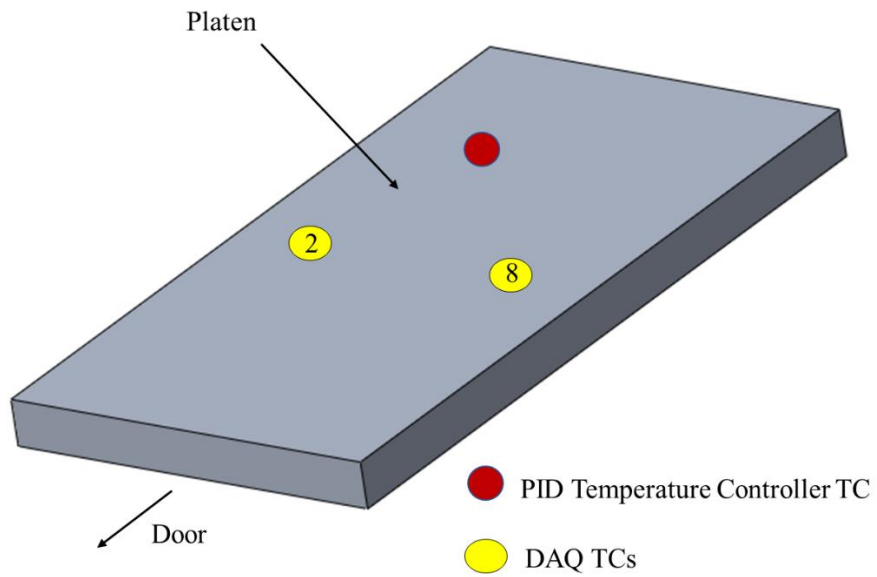


Figure 98: Tests 10-11 Thermocouple Configuration on Platen

D.6 Test 12 Setup

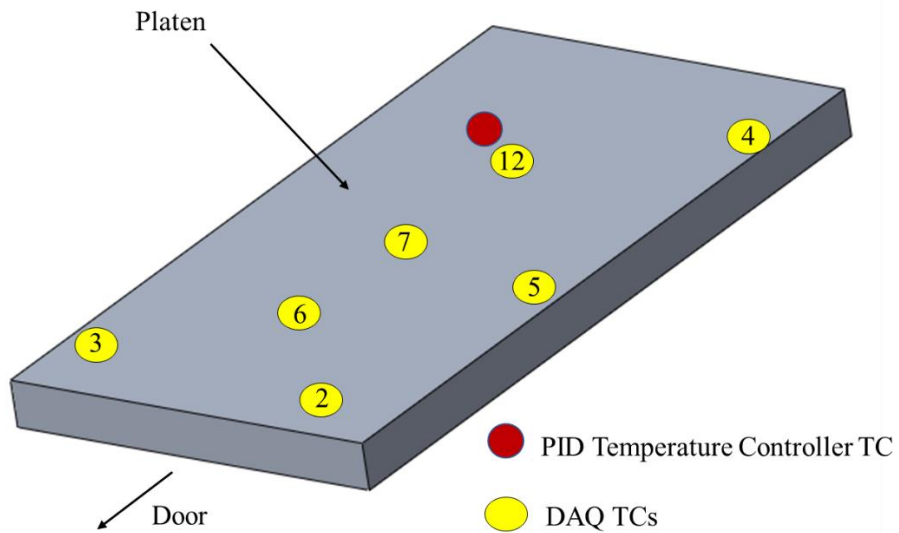


Figure 99: Test 12 Thermocouple Configuration on Platen

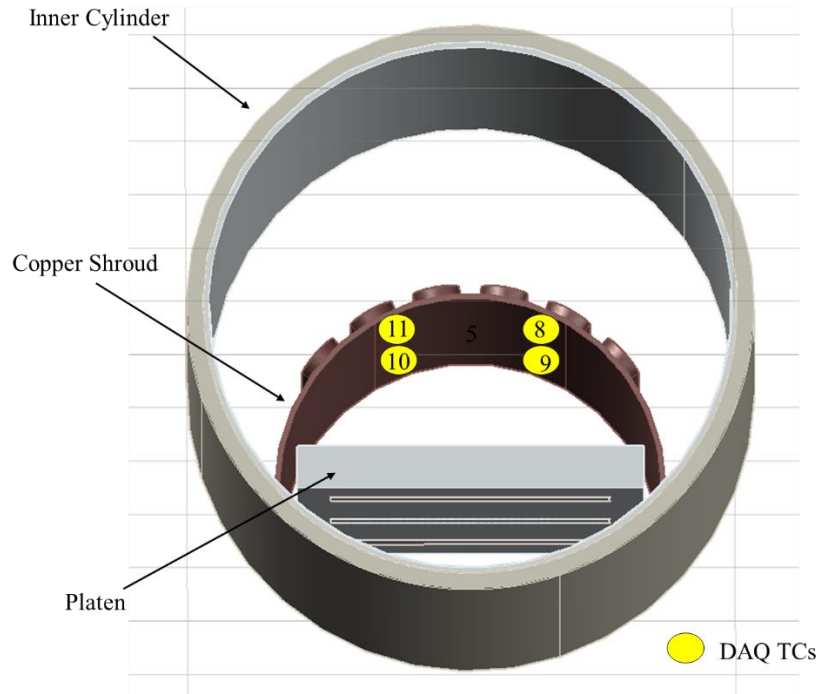


Figure 100: Test 12 Thermocouple Configuration in Chamber

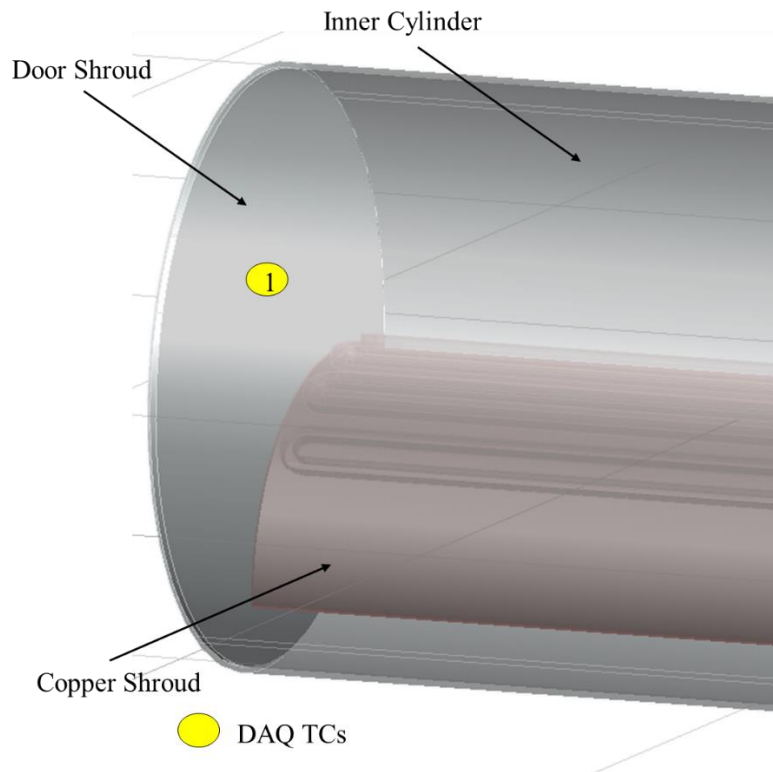


Figure 101: Test 12 Thermocouple Configuration on Door Shroud

D.7 Test 13 Setup

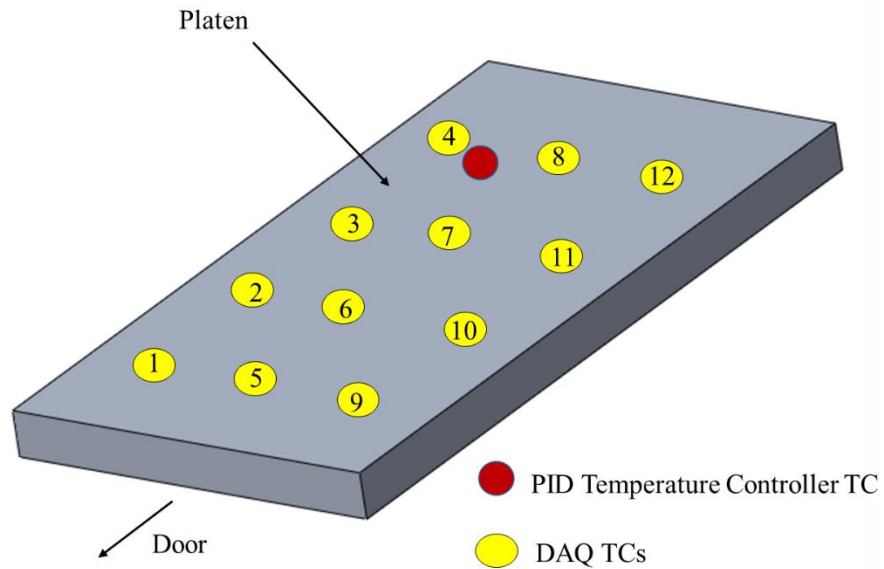


Figure 102: Test 13 Thermocouple Configuration on Platen

D.8 Tests 14-15 Setup

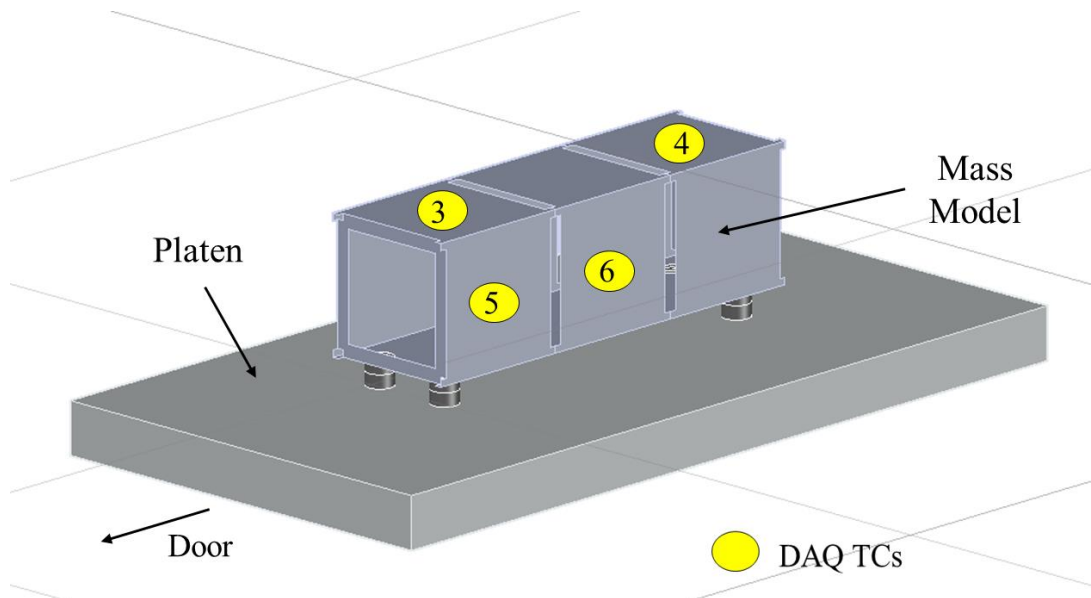


Figure 103: Tests 14-15 Thermocouple Configuration on Mass Model (Right and Top)

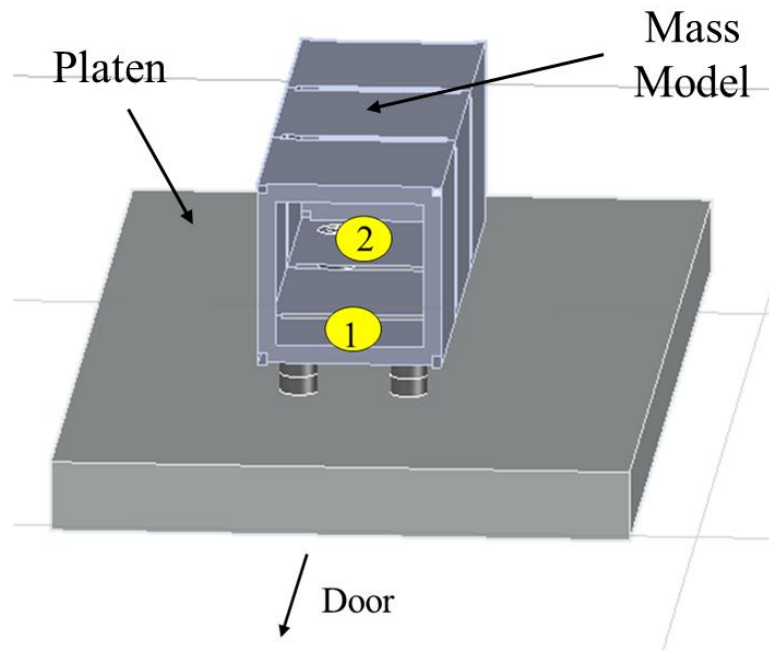


Figure 104: Tests 14-15 Thermocouple Configuration on Mass Model (Bottom)

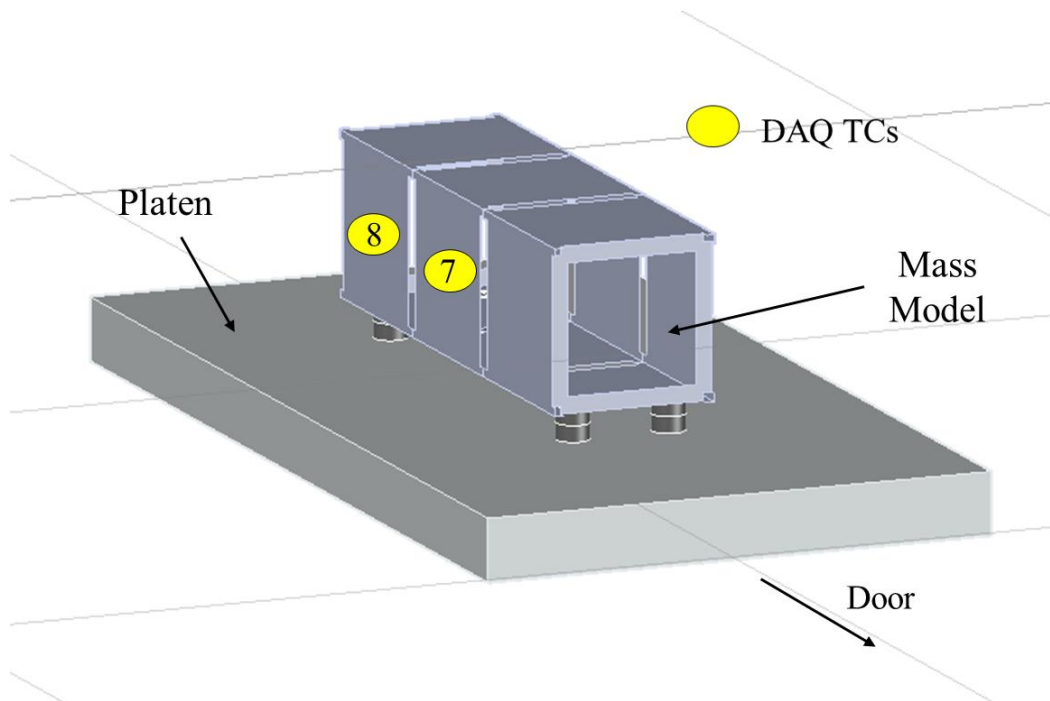


Figure 105: Tests 14-15 Thermocouple Configuration on Mass Model (Left)

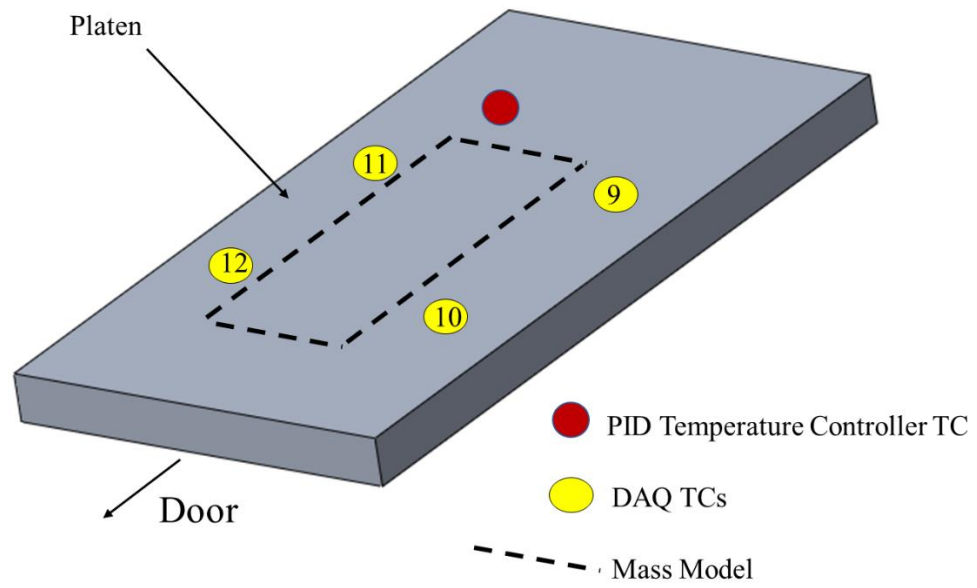


Figure 106: Tests 14-15 Thermocouple Configuration on Platen

Appendix E

ANALYTICAL MODEL CALCULATIONS

Constants:

$$\sigma = 5.67E - 8 \left[\frac{W}{m^2 K^4} \right] \quad \text{Stefan-Boltzmann Constant}$$

$$Q_{in} = 0.7500 * 475 = 356.2500 [W] \quad \text{Power from each heater}$$

$$\rho_{AL} = 2700 \left[\frac{kg}{m^3} \right] \quad \text{Density of Aluminum 6061}$$

$$\rho_{SS} = 8030 \left[\frac{kg}{m^3} \right] \quad \text{Density of 304 Stainless Steel}$$

$$V_{heater} = .2540 * .0190 * 0.0415 = 2.0028E - 4 [m^3] \quad \text{Volume of heater}$$

$$V_{platen} = (0.3556 * 0.0381 * 0.6096) - (3 * V_{heater}) = 0.0077 [m^3]$$

Volume of Platen

$$m_{heater} = \rho_{SS} * V_{heater} = 1.6082 [kg] \quad \text{Mass of heater}$$

$$m_{platen} = \rho_{AL} * V_{platen} = 20.6773 [kg] \quad \text{Mass of platen}$$

$$C_{pAl} = 896 \left[\frac{J}{kgK} \right] \quad \text{Specific Heat of Aluminum 6061}$$

$$S_{Aplaten} = 3 * (0.2540 * 0.0415) = 0.0316 [m^2]$$

Surface Areas of Platen in Contact with the Heaters

$$R_{cAlSS} = 3.3000E - 4 \left[\frac{Km^2}{W} \right] \quad \text{Aluminum-Stainless Steel Area Specific Contact Resistance}$$

$$R_{cplaten} = \frac{R_{cAlSS}}{S_{Aplaten}} = 0.0104 \left[\frac{K}{W} \right] \quad \text{Contact Resistance Between Platen and Heaters}$$

$$T_o = 290.1500 [K] \quad \text{Initial Temperature}$$

$$\epsilon_{Al} = 0.5000 \quad \text{Emissivity of Aluminum}$$

$$A_{platenrad} = (2 * 0.0381 * 0.3556) + (2 * 0.0381 * 0.6096) + (0.3556 * 0.6096) =$$

$$0.5071 [m^2] \quad \text{Area of platen that radiates}$$

$$dt = 25 * 60 [sec] \quad \text{Total time of Conduction}$$

Steady State Calculations:

$$T_2 = \left((3 * Q_{in} - R_{cplaten}) * \frac{dt}{m_{platen} * C_{pAl}} \right) + T_o = 376.6791 [K]$$

Temperature of Platen after Conduction

$$Q_{outrad} = sig * \epsilon_{Al} * A_{platenrad} * (T_2^4 - T_o^4) = 187. [W] \quad \text{Heat transfer via Radiation}$$

$$t_{85min} = 85 * 60 [sec] \quad \text{Total time of Radiation}$$

$$T_3 = \left(-Q_{outrad} * \frac{t_{85min}}{m_{platen} * C_{pAl}} \right) + T_2 = 325.0549 [K]$$

Temperature of Platen After 85 minutes of Radiation

Appendix F

TESTS RESULTS

This appendix provides the test results from each test conducted for this thesis. Details about manual operations made during the test are provided when applicable.

F.1 Test 1 Data

During Test 1, the 12-channel temperature logger ran out of battery power after approximately 36 minutes. For this reason, data was not collected for the entirety of the test.

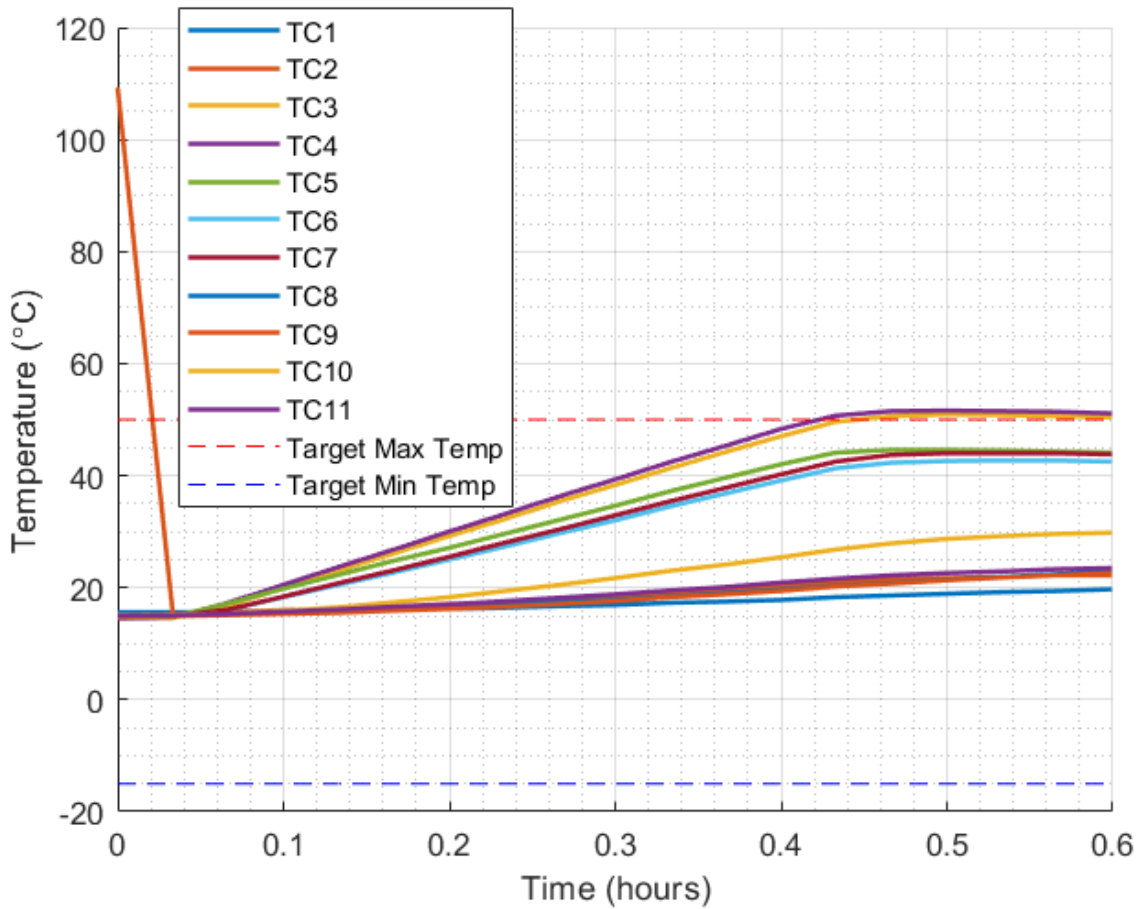


Figure 107: Thermocouple Data from Test 1

F.2 Test 2 Data

For Test 2, the cooling system was activated at hour zero and at hour 4.75. The door shroud valve was opened during the first hour of the test as well as between hours 4.75 and 5.

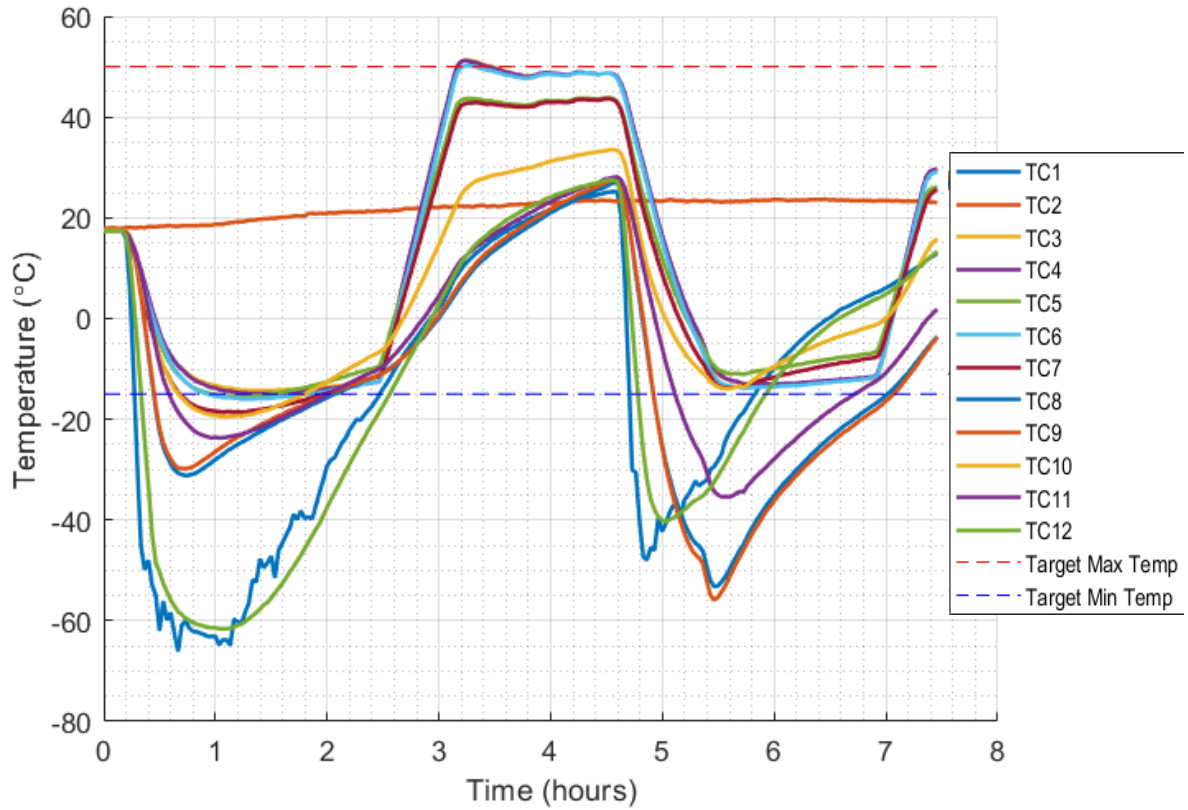


Figure 108: Thermocouple Data from Test 2

F.3 Test 3 Data

For Test 3, the cooling system was activated at hour zero and just before hour five. The door shroud valve was opened during the first 17 minutes of the test, just before hour two, at about 5.5 hours.

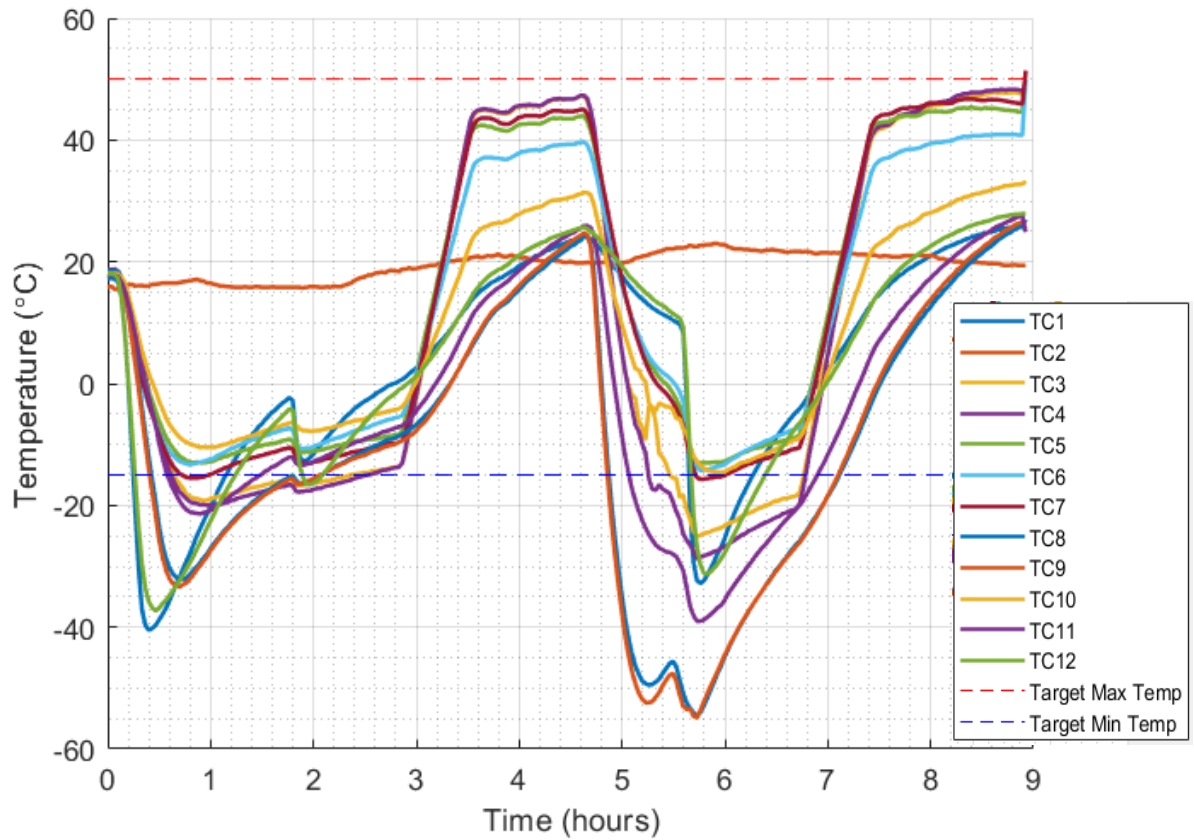


Figure 109: Thermocouple Data from Test 3

F.4 Test 4 Data

For Test 4, the door shroud LN₂ valve was opened during the first 26 minutes of the test. It was also opened just before hour three, just after hour four, and between hours six and seven. The LN₂ supply was expended just before hour seven, which is why the second cold soak was not completed.

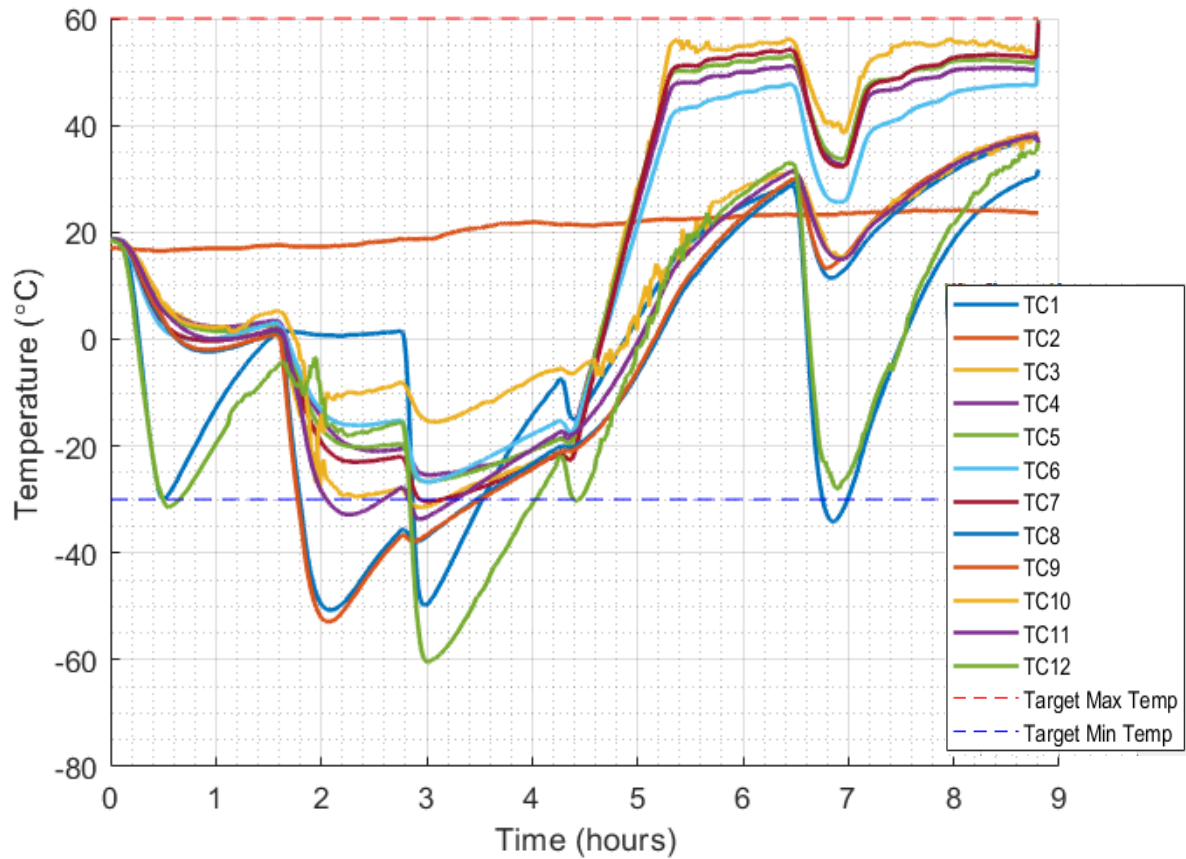


Figure 110: Thermocouple Data from Test 4

F.5 Test 5 Data

For Test 5, a single 90 minute cold soak was conducted. The door shroud LN₂ valve was opened for 20 minutes after 30 minutes of testing. It was also opened for thirteen minutes after one hour of testing, for 15 minutes after 1.5 hours of testing, for 15 minutes after almost two hours of testing, and finally for about 30 minutes after about 2.5 hours of testing. The LN₂ supply was expended after 3.5 hours of testing

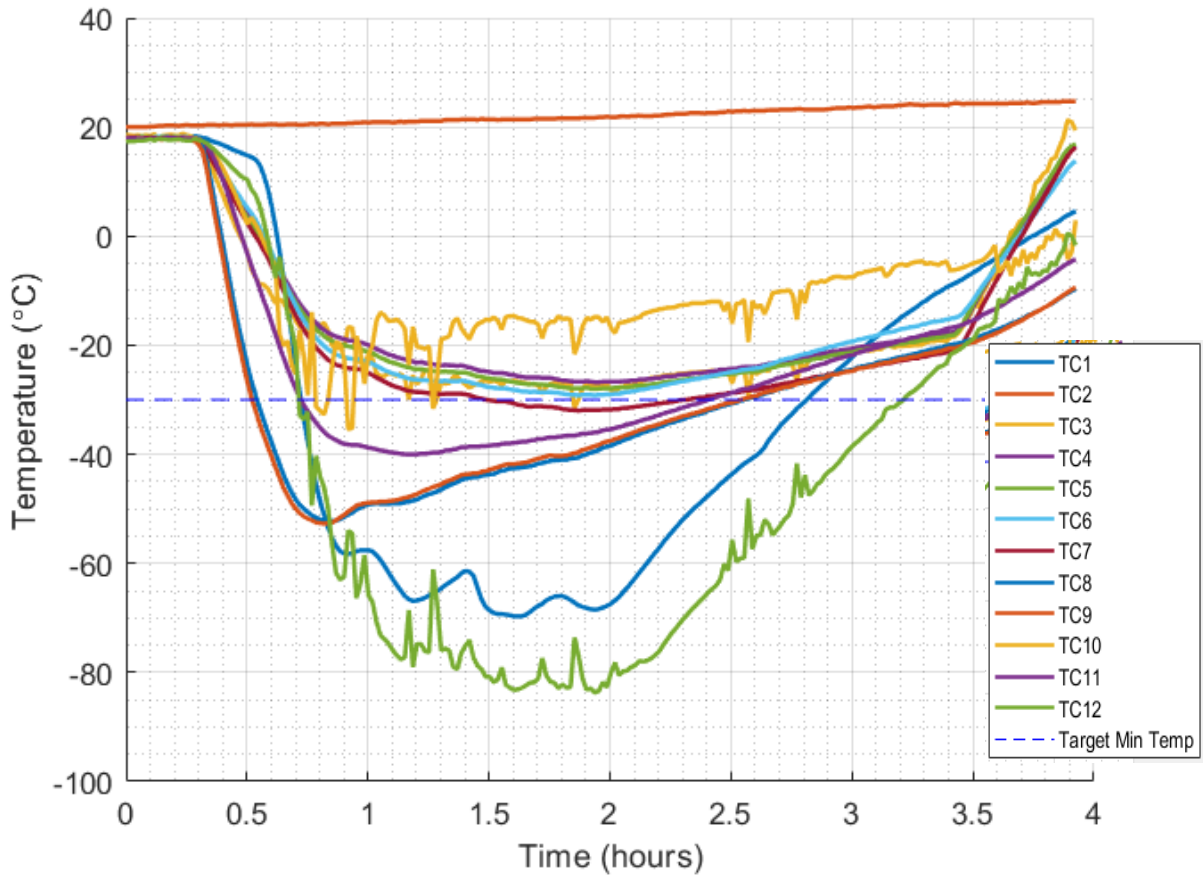


Figure 111: Thermocouple Data from Test 5

F.6 Test 6 Data

For Test 6, the door shroud LN₂ valve was opened just after hour one for only three minutes as well as just after 1.5 hours for only four minutes. The door shroud LN₂ valve was opened again for nine minutes after about 5.5 hours.

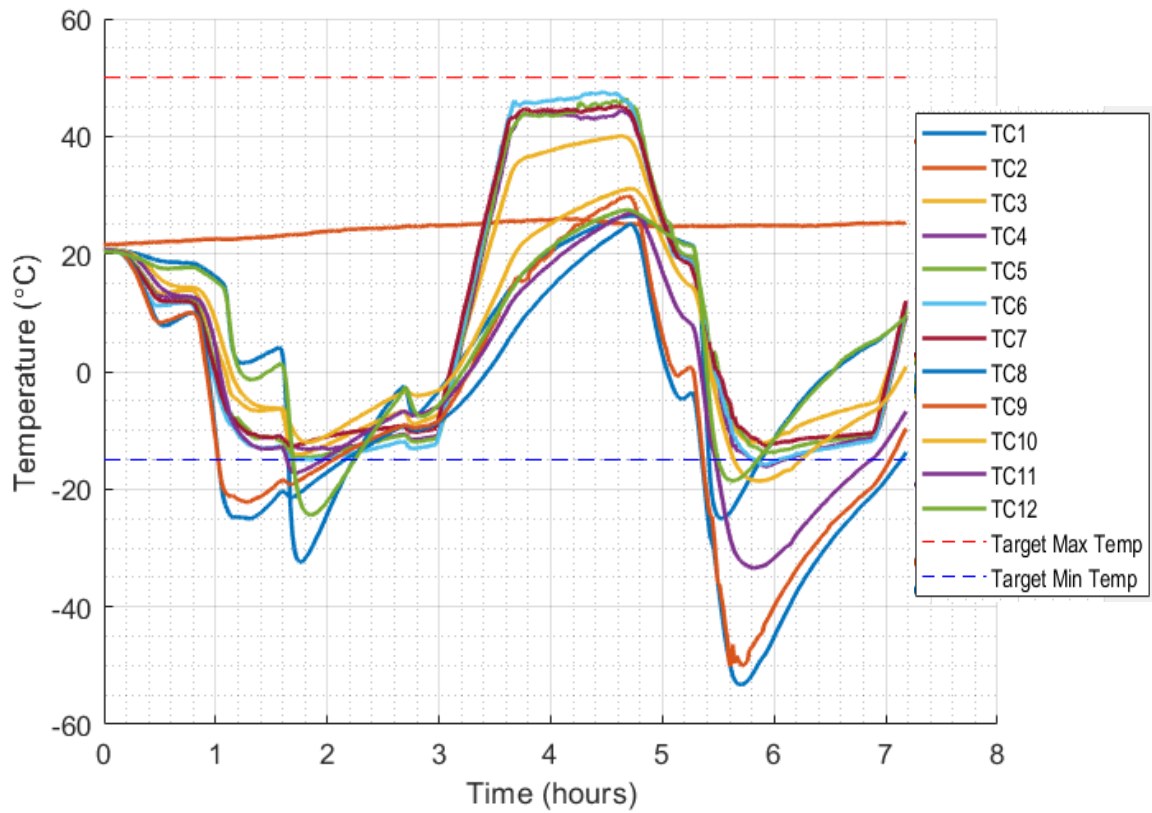


Figure 112: Thermocouple Data from Test 6

F.7 Test 7 Data

For Test 7, the door shroud LN₂ valve was manually opened after about 2.5 hours for about ten minutes. It was also opened for about nine minutes just before hour seven. Note that the polarity of TC3 was unintentionally flipped during this test.

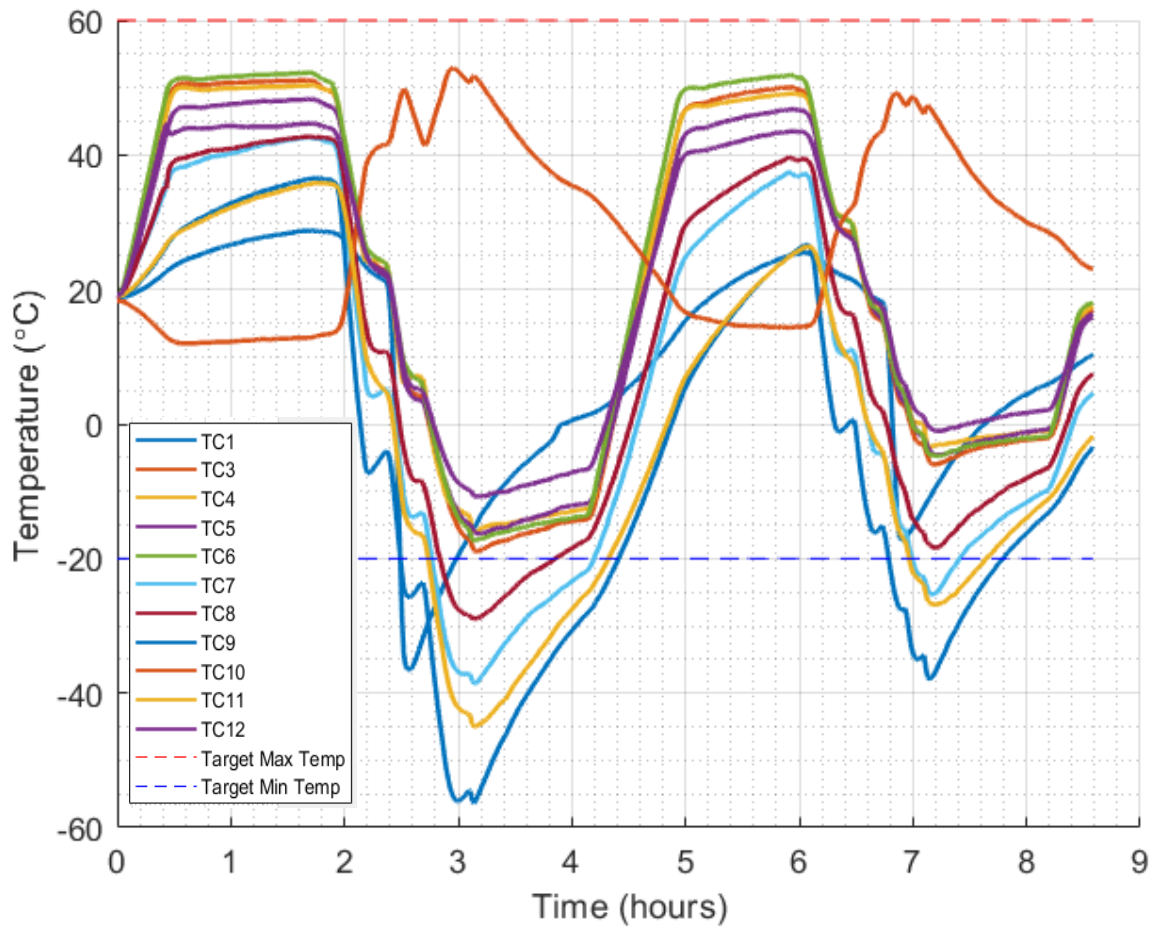


Figure 113: Thermocouple Data from Test 7

F.8 Test 8 Data

For Test 8, the door shroud LN₂ valve was opened for five minutes at hour two as well as for three minutes just before 2.5 hours. A deeper bucket for the exhaust hose to be submerged in was also introduced for this test. Note that the polarity of TC3 was flipped during this test.

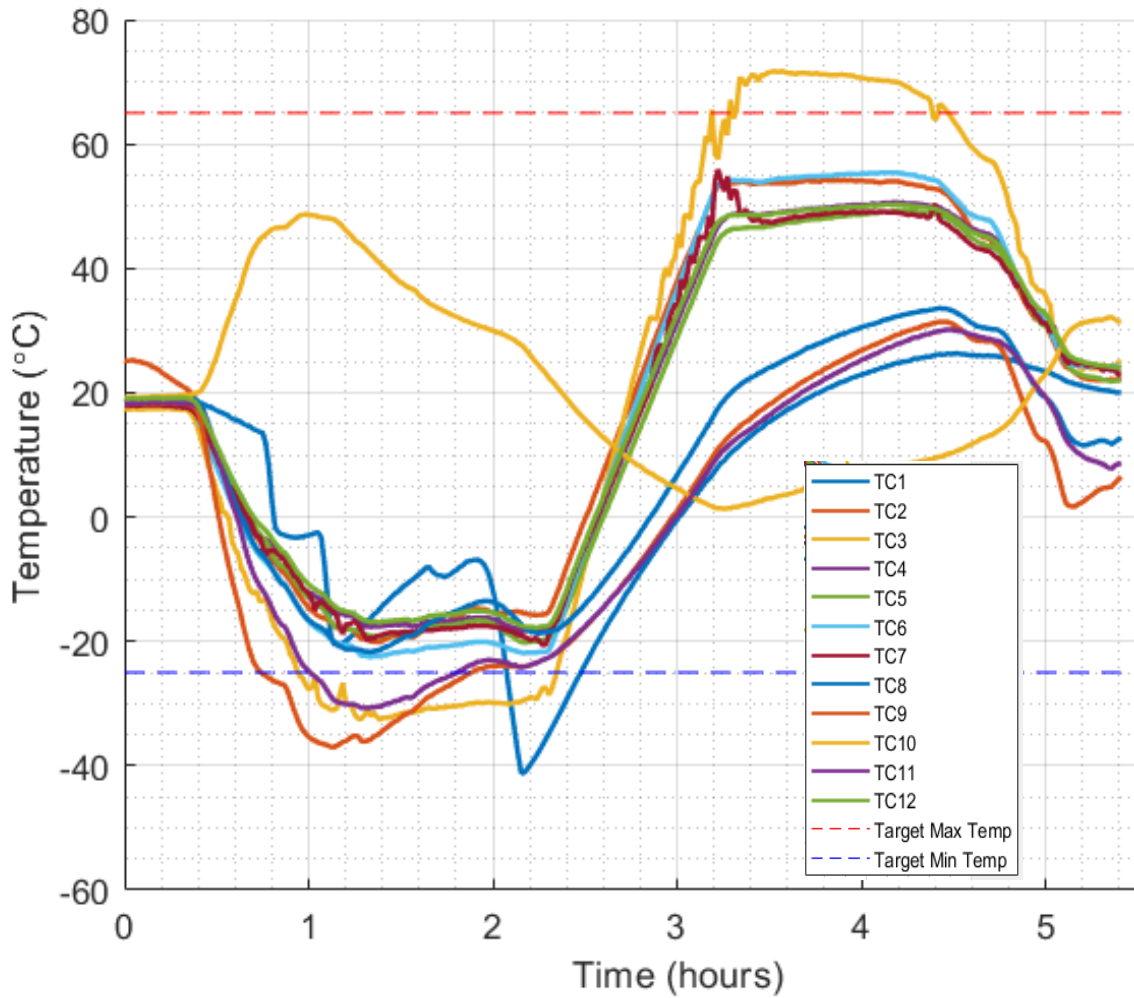


Figure 114: Thermocouple Data from Test 8

F.9 Test 9 Data

For Test 9, the door shroud LN₂ valve was manually opened just after one hour of testing for about four minutes. It was also opened just after two hours of testing for about three minutes. The door shroud LN₂ valve was opened again just before hour six for about two minutes and again just after hour six for about four minutes. Note that the polarity of TC3 was unintentionally flipped during this test.

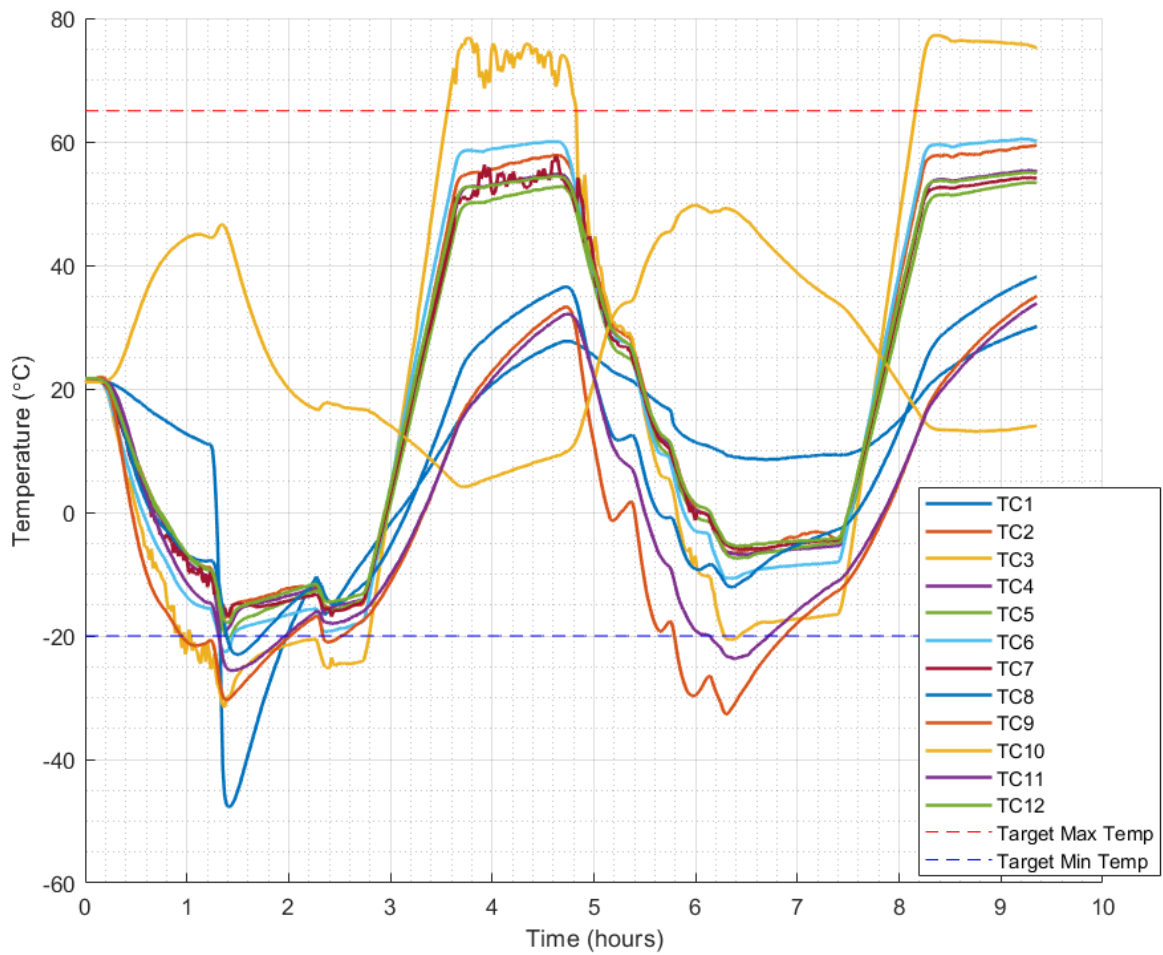


Figure 115: Thermocouple Data from Test 9

F.10 Test 10 Data

For Test 10, the door shroud LN₂ valve was only activated for about six minutes after 45 minutes of testing.

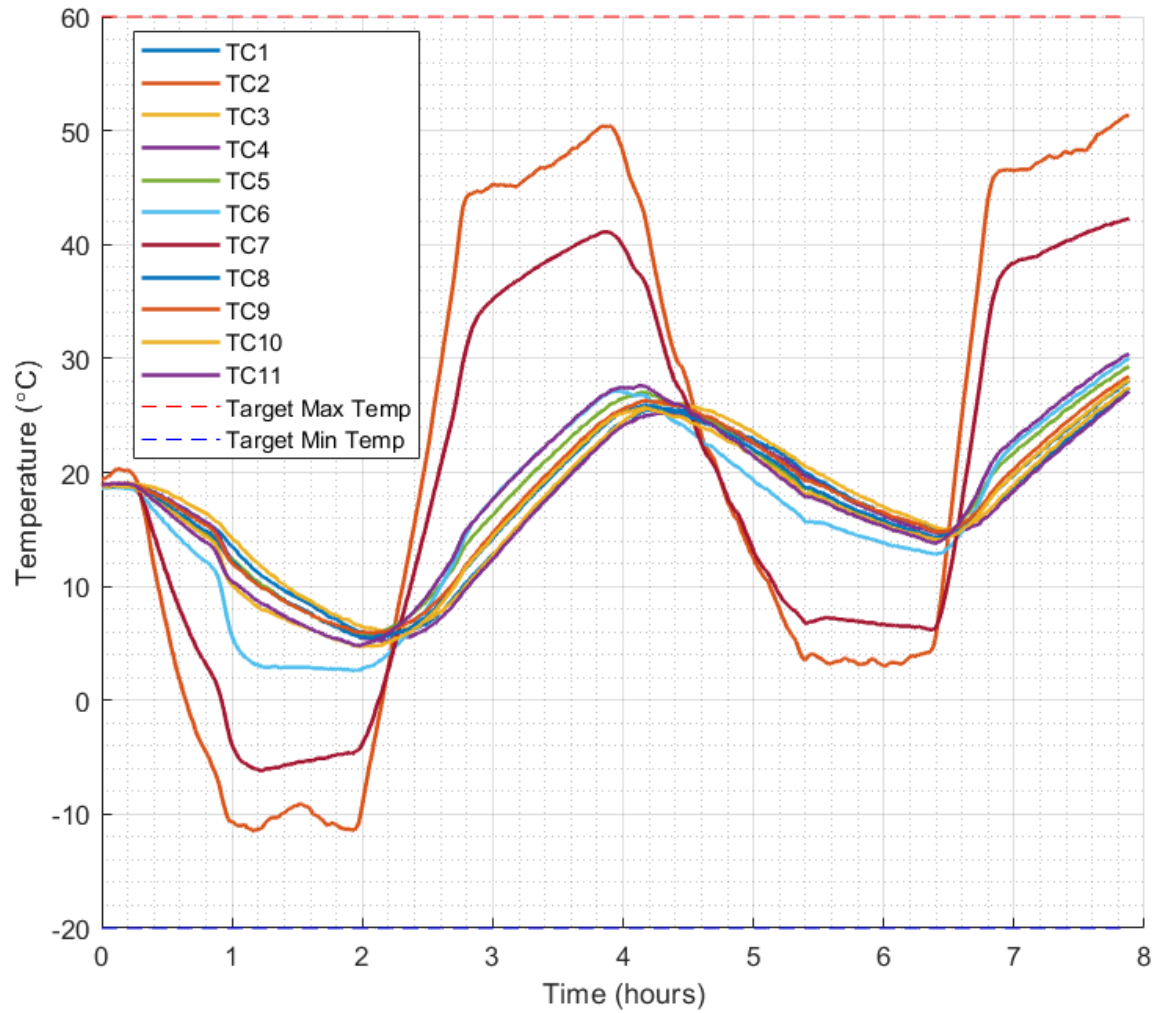


Figure 116: Thermocouple Data from Test 10

F.11 Test 11 Data

For Test 11, the door shroud LN₂ valve was not opened for any part of the test.

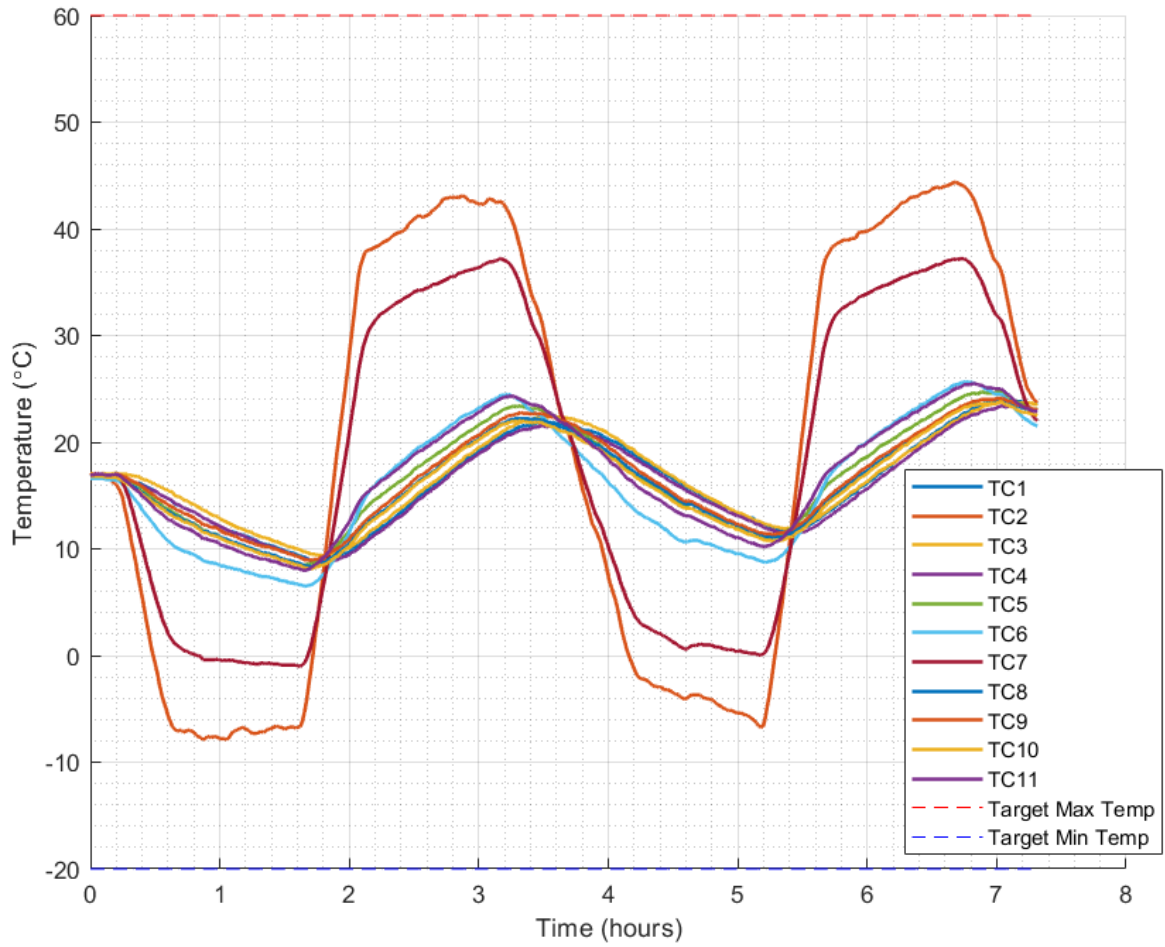


Figure 117: Thermocouple Data from Test 11

F.12 Test 12 Data

For Test 12, the door shroud LN₂ valve was opened for about seven minutes at hour one of testing. It was not opened at any other time during the test.

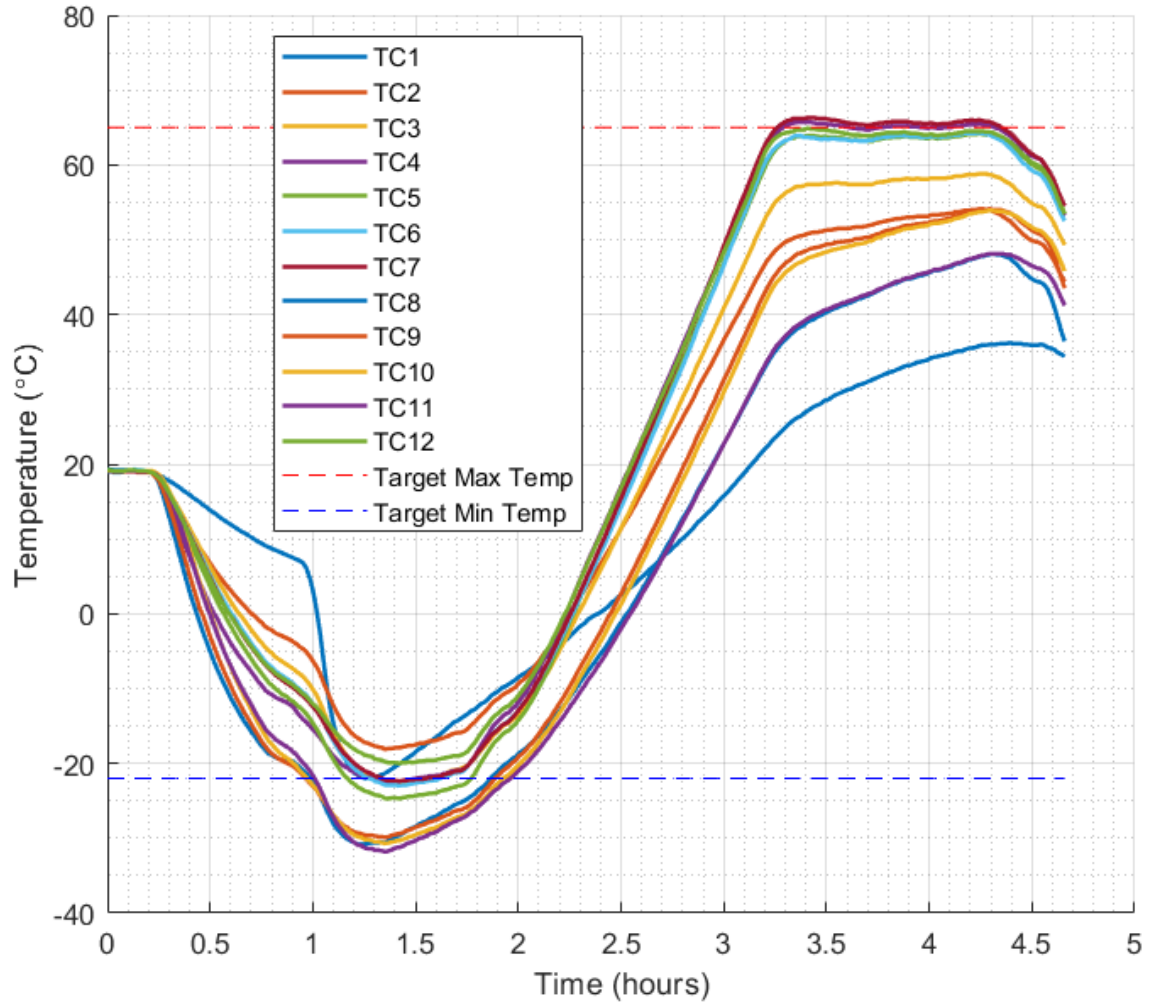


Figure 118: Thermocouple Data from Test 12

F.13 Test 13 Data

For Test 13, the door shroud LN₂ valve was not opened at any time during the test.

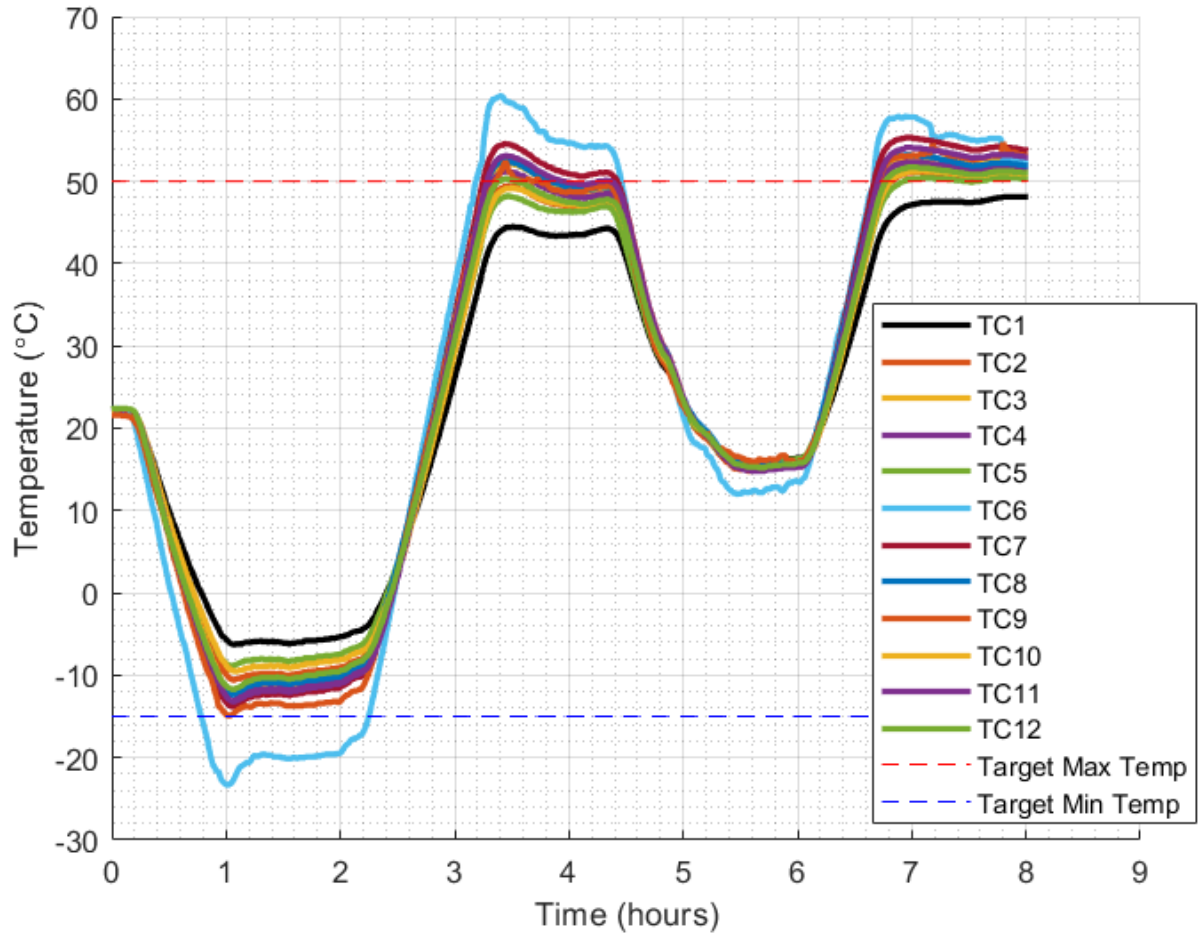


Figure 119: Thermocouple Data from Test 13

F.14 Test 14 Data

For Test 14, the door shroud LN₂ valve was not opened at any time during the test.

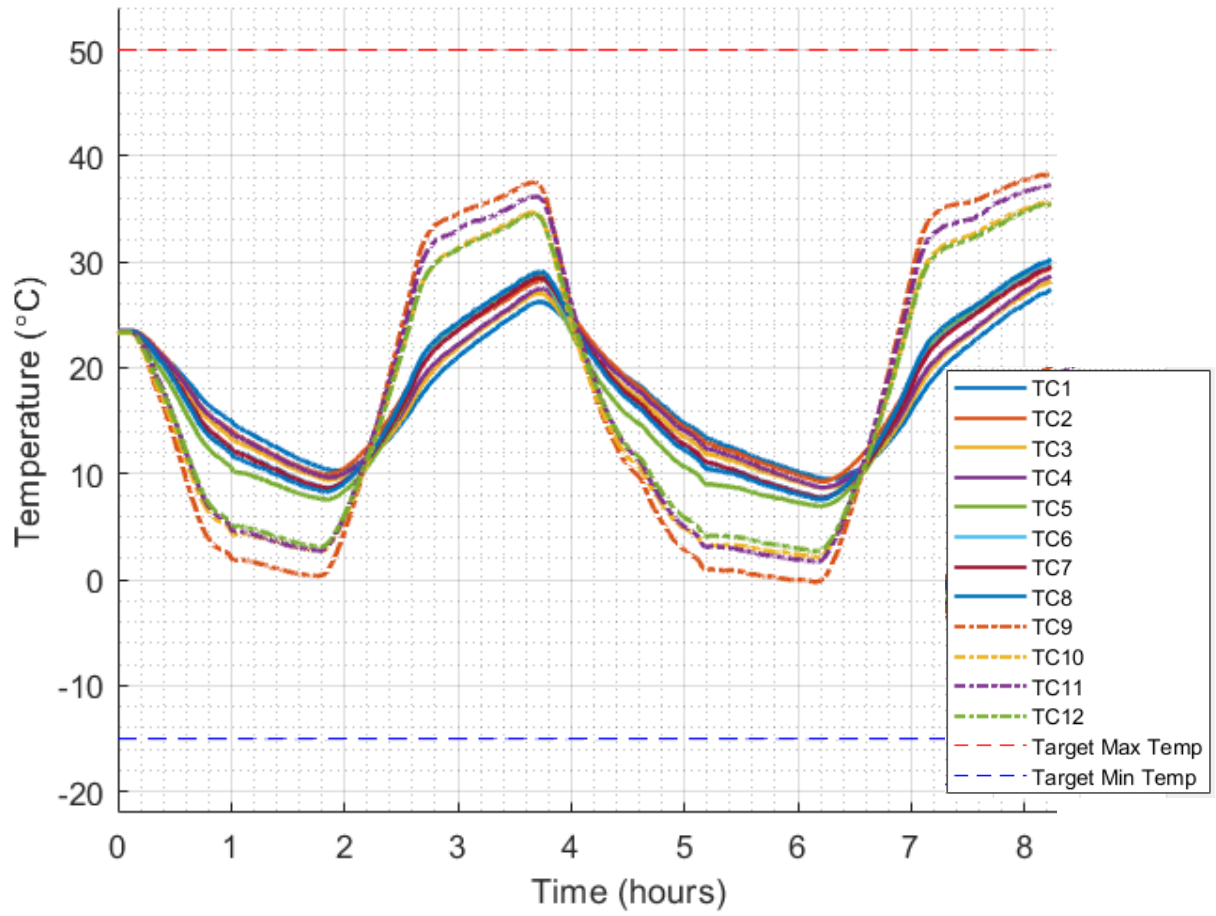


Figure 120: Thermocouple Data from Test 14

F.15 Test 15 Data

For Test 15, the door shroud LN₂ valve was not manually opened at any time during the test. The vertical lines shown in Figure 121: *Thermocouple Data from Test 15* represent the start and stop times of the period of time that the temperature logger was not recording data due to a dead battery. The DAQ thermocouple data is linearly interpolated between these two vertical lines.

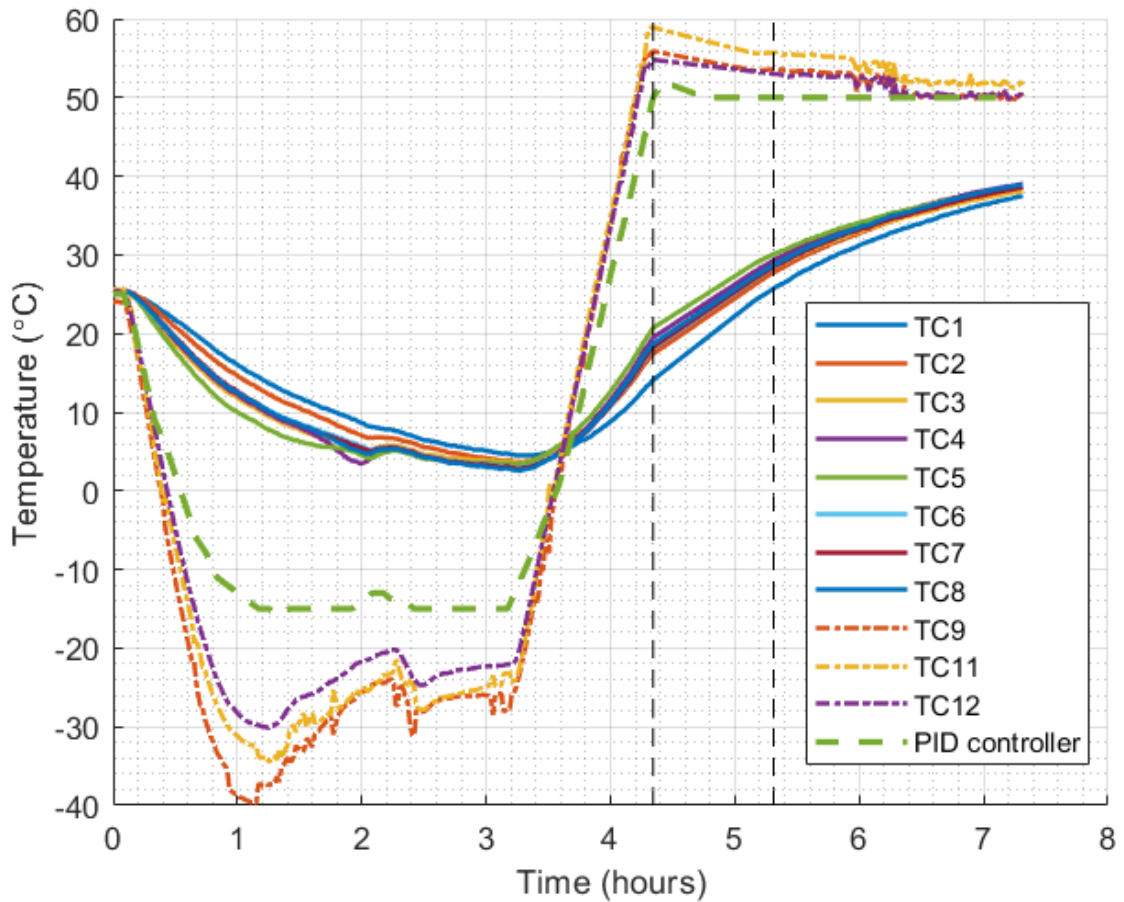


Figure 121: Thermocouple Data from Test 15

Appendix G

THERMOCOUPLE BUILD/REPAIR PROCEDURE

The thermocouples in use in the Blue TVAC may need to be replaced, rebuilt, or repaired in the future. Instructions for building a thermocouple are included below. A Philips screwdriver, wire strippers, and wire cutters are needed for this procedure.

1. Unscrew the two screws on the back of the thermocouple connector shown in Figure 122



Figure 122: Screws on Back of Thermocouple Connector

2. Unscrew the two screws inside the thermocouple connector shown in Figure 123

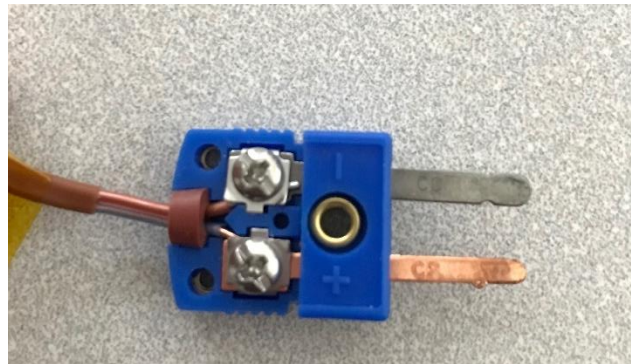


Figure 123: Screws Inside Thermocouple Connector

3. If needed, strip the insulative coating from the thermocouple wires as shown in Figure 124

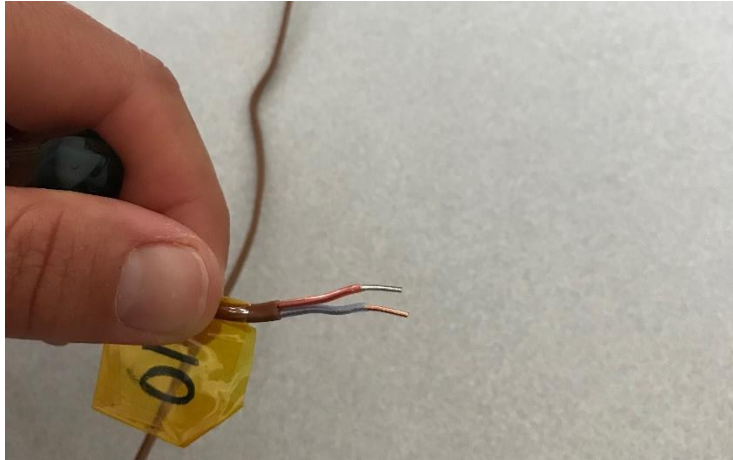


Figure 124: Stripped Thermocouple Wires

4. If needed, cut the exposed thermocouple wires so that approximately 1 cm of each wire is exposed.
5. Place the circular insulative disk around the thermocouple wires as shown in Figure 125. Ensure that the exposed wires are NOT touching.

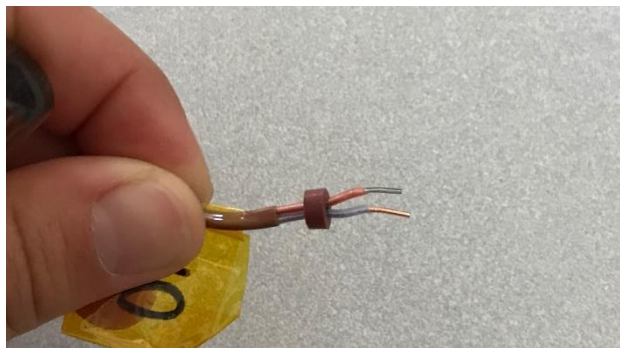


Figure 125: Thermocouples positioned in Insulative Disk

6. Position the bronze colored thermocouple wire between the bronze colored probe and the small plate and position the silver colored thermocouple wire between the silver colored probe and the small plate. This is shown in Figure 126.

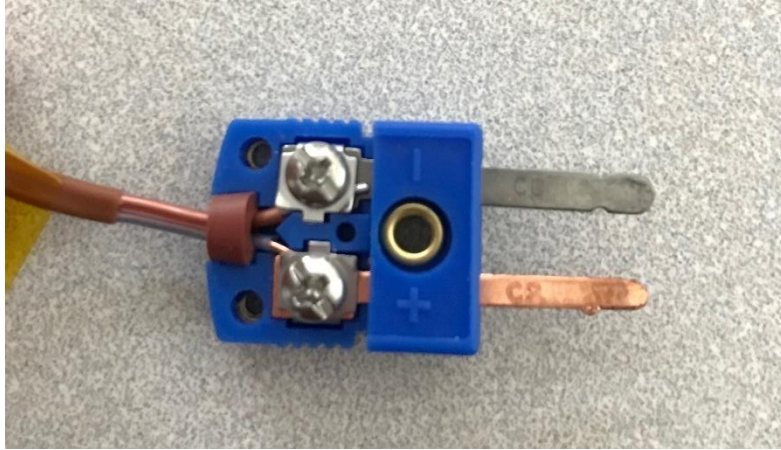


Figure 126: Exposed Thermocouple Wires Positioned Between Probes and Plates

7. Screw the two internal screws back into place. Ensure that the exposed thermocouple wires are in contact with the probes and are not loose.
8. Screw the external screws and plastic jacket back into place as shown in Figure 127.

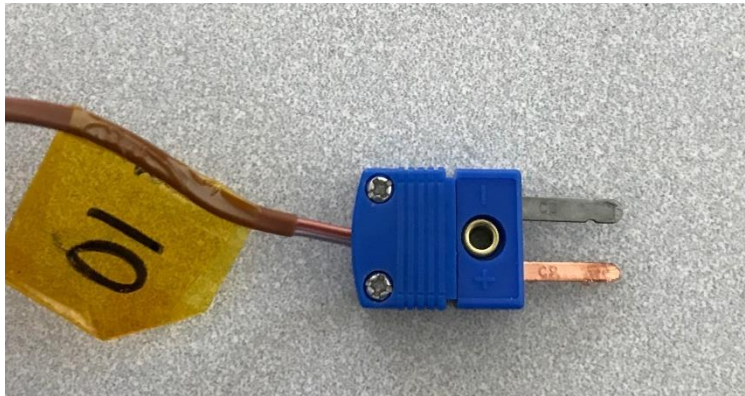


Figure 127: Assembled Thermocouple

Appendix H

THERMAL MODEL RESULTS

This appendix provides additional color maps from the thermal vacuum simulations that included the mass model.

H.1 Additional Cooling Phase Simulation Results

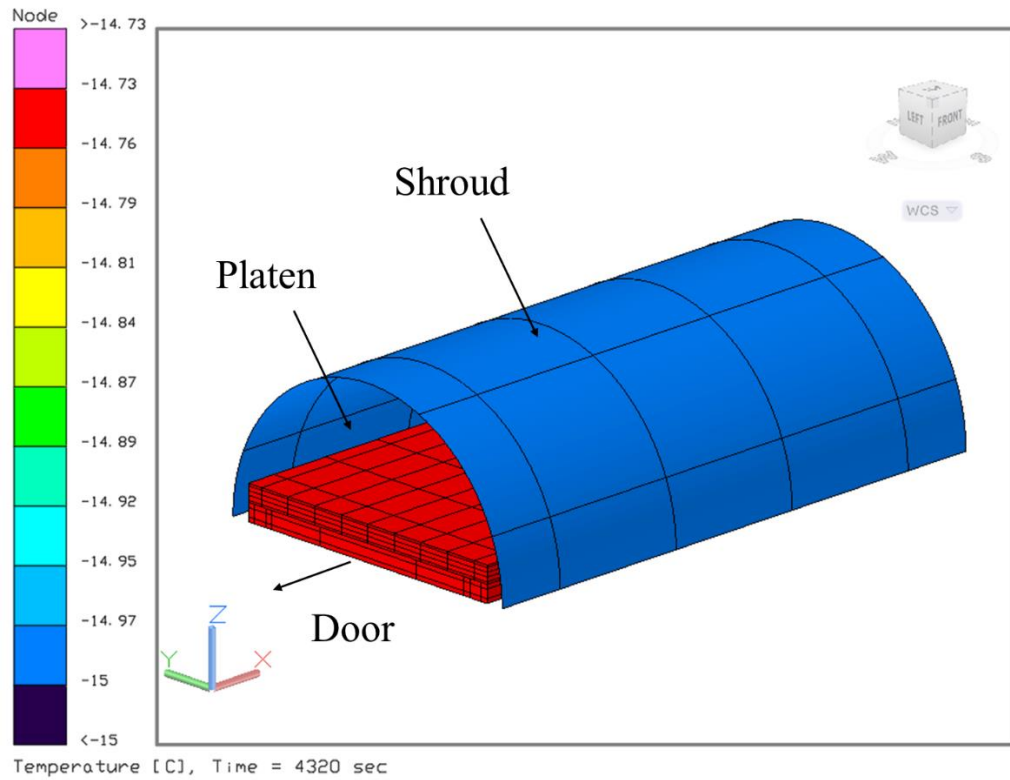


Figure 128: Predicted Temperature of Shroud During Cooling Phase with Mass Model

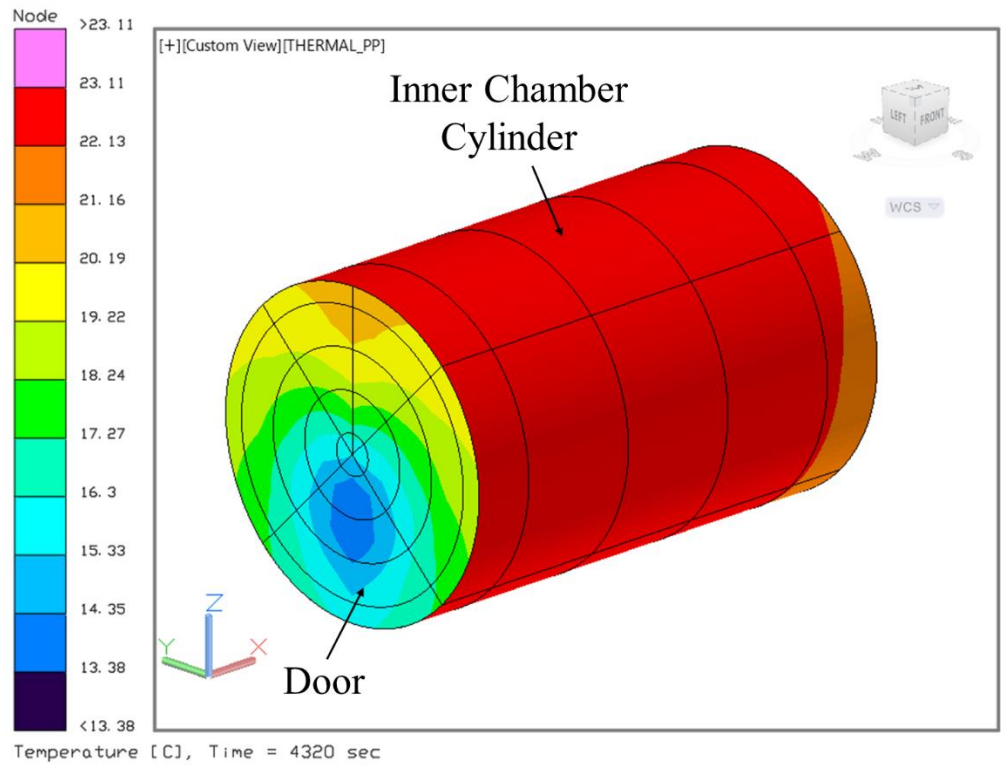


Figure 129: Predicted Temperature of Door and Inner Cylinder During Cooling Phase with Mass Model

H.2 Additional Cold Soak Phase Simulation Results

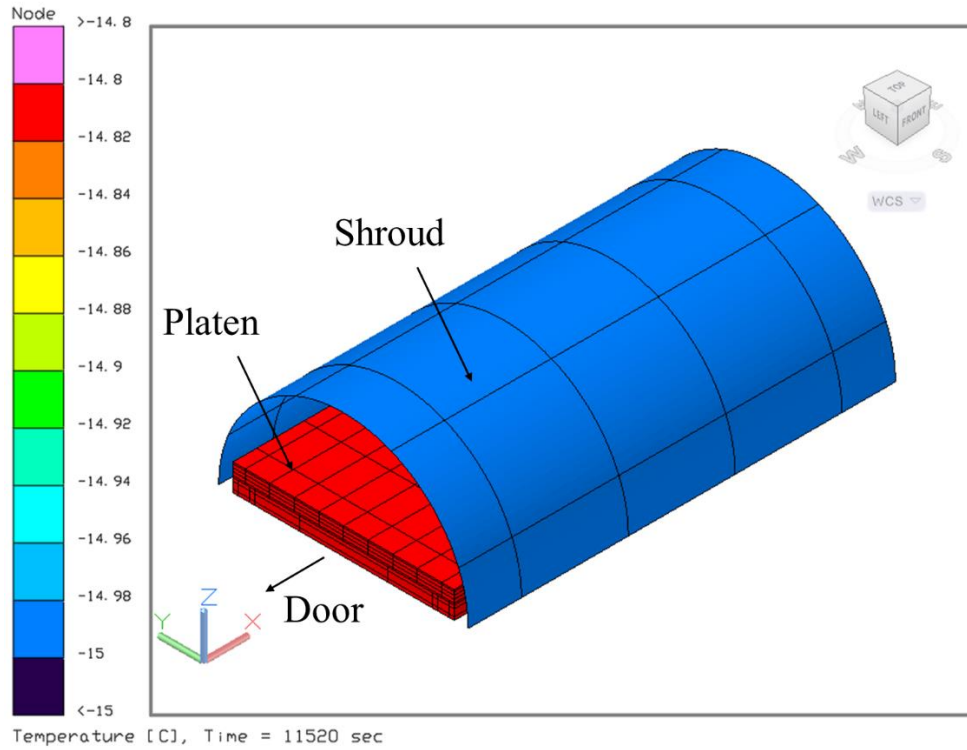


Figure 130: Predicted Temperature of Shroud During Cold Soak Phase with Mass Model

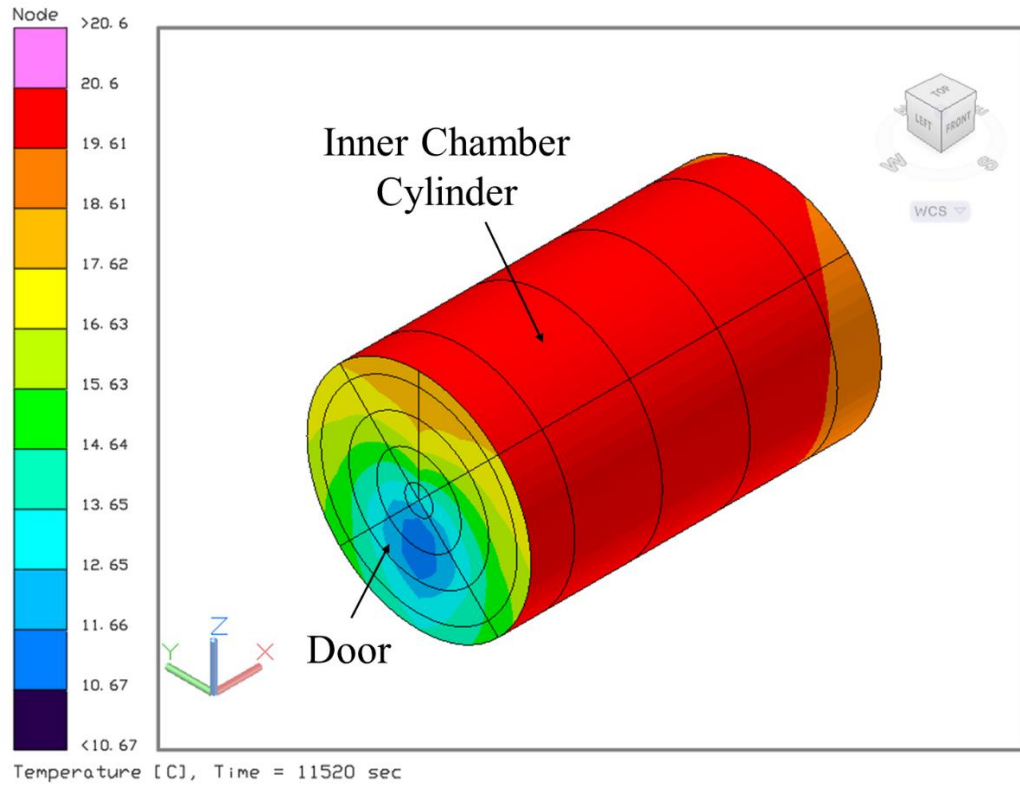


Figure 131: Predicted Temperature of Door and Inner Cylinder During Cold Soak Phase with Mass Model

H.3 Additional Heating Phase Simulation Results

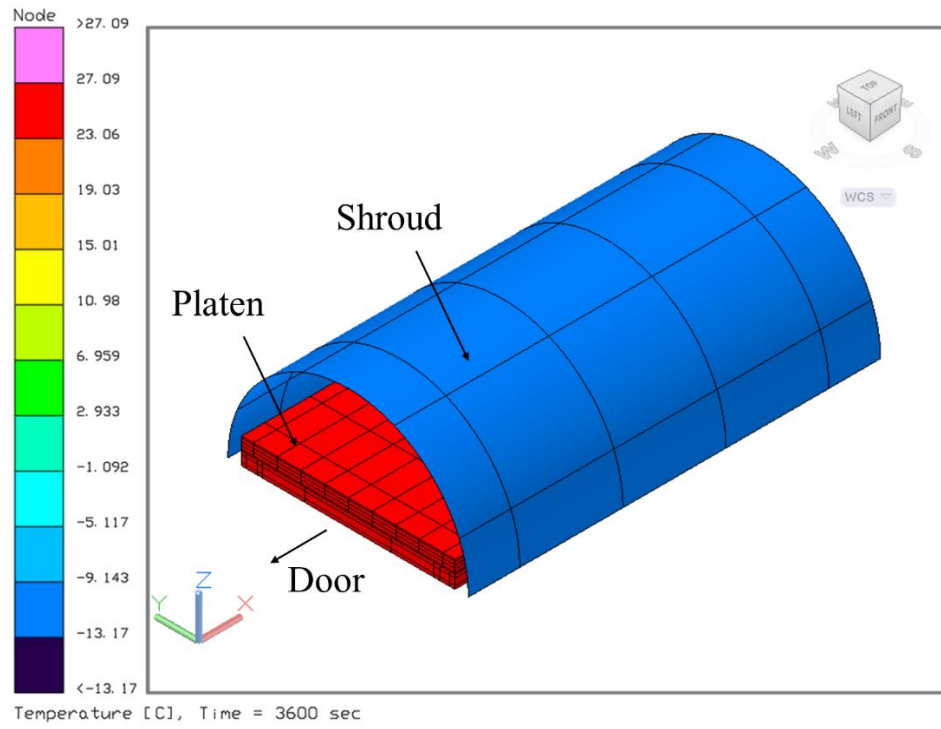


Figure 132: Predicted Temperature of Shroud During Heating Phase with Mass Model

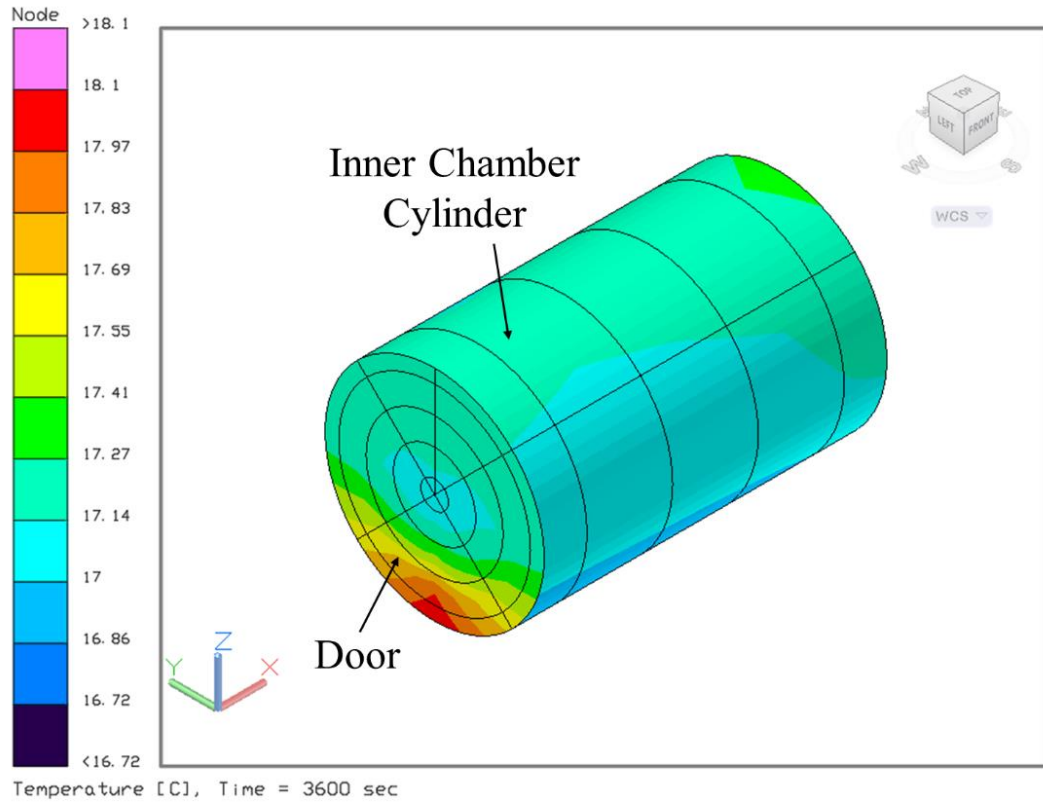


Figure 133: Predicted Temperature of Door and Inner Cylinder During Heating Phase with Mass Model

H.4 Additional Hot Soak Phase Simulation Results

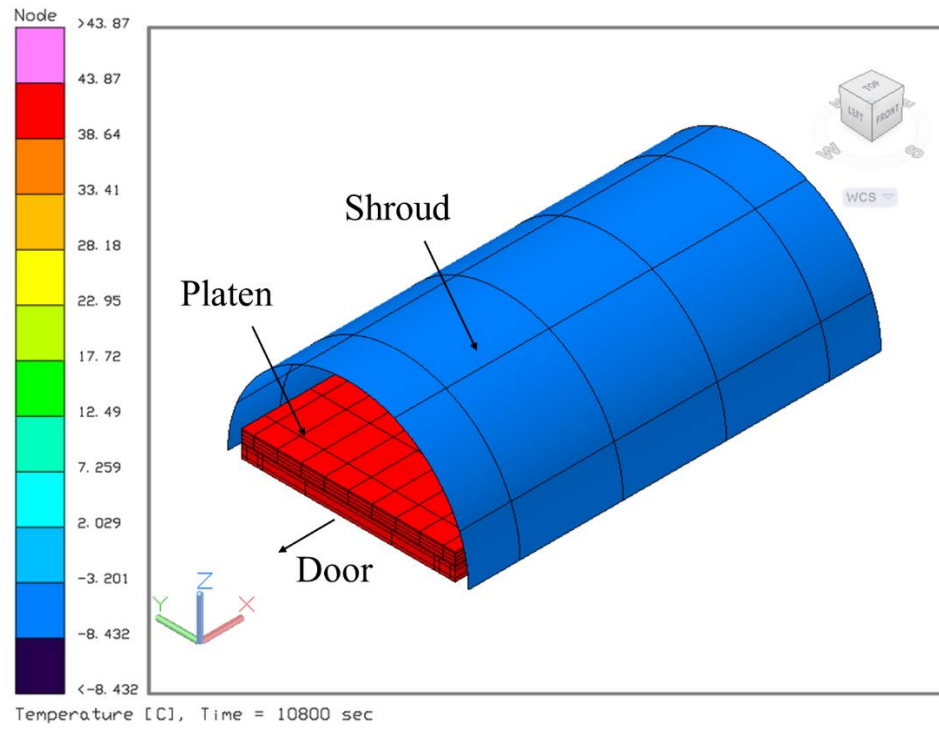


Figure 134: Predicted Temperature of Shroud During Hot Soak Phase with Mass Model

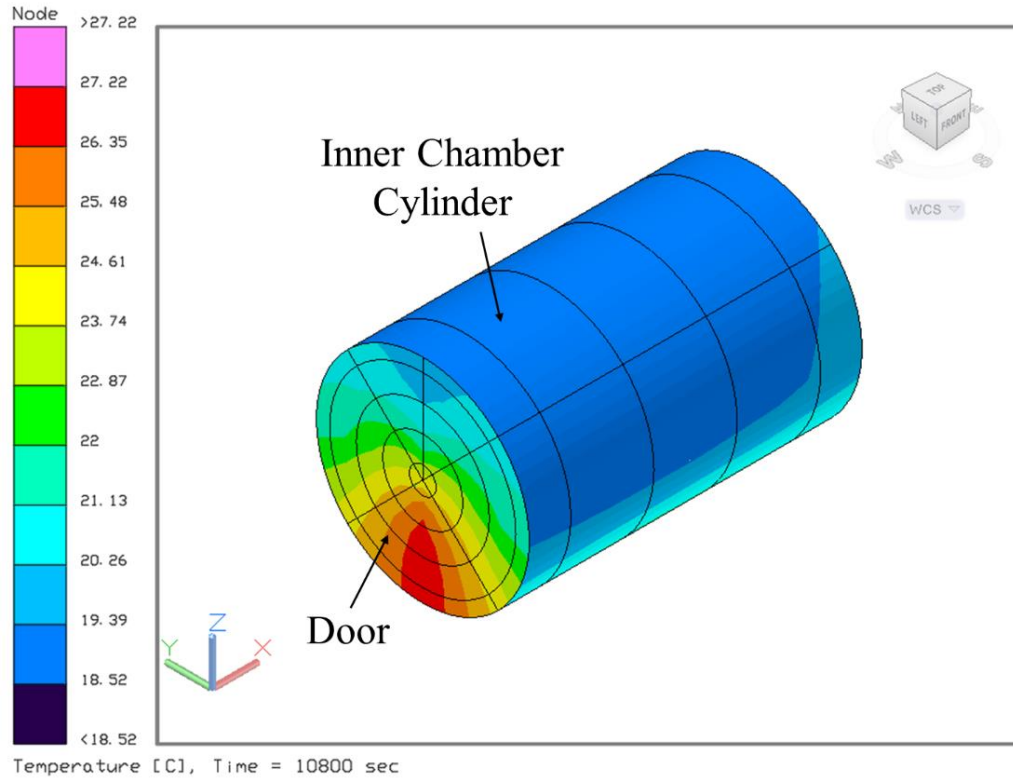


Figure 135: Predicted Temperature of Door and Inner Cylinder During Hot Soak Phase with Mass Model